

**April 2012**

**Scientific Documentation of the NCEP Nonhydrostatic Multiscale Model on the  
B grid (NMMB). Part 1 Dynamics**

**Zavisa Janjic  
Robert Gall**

**Research Applications Laboratory  
Joint Numerical Testbed  
Developmental Testbed Center**

---

**NATIONAL CENTER FOR ATMOSPHERIC RESEARCH  
P. O. Box 3000  
BOULDER, COLORADO 80307-3000  
ISSN Print Edition 2153-2397  
ISSN Electronic Edition 2153-2400**

## NCAR TECHNICAL NOTES

<http://www.ucar.edu/library/collections/technotes/technotes.jsp>

The Technical Notes series provides an outlet for a variety of NCAR Manuscripts that contribute in specialized ways to the body of scientific knowledge but that are not suitable for journal, monograph, or book publication. Reports in this series are issued by the NCAR scientific divisions. Designation symbols for the series include:

*EDD – Engineering, Design, or Development Reports*  
Equipment descriptions, test results, instrumentation,  
and operating and maintenance manuals.

*IA – Instructional Aids*  
Instruction manuals, bibliographies, film supplements,  
and other research or instructional aids.

*PPR – Program Progress Reports*  
Field program reports, interim and working reports,  
survey reports, and plans for experiments.

*PROC – Proceedings*  
Documentation or symposia, colloquia, conferences,  
workshops, and lectures. (Distribution may be limited to  
attendees).

*STR – Scientific and Technical Reports*  
Data compilations, theoretical and numerical  
investigations, and experimental results.

*The National Center for Atmospheric Research (NCAR) is operated by the nonprofit University Corporation for Atmospheric Research (UCAR) under the sponsorship of the National Science Foundation. Any opinions, findings, conclusions, or recommendations expressed in this publication are those of the author(s) and do not necessarily reflect the views of the National Science Foundation.*

## **Nonhydrostatic Multiscale Model on the B grid (NMMB). Part 1 Dynamics**

**Zavisa Janjic**

Environmental Modeling Center,  
National Centers for Environmental Prediction, Camp Springs, MD

**Robert Gall**

Development Manager, Hurricane Forecast Improvement Program,  
NOAA/OST, Silver Spring, MD

## Table of Contents

<b>LIST OF FIGURES</b> .....	v
<b>1.0 INTRODUCTION</b> .....	1
1.1 Overview of the Nonhydrostatic Multi-Scale Model on the B grid (NMMB) .....	3
<b>2.0 MODEL EQUATIONS</b> .....	6
<b>3.0 HORIZONTAL COORDINATE</b> .....	12
<b>4.0 HORIZONTAL GRID</b> .....	14
4.1 The B Grid.....	14
4.2 Comments on the choice of the B grid .....	14
<b>5.0 VERTICAL COORDINATE AND VERTICAL STAGGERING</b> .....	22
<b>6.0 TEMPORAL DISCRETIZATION</b> .....	26
6.1 Overview of the time differencing approach .....	26
6.2 Stabilization of Adams-Bashforth Time Differencing.....	26
6.3 The Crank-Nicholson Differencing Scheme.....	28
6.4 Time integration of the fast adjustment process .....	29
6.5 Time integration of vertically propagating sound waves.....	29
<b>7.0 TIME DISCRETE EQUATIONS</b> .....	30
7.1 Time differencing .....	31
7.2 Solution of the coupled equations.....	33
7.3 Time stepping and time step .....	36
<b>8.0 SPATIAL DISCRETE EQUATIONS</b> .....	38
8.1 Mass divergence and hydrostatic continuity equation .....	38
8.2 Hydrostatic pressure gradient force and the omega-alpha term.....	39
8.3 Horizontal advection of momentum .....	43
8.4 Horizontal advection of temperature and other mass point variables.....	48
8.5 Vertical Advection.....	49
8.6 Nonhydrostatic pressure gradient force, momentum conservation, omega-alpha term.....	49
8.7 Polar filtering .....	51
<b>9.0 GENERAL COMMENTS ON CONSERVATION PROPERTIES IN THE NMMB</b> .....	54
<b>10.0 BOUNDARY CONDITIONS</b> .....	57
10.1 Lateral and Polar Boundary Conditions .....	57
10.2 Vertical Boundary Conditions.....	60
<b>11.0 TURBULENT MIXING AND MODEL FILTERS</b> .....	61
11.1 Explicit Lateral Diffusion .....	61
11.2 Horizontal Divergence Damping .....	62
11.3 Filters .....	64
<b>12.0 REFERENCES</b> .....	72

## List of Figures

- Figure 1: The left hand figure shows a domain centered at 38N, 92W plotted on a regular latitude longitude map background. The right hand figure shows the same domain projected on a rotated latitude longitude map background.
- Figure 2: The B grid and grid distances  $\Delta x$ ,  $\Delta y$  and  $d$ .
- Figure 3: The staggered and semi-staggered grids C, B, E and Z and coordinate systems used in finite differencing.
- Figure 4: The ratio  $\nu_C/f$  as a function of  $X$  and  $Y$  in case of Charney-Phillips vertical staggering (see text for details).
- Figure 5: The ratios  $\nu_B/f$  (upper panel) and  $\nu_C/f$  (lower panel) as functions of  $X$  and  $Y$  in case of Lorenz vertical staggering (see text for details).
- Figure 6: Relative frequencies  $\nu_B/\nu$  (upper panel) and  $\nu_C/\nu$  (lower panel) as functions of  $X$  and  $Y$  in case of Charney-Phillips vertical staggering (see text for details).
- Figure 7: Examples of thicknesses of 64 NMMB layers in Pa depending on surface pressure, 1000 hPa (upper left panel), 750 hPa (upper right panel) and 500 hPa (lower left panel). Transition to hydrostatic pressure coordinate occurs at about 300 hPa, and the top of the model atmosphere is at 10 hPa. Cumulative distribution of topography height in medium resolution global NMMB is also shown in 100 m bins (lower right panel).
- Figure 8: The difference between the Charney-Phillips and the Lorenz vertical staggering.
- Figure 9: Amplification factors for the computational mode (red) and the physical mode (green) in the Adams-Bashforth time differencing scheme. Wave number in radians is shown along the abscissa with the  $4\Delta x$  wave in the center, the  $2\Delta x$  wave to the right and infinite wave number on the left.
- Figure 10: Same as figure 9 except the amplification factor scale near 1 is amplified. The green line shows the physical mode amplification factor for the Adams-Bashforth scheme (6.2.1), while the orange line corresponds to the modified scheme (6.2.2).
- Figure 11: Time stepping process in the NMMB.
- Figure 12: Schematic representation of mass fluxes in between h points on the B grid.
- Figure 13: Stencil of stream function points used to derive analog of the C grid energy and enstrophy conserving scheme on the B grid.
- Figure 14: Schematic representation of fluxes in between h points on the B grid.
- Figure 15: Lateral boundary conditions used in NMMB when used as a regional model.
- Figure 16: Schematic representation of the distribution of variables near the North Pole.
- Figure 17: Remapping variable values from real to ghost latitudinal circles near the poles.
- Figure 18: Schematic representation of fluxes in between h points on the B grid.

## 1.0 INTRODUCTION

Regional numerical weather prediction (NWP) models have reached the limits of validity of the hydrostatic approximation, and the global ones are rapidly approaching these limits. Vast experience with nonhydrostatic models has been accumulated in simulating convective clouds and storms, particularly in academic circles, but the techniques developed and used may not be directly or entirely applicable in operational NWP since NWP deals with phenomena on a much wider range of temporal and spatial scales. In response to this situation, over the last two decades or so, nonhydrostatic models specifically intended for weather forecasting have been developed and implemented (e.g., Davies et al., 2005; Doms and Schaettler, 1997; Janjic et al., 2001; Janjic, 2003; Room et al., 2006; Saito et al., 2007; Skamarock and Klemp, 2008; Steppeler et al., 2003; Yeh et al., 2002).

Concerning the criteria that a successful nonhydrostatic NWP model should satisfy, there are several, rather obvious choices. The accuracy of the nonhydrostatic model must not be inferior to that of mature hydrostatic models running at the same resolution. Moreover, particularly having in mind the uncertainties concerning the benefits that can be expected from nonhydrostatic dynamics at transitional, single digit resolutions in kilometers, the nonhydrostatic model should be sufficiently computationally efficient. Finally, the model dynamics should be capable of reproducing strongly nonhydrostatic flows at very high resolutions. Although such resolutions are beyond the resolutions that could be used in NWP in the near future, this condition must be satisfied in order to demonstrate that the model is indeed nonhydrostatic.

The new unified Nonhydrostatic Multiscale Model on the Arakawa B grid (NMMB) has been under development at the National Centers for Environmental Prediction (NCEP) within the new NOAA Environmental Modeling System (NEMS) framework (Janjic, 2005; Janjic and Black, 2007). The model is designed for a broad range of spatial and temporal scales so that it can be applied to a variety of applications from LES studies to weather forecasting and climate simulations on regional and global scales. The NMMB represents the second generation of nonhydrostatic models developed at NCEP. Except for being redesigned for the B grid, the model formulation follows the general modeling philosophy of its predecessor, the NCEP's regional Nonhydrostatic Mesoscale Model dynamic core in the Weather Research and Forecasting framework (WRF NMM) (Janjic et al., 2001, 2010; Janjic, 2003). The WRF NMM has been used for various applications at NCEP and elsewhere since the early 2000s, and since 2006 it has been the main short-range forecasting regional North American Model (NAM).

The NCEP grid point nonhydrostatic models have been developed building on NWP experience. As in their hydrostatic predecessors, mass-based hydrostatic vertical coordinates have been used. With the mass (hydrostatic pressure) coordinate the nondivergent flow remains on coordinate surfaces. Note that a similar argument applies to adiabatic flows in isentropic coordinates. However, important flow regimes on the meso scales are characterized by weak stability and strong diabatic forcing, which renders the isentropic coordinates less appealing (although still applicable) on these

scales. With this choice, the mass, as well as a number of other first order and quadratic quantities can be conserved in the discrete system in a straightforward way.

The nonhydrostatic dynamics were formulated by relaxing the hydrostatic approximation in hydrostatic NWP formulation based on modeling principles proven in practice. These principles were applied in several generations of models preceding the NMM and NMMB (e.g., Janjic 1977, 1979, 1984a, 1984b), and have been thoroughly tested in NWP and regional climate applications, although the specific numerical schemes employed have evolved significantly over time, and over about two orders of magnitude in resolution. In this way, the validity of the hydrostatic model was extended to nonhydrostatic motions, and at the same time the preferable features of the hydrostatic formulation were preserved in the hydrostatic limit.

The system of nonhydrostatic equations in the general mass based vertical coordinate is split into two parts: (a) the part that corresponds to the hydrostatic system, except for higher order corrections due to vertical acceleration, and (b) the system of equations that allows computation of the corrections due to the vertical acceleration. The separation of the nonhydrostatic contributions shows in a transparent way where, how and to what extent the hydrostatic approximation affects the equations. This approach does not require any linearization or additional approximation. The resulting system of nonhydrostatic equations has only one additional prognostic equation for nonhydrostatic pressure. Given the hydrostatic pressure, nonhydrostatic pressure and temperature, the geopotential is uniquely defined, and vertical velocity and vertical acceleration are computed from geopotential. Of course, the vertical velocity reduces to a consistent discrete approximation, so that internal consistency is preserved in the discrete system.

The nonhydrostatic dynamics extension is implemented through an add-on nonhydrostatic module. The nonhydrostatic module can be turned on and off depending on resolution in order to eliminate the computational overhead at coarse and transitional resolutions where the impact of nonhydrostatic effects is not detectable. More importantly, this feature allows easy comparison of hydrostatic and nonhydrostatic solutions at various resolutions using an identical hydrostatic core.

The “isotropic” quadratic conservative finite-volume horizontal differencing employed in the model conserves a variety of basic and derived dynamical and quadratic quantities and preserves some important properties of differential operators. Among these, the conservation of energy and enstrophy improves the accuracy of the nonlinear dynamics of the model on all scales (Arakawa, 1966; Janjic, 1984a, 1984b).

Currently, the NMMB uses the regular latitude-longitude grid for the global domain, and a rotated latitude-longitude grid in regional applications. With the Equator of the rotated system running through the middle of the regional integration domain, more uniform grid distances are obtained. In the vertical, the hybrid pressure-sigma coordinate has been chosen as the primary option. “Across the pole” polar boundary conditions are specified in the global limit and the polar filter acting on tendencies selectively slows down the wave components of the basic dynamical variables that would otherwise propagate faster in the zonal direction than the fastest wave propagating in the meridional direction. The multiple movable nesting capability is also available.

In very high resolution tests, a two-dimensional model based on the described principles successfully reproduced the classical two-dimensional nonhydrostatic solutions and thus demonstrated the validity of the concept (Janjic et al., 2001; Janjic, 2004). The high resolution tests using the regional version of the model indicate that the impact of nonhydrostatic dynamics becomes detectable at about 8 km resolution provided almost all dissipative mechanisms in the model are turned off, and noticeable at about 1 km resolution (Janjic et al., 2001; Janjic, 2003, 2004). The extra computational cost of the nonhydrostatic dynamics is on the order of 10% in global applications, or nonexistent if the nonhydrostatic extension is switched off at coarser resolutions. However, the relatively low cost of the nonhydrostatic dynamics allows its application even at transitional resolutions where the benefits due to the nonhydrostatic dynamics are small or uncertain.

The model has been computationally robust, efficient and reliable in operational applications and pre-operational tests. As indicated by regular runs carried out at NCEP, the NMMB produces good medium range forecasts, and its computational efficiency compares favorably with other medium range forecasting models.

### **1.1 Overview of the Nonhydrostatic Multi-Scale Model on the B grid (NMMB)**

This technical note focuses on the scientific and algorithmic approaches in the NMMB dynamics. Discussed are the NMMB dynamics solver, boundary conditions and the horizontal diffusion and other dissipative processes. The other components of the NMMB such as physical package, data assimilation, verification and the software framework are discussed elsewhere.

The NMMB dynamics solver includes fast waves, advection, thermodynamic processes, a nonhydrostatic add-on module, lateral diffusion, horizontal divergence damping, coupling of the sub-grids of the semi-staggered grid B, boundary conditions, polar filtering and nesting capabilities. It also includes transport of various components of the atmosphere such as moisture variables and other tracers. This system together with various options for physics, initialization and post processing are combined within the NEMS framework to produce end-to-end multiscale simulations.

#### *Major Features of the NMMB Dynamics Solver*

General requirements considered when building the NMMB core include:

- Modeling principles proven in NWP and regional climate applications;
- Numerical methods that control the nonlinear energy cascade and minimize generation of small-scale computational noise;
- Full compressible equations split into hydrostatic and nonhydrostatic contributions;
- Easy comparison of hydrostatic and nonhydrostatic solutions;
- Reduced computational effort at lower resolutions;

- Robustness and computational efficiency.

With these requirements taken into account, the main characteristics of the NMMB dynamics solver are:

- *Equations:* Fully compressible, Eulerian, nonhydrostatic with hydrostatic option.
- *Prognostic variables:* Horizontal vector wind components, temperature, nonhydrostatic pressure and hydrostatic surface pressure. In addition any number of scalars such as turbulent kinetic energy (TKE), water vapor mixing ratio, rain/snow mixing ratio, cloud water/ice mixing ratio, various aerosols and other tracers.
- *Horizontal Coordinate:* Rotated latitude-longitude for regional applications, and latitude-longitude coordinate with polar filter for global applications.
- *Vertical Coordinate:* Terrain-following hydrostatic-pressure based hybrid coordinate transitioning into the pure hydrostatic pressure coordinate near the top of the model atmosphere. The transition occurs at a specified pressure surface preferably below the Tropopause. Top of the model is a constant pressure surface.
- *Horizontal Grid:* Arakawa B-grid staggering.
- *Vertical Grid:* Lorenz staggering.
- *Time Integration:* Forward-backward for fast waves, implicit for vertically propagating sound waves, Adams-Bashforth for horizontal advection and Coriolis terms, and Crank-Nicholson for vertical advection.
- *Spatial Discretization:* Conservation of mass, momentum, energy, enstrophy and a number of other first order and quadratic quantities. Positive definiteness and monotonicity are preserved by tracer advection.
- *Lateral Turbulent Mixing and Model Filters:* Smagorinsky nonlinear lateral diffusion, horizontal divergence damping and coupling of the sub grids of the semi-staggered grid B by modifying the divergence term in the mass continuity equation (2.12).
- *Initial conditions:* Can be derived from a variety of sources including interpolation from existing grids, and various data assimilation systems.
- *Lateral Boundary Conditions:* Specified from a larger domain model or on the fly from the parent run.
- *Top Boundary Conditions:* Vertical velocity in the pressure coordinate system at the top boundary (a constant pressure level) is zero; nonhydrostatic pressure is equal to hydrostatic pressure. There is no special filtering applied near the top boundary.
- *Bottom Boundary Conditions:* Vertical velocity in the hybrid coordinate is zero, vertical derivative of the nonhydrostatic pressure deviation is zero. Physical boundary conditions are specified by surface physics schemes.

- *Earth's Rotation*: Coriolis terms included.
- *Nesting*: Simultaneous or sequential, running one way, two-way and two-way fixed or moving nests.

Extended WRF NMM and GFS physical parameterizations are available. These parameterizations include:

- *Microphysics*: Bulk schemes ranging from simplified physics suitable for mesoscale modeling to sophisticated mixed-phase physics for cloud resolving models.
- *Cumulus parameterizations*: Adjustment and mass-flux schemes.
- *Surface Physics*: Multi-layer full vegetation and soil moisture models, including snow cover and sea ice.
- *Planetary Boundary Layer and Free Atmosphere Turbulence*: Turbulent kinetic energy prediction and non-local schemes.
- *Atmospheric Radiation*: Longwave and shortwave schemes with multiple spectral bands. Cloud effects and surface fluxes are included.

Model initialization techniques available are:

- GSI (grid point statistical Interpolation);
- NPS (NEMS Preprocessing System), interpolation from other model grids;
- Digital filter.

## 2.0 MODEL EQUATIONS

Let  $s$  denote a generalized mass based terrain following vertical coordinate that varies from 0 at the model top to 1 at the surface (e.g., Eckermann, 2009). Let  $\pi$  be the hydrostatic pressure, and let  $\pi_{sfc}$  and  $\pi_T$  be the hydrostatic pressures at the surface and at the top of the model atmosphere, respectively. Then, the difference in hydrostatic pressure between the base and the top of the model column is  $\mu = \pi_{sfc} - \pi_T$ . Here,  $\pi_T$  is a nonnegative constant, whereas  $\pi_{sfc}$  is a function of time and horizontal position. In the hybrid coordinate the hydrostatic pressure is computed from the formula

$$\pi(x, y, s, t) = \pi_T + \sigma_1(s)H + \sigma_2(s)\mu(x, y, t), \quad (2.0)$$

where  $H$  is the constant depth of the hydrostatic pressure coordinate layer at the top of the model atmosphere,  $\sigma_1$  is zero at the top and the bottom of the model atmosphere, and  $\sigma_2$  increases from 0 to 1 from top to bottom.

The hypsometric equation

$$\frac{\partial \Phi}{\partial \pi} = -\alpha \quad (2.1)$$

relates the geopotential  $\Phi$  to the hydrostatic pressure. Assuming that the atmosphere is dry, the specific volume is related to the temperature  $T$  and pressure  $p$  by the ideal gas law  $\alpha = RT/p$ ,  $R$  being the gas constant. Note that the ideal gas law does not involve the hydrostatic pressure but rather the actual pressure,  $p$ , hereafter referred to as nonhydrostatic pressure. Using the ideal gas law, from (2.1)

$$\frac{\partial \Phi}{\partial s} = -\frac{RT}{p} \frac{\partial \pi}{\partial s}. \quad (2.2)$$

Upon integration of (2.2) from the surface, where the geopotential is denoted by  $\Phi_{sfc}$ , to an arbitrary level  $s$ ,

$$\Phi = \Phi_{sfc} + \int_s^1 \frac{RT}{p} \frac{\partial \pi}{\partial s'} ds'. \quad (2.3)$$

Using (2.1), the third equation of motion may be written as

$$\frac{dw}{dt} = g \left( \frac{\partial p}{\partial \pi} - 1 \right). \quad (2.4)$$

Defining the ratio of the vertical acceleration and gravity  $g$ ,

$$\varepsilon \equiv \frac{1}{g} \frac{dw}{dt}, \quad (2.5)$$

(2.4) may be rewritten as

$$\frac{\partial p}{\partial \pi} = 1 + \varepsilon, \quad (2.6)$$

which defines the relationship between the hydrostatic and the nonhydrostatic pressures. Integrating (2.6) with respect to  $\pi$ , one obtains the nonhydrostatic pressure at an arbitrary hydrostatic pressure, or on a coordinate surface  $s$ ,

$$p = \int_{\pi_T}^{\pi} \frac{\partial p}{\partial \pi'} d\pi' = \int_0^s (1 + \varepsilon) \frac{\partial \pi'}{\partial s'} ds'. \quad (2.7)$$

As can be seen from (2.6) and (2.7), should  $\varepsilon$  vanish, the pressure and the hydrostatic pressure become equivalent.

In the hydrostatic  $s$  coordinate system, the time derivative of a fluid property  $q$  following the motion of an air parcel may be written as

$$\frac{dq}{dt} = \left( \frac{\partial q}{\partial t} \right)_s + \mathbf{v} \cdot \nabla_s q + \left( \dot{s} \frac{\partial \pi}{\partial s} \right) \frac{\partial q}{\partial \pi}. \quad (2.8)$$

Here,  $\dot{s}$  is the vertical velocity and the subscripts indicate the variable that is kept constant while the differentiation is performed.

The nonhydrostatic continuity equation takes the form

$$w = \frac{1}{g} \left[ \left( \frac{\partial \Phi}{\partial t} \right)_s + \mathbf{v} \cdot \nabla_s \Phi + \left( \dot{s} \frac{\partial \pi}{\partial s} \right) \frac{\partial \Phi}{\partial \pi} \right] + W(\lambda, \varphi, t), \quad (2.9)$$

i.e., reduces to the definition of the vertical velocity  $w$ , with  $W$  denoting an integration constant that may depend on horizontal coordinates and time. For simplicity of exposition, in subsequent derivations we assume that  $W$  is zero. The familiar hydrostatic mass continuity equation

$$\left[ \frac{\partial}{\partial t} \left( \frac{\partial \pi}{\partial s} \right) \right]_s + \nabla_s \cdot \left( \mathbf{v} \frac{\partial \pi}{\partial s} \right) + \frac{\partial}{\partial s} \left( \dot{s} \frac{\partial \pi}{\partial s} \right) = 0 \quad (2.10)$$

also follows from the nonhydrostatic continuity equation.

Using the material surface boundary conditions  $\dot{s} \equiv ds/dt$  at  $s=0$  and  $s=1$ , one may obtain two equations from (2.10). The first one gives the tendency of the hydrostatic surface pressure

$$\frac{\partial \mu}{\partial t} = - \int_0^1 \nabla_{s'} \cdot \left( \mathbf{v} \frac{\partial \pi}{\partial s'} \right) ds', \quad (2.11)$$

and the second one is used to calculate the vertical velocity term

$$\left( \dot{s} \frac{\partial \pi}{\partial s} \right)_s = - \left( \frac{\partial \pi}{\partial t} \right)_s - \int_0^s \nabla_{s'} \cdot \left( \mathbf{v} \frac{\partial \pi}{\partial s'} \right) ds'. \quad (2.12)$$

Using the relations (2.1) and (2.6), in the case of a nonhydrostatic atmosphere one obtains

$$- \frac{1}{\rho} \nabla_z p \equiv - (1 + \varepsilon) \nabla_s \Phi - \alpha \nabla_s p. \quad (2.13)$$

Using (2.13), the inviscid nonhydrostatic equation for the horizontal part of the wind takes the form

$$\frac{d\mathbf{v}}{dt} = - (1 + \varepsilon) \nabla_s \Phi - \alpha \nabla_s p + \mathbf{f} \mathbf{k} \times \mathbf{v}. \quad (2.14)$$

Again, for vanishing  $\varepsilon$ , (2.14) reduces to the form used in hydrostatic models.

The first law of thermodynamics for adiabatic processes has the form

$$c_p \frac{dT}{dt} = \alpha \frac{dp}{dt} \quad (2.15)$$

in which  $c_p$  is the specific heat at constant pressure. In hydrostatic models, the derivative  $dp/dt$  is replaced by the derivative of hydrostatic pressure  $d\pi/dt$ , often denoted by the Greek letter omega ( $\omega$ ). For this reason, the right hand side of the equation is frequently referred to as the “omega–alpha” term. The derivative of pressure can be separated into a component  $\omega_1$  which reduces to the hydrostatic expression when  $\varepsilon$  vanishes, and a component  $\omega_2$  which vanishes with vanishing  $\varepsilon$ . Note that, generally,  $p = p(x, y, \pi, t)$ . Then

$$\frac{\partial p}{\partial t} = \left( \frac{\partial p}{\partial \pi} \right)_t \frac{\partial \pi}{\partial t} + \left( \frac{\partial p}{\partial t} \right)_\pi = (1 + \varepsilon) \frac{\partial \pi}{\partial t} + \left( \frac{\partial p}{\partial t} \right)_\pi, \quad (2.16)$$

where the subscripts indicate the variable that is kept constant while the differentiation is performed. In addition, as can be seen from (2.6),

$$\left( \dot{s} \frac{\partial \pi}{\partial s} \right) \frac{\partial p}{\partial \pi} = (1 + \varepsilon) \left( \dot{s} \frac{\partial \pi}{\partial s} \right). \quad (2.17)$$

Thus,  $dp/dt$  is written in the form

$$\frac{dp}{dt} = \omega_1 + \omega_2 \quad (2.18)$$

where

$$\omega_1 \equiv (1 + \varepsilon) \frac{\partial \pi}{\partial t} + \mathbf{v} \cdot \nabla_s p + (1 + \varepsilon) \left( \dot{s} \frac{\partial \pi}{\partial s} \right), \quad (2.19)$$

or taking into account (2.12),

$$\omega_1 = \mathbf{v} \cdot \nabla_s p - (1 + \varepsilon) \int_0^s \nabla_{s'} \cdot \left( \mathbf{v} \frac{\partial \pi}{\partial s'} \right) ds'. \quad (2.20)$$

Note that the contribution of the second term of the pressure gradient force in (2.13) to the kinetic energy generation is compensated by the contribution of the horizontal advection of pressure in (2.19). The second part of  $\omega$  is defined by

$$\omega_2 \equiv \frac{\partial p}{\partial t} - (1 + \varepsilon) \frac{\partial \pi}{\partial t}. \quad (2.21)$$

Note that the term (2.21) vanishes for vanishing  $\varepsilon$ .

In view of the separation of omega into two parts, the thermodynamic equation is separated into two parts as well,

$$\left( \frac{\partial T}{\partial t} \right)_1 = -\mathbf{v} \cdot \nabla_s T - \left( \dot{s} \frac{\partial \pi}{\partial s} \right) \frac{\partial T}{\partial \pi} + \frac{1}{c_p} (\alpha \omega_1) \quad (2.22)$$

and

$$\left( \frac{\partial T}{\partial t} \right)_2 = \frac{1}{c_p} (\alpha \omega_2). \quad (2.23)$$

With the aid of (2.20), (2.22) may be rewritten as

$$\left( \frac{\partial T}{\partial t} \right)_1 = -\mathbf{v} \cdot \nabla_s T - \left( \dot{s} \frac{\partial \pi}{\partial s} \right) \frac{\partial T}{\partial \pi} + \frac{\alpha}{c_p} \left[ \mathbf{v} \cdot \nabla_s p - (1 + \varepsilon) \int_0^s \nabla_{s'} \cdot \left( \mathbf{v} \frac{\partial \pi}{\partial s'} \right) ds' \right]. \quad (2.24)$$

Again, when  $\varepsilon$  vanishes, (2.22) and (2.24) take the form used in hydrostatic models, and the equation for the second part (2.23) takes the trivial form  $(\partial T / \partial t)_2 = 0$ .

The nonhydrostatic system of equations is closed by applying the operator (2.8) to the continuity equation (2.9) in order to obtain the vertical acceleration  $dw/dt$ . Then, from (2.5),

$$\varepsilon = \frac{1}{g} \frac{dw}{dt} = \frac{1}{g} \left[ \left( \frac{\partial w}{\partial t} \right)_s + \mathbf{v} \cdot \nabla_s w + \left( \dot{s} \frac{\partial \pi}{\partial s} \right) \frac{\partial w}{\partial \pi} \right]. \quad (2.25)$$

The parameter  $\varepsilon$  is the central point of the extended, nonhydrostatic dynamics. Assume for a moment that  $\varepsilon$  is zero. Then, Eqs. (2.2), (2.10), (2.14) and (2.24), together with the gas law, represent the set of equations describing the hydrostatic, inviscid, adiabatic atmosphere. However, the presence of nonzero  $\varepsilon$  in (2.6), (2.14) and (2.24) demonstrates in a transparent way where, how, and to what extent relaxing the hydrostatic approximation affects the familiar hydrostatic equations. Note that the

system of equations developed above bears a close relation to the system discussed by Laprise (1992).

On the synoptic scales,  $\varepsilon$  is small and approaches the computer round-off error. However, in case of vigorous convective storms, or strong vertical accelerations in flows over steep obstacles, the vertical velocity can reach the order of  $10ms^{-1}$  over a period on the order of  $1000s$ . This yields an estimate of the vertical acceleration on the order of  $10^{-2}ms^{-2}$ , and consequently,  $\varepsilon$  on the order of  $10^{-3}$ . As can be seen from (2.6), for this value of  $\varepsilon$  the nonhydrostatic deviation of pressure can reach  $100Pa$ . Bearing in mind that the typical synoptic scale horizontal pressure gradient is of the order of  $100Pa$  over  $100km$ , this suggests that significant local nonhydrostatic pressure gradients and associated circulations may develop on small scales. Nevertheless,  $\varepsilon$  remains much smaller than unity in atmospheric flows, and therefore, the nonhydrostatic effects in (2.6), (2.14) and (2.24) are of a higher order magnitude. An important consequence of this situation for the discretization is that high accuracy of computation of  $\varepsilon$  does not appear to be of paramount importance, since the computational errors are of even higher order than  $\varepsilon$ .

As can be seen from (2.2), the geometric height  $z$  is uniquely defined by the hydrostatic and nonhydrostatic pressures  $\pi$  and  $p$ , and temperature  $T$ . Thus, if these three variables are known, the vertical velocity  $w$  can be computed using the definition (2.8), or the nonhydrostatic continuity equation (2.9). Hence,  $w$  (and consequently  $\varepsilon$ ) cannot be considered as an independent prognostic variable. Nevertheless, for internal consistency, the vertical velocity  $w$  still must satisfy the prognostic vertical equation of motion (2.4).

In meso and large scale atmospheric flows  $\varepsilon \ll 1$ , and therefore the hydrostatic approximation can be safely used. Experiments have shown that impact of nonhydrostatic dynamics becomes detectable at resolutions  $<10km$ , and important at the resolution of about  $1km$ .

So far the equations for the dry atmosphere have been discussed. In real data applications, the presence of moisture and condensate affects the density and heat capacity of the air which also should be taken into account. In order to do that, the temperature  $T$  in (2.2) and (2.3) is replaced by virtual temperature

$$T_v = T(1 + 0.608q - c), \quad (2.26)$$

where  $q$  is specific humidity and  $c$  is condensate. The heat capacity  $c_p$  appearing in (2.15) and (2.22)-(2.24) takes on the value corresponding to the mixture of dry air, water vapor and condensate

$$c_p (m^{dry} + m^{vapor} + m^{liquid}) = c_p^{dry} m^{dry} + c_p^{vapor} m^{vapor} + c_p^{liquid} m^{liquid}, \quad (2.27)$$

or after rearrangement,

$$c_p = c_p^{dry} \left[ 1 + \left( \frac{c_p^{vapor}}{c_p^{dry}} - 1 \right) q + \left( \frac{c_p^{liquid}}{c_p^{dry}} - 1 \right) c \right]. \quad (2.28)$$

Here  $m$  is mass, and the superscripts *dry*, *vapor* and *liquid* denote, respectively, the variables for dry air, water vapor and liquid condensate.

Thus the complete list of variables dealt with by the model dynamics includes

*Mass variables:*

- $\mu, \pi$  hydrostatic pressure (column mass weight) [Pa]
- $p$  nonhydrostatic pressure [Pa]
- $T$  temperature [K]
- $q$  specific humidity (advection only) [kg/kg]
- $c$  total water condensate (advection only) [kg/kg]
- various tracers (advection only)

*Wind variables:*

- $u, v$  wind components [m/s].

### 3.0 HORIZONTAL COORDINATE

On the global scale, the latitude-longitude coordinate system is used. In regional applications a transformed latitude-longitude coordinate system is employed in order to improve computational efficiency. The latter system is obtained by rotation of the natural, geodesic latitude-longitude in such a way that the intersection of the equator and zero meridian of the transformed system coincides with the center of the model domain. The transformed system provides a more uniform horizontal grid spacing by reducing to a large extent the meridian convergence, and, accordingly, allows use of a larger time step for the model time integration. The transformation and inverse transformation equations between the natural latitude-longitude coordinates  $(\lambda, \varphi)$  and the rotated system  $(\Lambda, \Phi)$  are

$$\Lambda = \arctan \frac{\cos \varphi \sin(\lambda - \lambda_0)}{\cos \varphi_0 \cos \varphi \cos(\lambda - \lambda_0) + \sin \varphi_0 \sin \varphi} \quad (3.1)$$

$$\Phi = \arcsin[\cos \varphi_0 \sin \varphi - \sin \varphi_0 \cos \varphi \cos(\lambda - \lambda_0)] \quad (3.2)$$

and

$$\lambda = \arctan \left[ \frac{\cos \varphi_0 \cos \Phi \sin \Lambda}{\cos \Lambda \cos \Phi - \sin \varphi_0 (\cos \varphi_0 \sin \Phi + \sin \varphi_0 \cos \Phi \cos \Lambda)} \right] + \lambda_0 \quad (3.4)$$

$$\varphi = \arcsin(\cos \varphi_0 \sin \Phi + \sin \varphi_0 \cos \Phi \cos \Lambda) \quad (3.3)$$

Here,  $\lambda_0$  and  $\varphi_0$  are the angles of rotation along the axes of of the coordinates  $(\lambda, \varphi)$ . Defining

$$C = \frac{\cos \varphi_0 \cos \varphi + \sin \varphi_0 \sin \varphi \cos(\lambda - \lambda_0)}{\cos\{\arcsin[\cos \varphi_0 \sin \varphi - \sin \varphi_0 \cos \varphi \cos(\lambda - \lambda_0)]\}}, \quad (3.5)$$

$$S = \frac{\sin \varphi_0 \sin(\lambda - \lambda_0)}{\cos\{\arcsin[\cos \varphi_0 \sin \varphi - \sin \varphi_0 \cos \varphi \cos(\lambda - \lambda_0)]\}}, \quad (3.6)$$

the horizontal wind in the rotated system  $\mathbf{V} = (U, V)$  expressed in terms of the wind in the natural latitude/longitude system  $\mathbf{v} = (u, v)$  is

$$U = Cu - Sv, \quad (3.6)$$

$$V = Su + Cv. \quad (3.7)$$

The inverse wind transformation has the form

$$u = CU + SV, \quad (3.7)$$

$$v = CV - SU. \quad (3.8)$$

Figure 1 shows an example of a rotated grid in a typical limited area application of the NMMB.

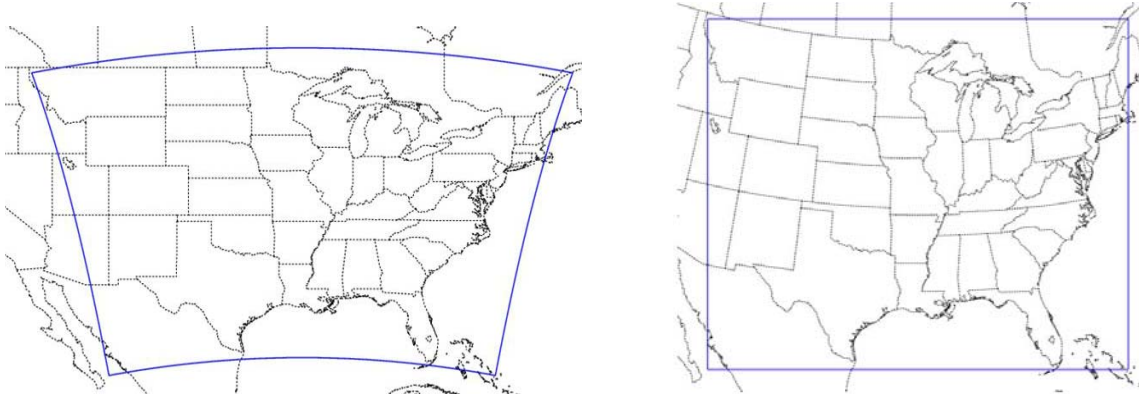


*Figure 1. The left hand figure shows a domain centered at 38N, 92W plotted on a regular latitude longitude map background. The right hand figure shows the same domain projected on a rotated latitude longitude map background.*

## 4.0 HORIZONTAL GRID

### 4.1 The B Grid

The NMMB is formulated on the B grid for reasons discussed in section 4.2. Figure 2 illustrates the staggering on the B-grid where  $h$  represents mass points (temperature, pressure, height, any mass or passive variable) and  $\mathbf{v}$  represents the horizontal velocity vector. The grid distances  $\Delta x$ ,  $\Delta y$  and  $d$  are also shown.

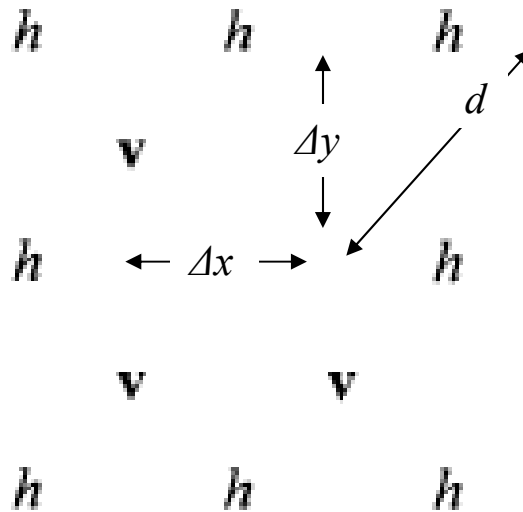


Figure 2. The B grid and grid distances  $\Delta x$ ,  $\Delta y$  and  $d$ .

### 4.2 Comments on the choice of the B grid

Winninghoff (1968) and Arakawa and Lamb (1977) examined the frequencies of gravity-inertia waves obtained using second-order centered differences on various types of rectangular horizontal grids. Compared to other grids considered, generally better agreements with the exact frequencies were obtained on the staggered grid C, and on the semi-staggered grid B (or E) shown in Figure 3. The symbol  $h$  in the figure denotes the mass point variables, while the horizontal velocity vector and the velocity components are denoted, respectively, by  $\mathbf{v}$ ,  $u$  and  $v$ . However, the staggered grid and the semi-staggered grids are not without problems, either. The problems on the staggered grid arise due to the averaging of the velocity components in the Coriolis force terms. On the other hand, in order to illustrate the problems on the semi-staggered grids, consider the shallow water equations

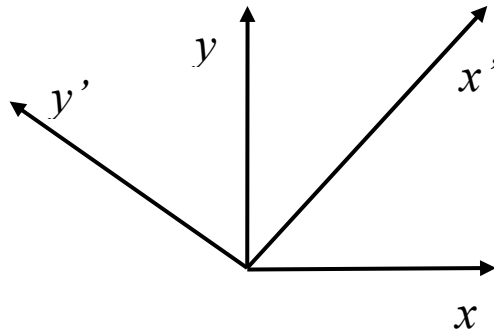
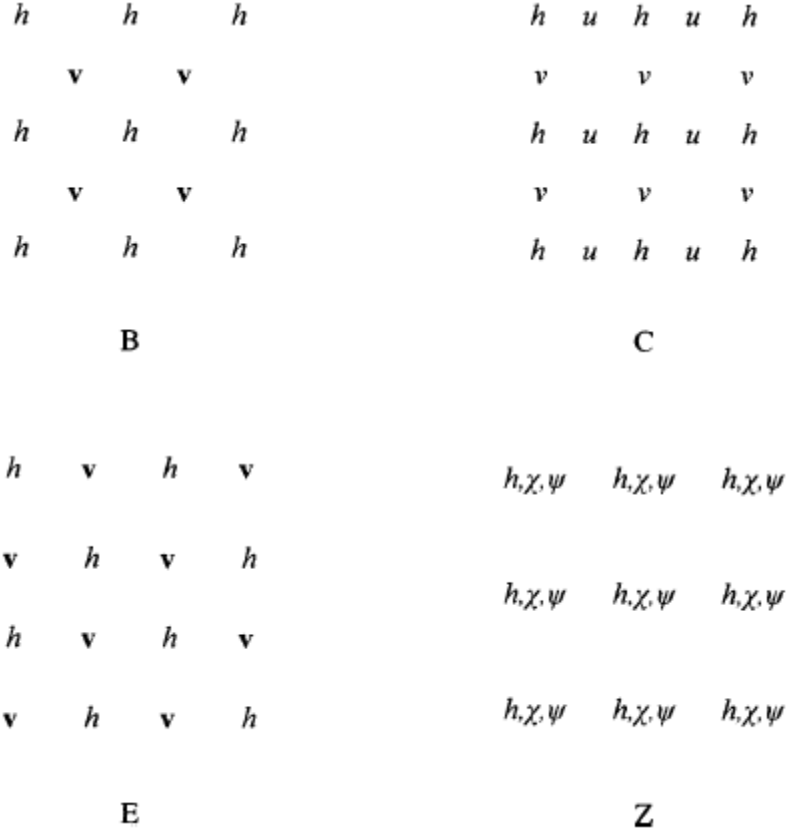


Figure 3. The staggered and semi-staggered grids C, B, E and Z and coordinate systems used in finite differencing.

$$\frac{\partial u}{\partial t} = -g \frac{\partial h}{\partial x} + fv, \quad \frac{\partial v}{\partial t} = -g \frac{\partial h}{\partial y} - fu, \quad \frac{\partial h}{\partial t} = -H \left( \frac{\partial u}{\partial x} + \frac{\partial v}{\partial y} \right). \quad (4.2.1)$$

Here,  $u$  and  $v$  are the velocity components,  $h$  is the height of the free surface,  $g$  is gravity,  $f$  is the Coriolis parameter assumed to be constant, and  $H$  is the mean depth of the fluid. The other symbols used have their usual meaning. The system (4.2.1) discretized in the most straightforward way, e.g., on the B grid, has the form

$$\frac{\partial u}{\partial t} = -g\delta_x \bar{h}^y + fv, \quad \frac{\partial v}{\partial t} = -g\delta_y \bar{h}^x - fu, \quad \frac{\partial h}{\partial t} = -H(\delta_x \bar{u}^y + \delta_y \bar{v}^x). \quad (4.2.2)$$

In (4.2.2), the symbol  $\delta$  and the overbar, respectively, represent the simplest two-point centered differencing and averaging operators applied in the direction indicated by the accompanying subscript or superscript. Following Janjic (1984a, 1984b), the velocity components on the B grid may be written in terms of the velocity potential  $\chi$  and the stream function  $\psi$  in the form

$$u = \delta_x \bar{\chi}^y - \delta_y \bar{\psi}^x, \quad v = \delta_y \bar{\chi}^x + \delta_x \bar{\psi}^y. \quad (4.2.3)$$

Then, after substituting the expressions (4.2.3) into the system (4.2.2), and rearrangement, one obtains

$$\frac{\partial \chi}{\partial t} = -gh + f\psi, \quad \frac{\partial \psi}{\partial t} = -f\chi, \quad \frac{\partial h}{\partial t} = -H(\delta_{xx} \bar{\chi}^{yy} + \delta_{yy} \bar{\chi}^{xx}), \quad (4.2.4)$$

where repeated subscripts and superscripts indicate repeated applications of the operators they are accompanying. As can be seen from (4.2.4), the only possible reason for the B grid problems is the insufficiently accurate computation of the Laplacian due to the averaging of the derivatives of the velocity potential  $\chi$  in the continuity equation. An inspection of the finite difference equations (4.2.4) reveals that they are defined on a nonstaggered grid, carrying all three variables  $\chi$ ,  $\psi$  and  $h$  at each grid point (Janjic 1984a, 1984b). This type of grid is also shown in Figure 3. It was named Z grid by Randall (1994). Thus, the B grid, together with the definitions (4.2.3), is equivalent to the Z grid. However, there is an important difference between the simulation of the gravity-inertia wave propagation on the grids B and Z. On the Z grid, the continuity equation can be written in the form

$$\frac{\partial h}{\partial t} = -H(\delta_{xx} \chi + \delta_{yy} \chi) \quad (4.2.5)$$

i.e., without averaging in the divergence term that was responsible for the B grid problems. However, an application of the Z grid in case of more complex equations would require costly conversions between the velocity components and the velocity potential and the stream function. A more complete comparison of the properties of the remaining two possibilities, the staggered grid C and the semi-staggered grids B and E can be found, e.g., in Janjic and Mesinger (1984, 1989). These considerations, however, do not give decisive advantage to either of the two choices. The problems on the semi-staggered grids B and E are restricted mainly to the shortest waves, while in the case of the slow internal modes, and/or weak stability, the C grid may develop problems in the entire range of the admissible wave numbers (cf. Arakawa and Lamb, 1977). In addition, there is an effective technique for filtering the low frequency, short-wave noise resulting from the inaccurate computation of the divergence term on the semi-staggered grids (Janjic, 1979). More sophisticated, nondissipative methods (“deaveraging” and “isotropisation”) for dealing with the problem also have been proposed (Janjic et al., 1998), leading to dramatic improvements of the finite-difference frequencies of the short gravity-inertia waves on the semi-staggered grids.

The results discussed so far are relevant for classical synoptic scale model design. In order to address the question of the choice of the horizontal grid as the mesoscales are approached, consider the linearized anelastic nonhydrostatic system

$$\begin{aligned}\frac{\partial u}{\partial t} &= -\frac{\partial P}{\partial x} + fv, & \frac{\partial v}{\partial t} &= -\frac{\partial P}{\partial y} - fu, & \frac{\partial w}{\partial t} &= -\frac{\partial P}{\partial z} + \theta, \\ \frac{\partial \theta}{\partial t} &= -N^2 w, & \frac{\partial u}{\partial x} + \frac{\partial v}{\partial y} + \frac{\partial w}{\partial z} &= 0.\end{aligned}\quad (4.2.6)$$

Here,  $P = c_p \theta_0 \pi'$ ,  $\theta = (g / \theta_0) \theta'$ ,  $\theta_0$  is the basic state potential temperature,  $\pi'$  is the Exner function perturbation,  $\theta'$  is the potential temperature perturbation and  $N$  is the Brunt-Vaisala frequency. Assuming, as usual, the solutions of the form

$$A = A_0 e^{i(kx + ly + mz - \nu t)}, \quad (4.2.7)$$

where  $A$  stands for any dependent variable appearing in (4.2.6),  $k$ ,  $l$  and  $m$  are the wave numbers in the directions of the coordinate axes  $x$ ,  $y$  and  $z$ , and  $\nu$  is the frequency, the frequency equation may be written in the form

$$\left(\frac{\nu}{f}\right)^2 = \frac{\left(\frac{N}{f}\right)^2 (k^2 + l^2) + m^2}{k^2 + l^2 + m^2}. \quad (4.2.8)$$

Defining, for brevity,  $X = kd$ ,  $Y = ld$ ,  $Z = m\Delta z$ , where  $d$  is the horizontal distance between two nearest points carrying the same variable, and  $\Delta z$  is the vertical grid size, (4.2.8) can be rewritten as

$$\left(\frac{\nu}{f}\right)^2 = \frac{\left(\frac{N}{f}\right)^2 (X^2 + Y^2) + Z^2 \left(\frac{d}{\Delta z}\right)^2}{X^2 + Y^2 + Z^2 \left(\frac{d}{\Delta z}\right)^2}. \quad (4.2.9)$$

The normalized frequencies on the grids B and C, respectively, are (communicated by Klemp)

$$\left(\frac{\nu_B}{f}\right)^2 = \frac{\left(\frac{N}{f}\right)^2 \cos^2\left(\frac{Z}{2}\right) \left[ \cos^2\left(\frac{Y}{2}\right) \sin^2\left(\frac{X}{2}\right) + \cos^2\left(\frac{X}{2}\right) \sin^2\left(\frac{Y}{2}\right) \right] + \left(\frac{d}{\Delta z}\right)^2 \sin^2\left(\frac{Z}{2}\right)}{\cos^2\left(\frac{Y}{2}\right) \sin^2\left(\frac{X}{2}\right) + \cos^2\left(\frac{X}{2}\right) \sin^2\left(\frac{Y}{2}\right) + \left(\frac{d}{\Delta z}\right)^2 \sin^2\left(\frac{Z}{2}\right)} \quad (4.2.10)$$

$$\left(\frac{\nu_C}{f}\right)^2 = \frac{\left(\frac{N}{f}\right)^2 \cos^2\left(\frac{Z}{2}\right) \left[ \sin^2\left(\frac{X}{2}\right) + \sin^2\left(\frac{Y}{2}\right) \right] + \left(\frac{d}{\Delta z}\right)^2 \cos^2\left(\frac{X}{2}\right) \cos^2\left(\frac{Y}{2}\right) \sin^2\left(\frac{Z}{2}\right)}{\sin^2\left(\frac{X}{2}\right) + \sin^2\left(\frac{Y}{2}\right) + \left(\frac{d}{\Delta z}\right)^2 \sin^2\left(\frac{Z}{2}\right)}. \quad (4.2.11)$$

Note that in the case of the Charney-Phillips vertical staggering the factor  $\cos^2(Z/2)$  following the term  $(N/f)^2$  should be replaced by unity in both formulas. This factor

should be present in the case of usually used, more convenient, Lorenz vertical distribution of variables. The difference between the Charney-Phillips and the Lorenz vertical staggering is discussed in Section 5 and illustrated in Figure 8.

As can be seen from (4.2.9)-(4.2.11), there are two terms in the numerator. On the B grid the averaging within the divergence term affects the first term, while on the C grid the averaging of the Coriolis force terms affects the second term. Which of the two terms will be dominating is not always clear and may depend on stability and the choice of the horizontal and vertical grid sizes.

Consider the Charney-Phillips staggering first. As already pointed out, in this case the factor  $\cos^2(Z/2)$  following the term  $(N/f)^2$  in (4.2.10) and (4.2.11) should be replaced by unity, i.e.,

$$\left(\frac{v_B}{f}\right)^2 = \frac{\left(\frac{N}{f}\right)^2 \left[ \cos^2\left(\frac{Y}{2}\right) \sin^2\left(\frac{X}{2}\right) + \cos^2\left(\frac{X}{2}\right) \sin^2\left(\frac{Y}{2}\right) \right] + \left(\frac{d}{\Delta z}\right)^2 \sin^2\left(\frac{Z}{2}\right)}{\cos^2\left(\frac{Y}{2}\right) \sin^2\left(\frac{X}{2}\right) + \cos^2\left(\frac{X}{2}\right) \sin^2\left(\frac{Y}{2}\right) + \left(\frac{d}{\Delta z}\right)^2 \sin^2\left(\frac{Z}{2}\right)}. \quad (4.2.12)$$

$$\left(\frac{v_C}{f}\right)^2 = \frac{\left(\frac{N}{f}\right)^2 \left[ \sin^2\left(\frac{X}{2}\right) + \sin^2\left(\frac{Y}{2}\right) \right] + \left(\frac{d}{\Delta z}\right)^2 \cos^2\left(\frac{X}{2}\right) \cos^2\left(\frac{Y}{2}\right) \sin^2\left(\frac{Z}{2}\right)}{\sin^2\left(\frac{X}{2}\right) + \sin^2\left(\frac{Y}{2}\right) + \left(\frac{d}{\Delta z}\right)^2 \sin^2\left(\frac{Z}{2}\right)}. \quad (4.2.13)$$

In case of very weak stability, say  $N = 0.0001$ , and  $f = 0.0001$ , the factor  $(N/f)^2 = 1$ , and from (4.2.9) and (4.2.12) it follows that

$$\left(\frac{v}{f}\right)^2 = \left(\frac{v_B}{f}\right)^2 = 1 \quad (4.2.14)$$

in the entire admissible wavenumber range. Thus, the horizontal group velocity is zero. On the other hand, the ratio  $v_C/f$  computed from (4.2.13) using the same values of  $N$  and  $f$ , and assuming that  $d/\Delta z = 30$  and  $Z = \pi/32$ , is shown in Figure 4 as a function of  $X$  and  $Y$ . As can be seen from the figure, the frequency on the C grid is not constant. This leads to a nonzero group velocity throughout the horizontal admissible wavenumber range, including the longest waves.

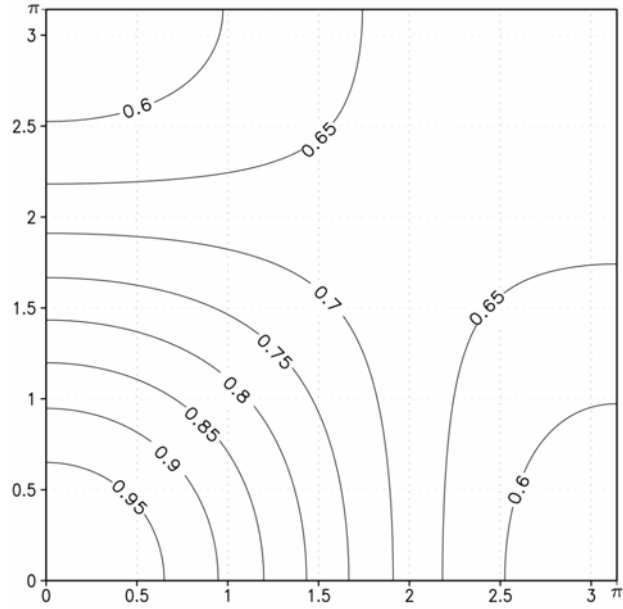


Figure 4. The ratio  $v_C / f$  as a function of  $X$  and  $Y$  in case of Charny-Phillips vertical staggering (see text for details).

The relative frequencies in the case of Lorenz staggering are shown in Figure 5. As can be seen from the figure, the relative frequencies on both the B (left panel) and C (right panel) grids are affected by this type of staggering. The relative frequency on the B grid is not constant, but remains very close to unity throughout the admissible horizontal wavenumber range. In contrast, significant deviations from the correct value can again be seen on the C grid, including the areas corresponding to the longest waves.

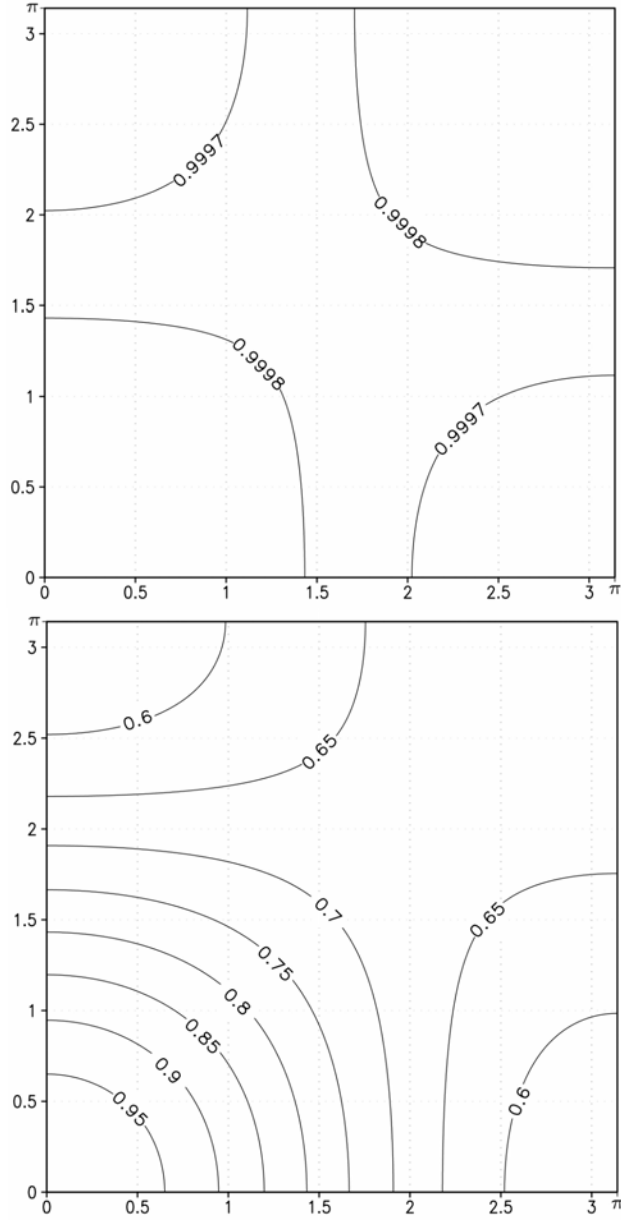


Figure 5. The ratios  $\nu_B/f$  (upper panel) and  $\nu_C/f$  (lower panel) as functions of  $X$  and  $Y$  in case of Lorenz vertical staggering (see text for details).

In current forecasting models the ratio  $d/\Delta z$  is of the order of 100. Since  $N$  is on the order of 0.01, in the case of large  $Z$  the two terms in the numerator of (4.2.10) and (4.2.11) can be similar magnitude. For example, let  $Z = \pi/4$ . For these values of  $d/\Delta z$ ,  $N$  and  $Z$ , the relative frequencies for both B and C grids, computed from formulas (4.2.10) and (4.2.11) and normalized by the continuous relative frequencies (4.2.9), are shown in Figure 6. As can be seen from the figure, the relative frequencies on the B grid (left panel) are affected by the discretization as well, but to a much smaller degree in the long wave range compared to the C grid (right panel).

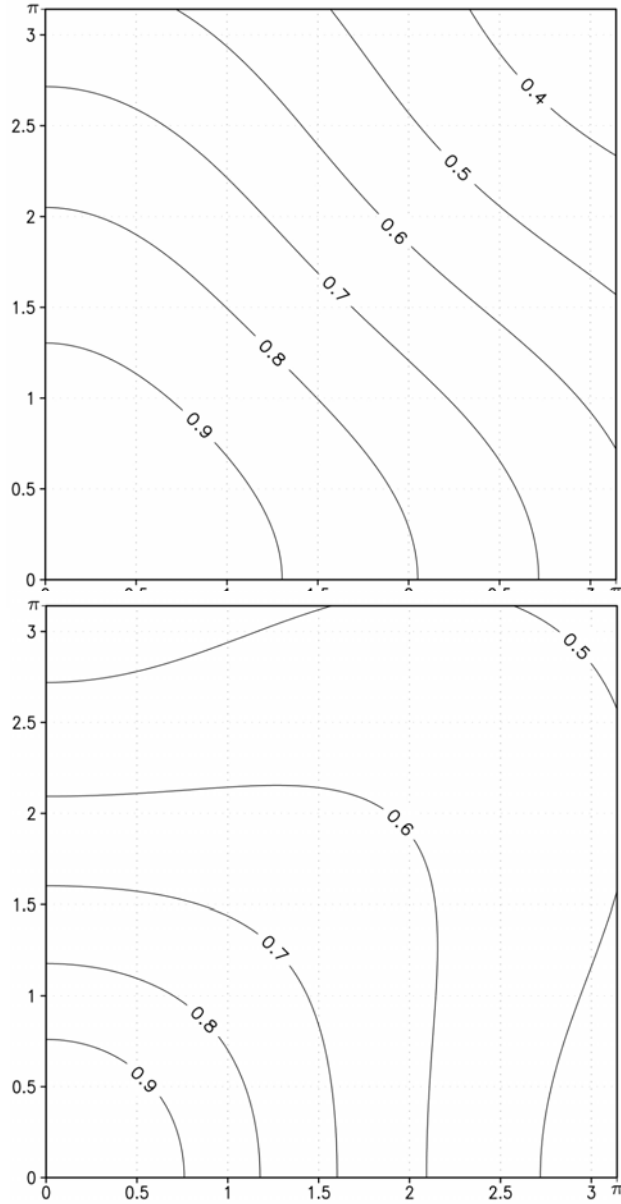


Figure 6. Relative frequencies  $\nu_B/\nu$  (upper panel) and  $\nu_C/\nu$  (lower panel) as functions of  $X$  and  $Y$  in case of Charny-Phillips vertical staggering (see text for details).

Since the problems on the semi-staggered grid B are restricted to the shortest resolvable scales, and they are less sensitive to the stability and the choice of the vertical and horizontal grid sizes, preference was given to the semi-staggered grid B.

## 5.0 VERTICAL COORDINATE AND VERTICAL STAGGERING

The old NCEP's operational regional hydrostatic model ("Eta") used a step-like representation of mountains originally proposed by Bryan (1969) in the z-vertical coordinate. This approach was modified for a sigma coordinate model by Mesinger et al (1988). The advantage of the step-like mountains is that the coordinate surfaces are quasi-horizontal. However, internal discontinuities are introduced at the vertical sides of the steps, and lateral boundary conditions are required at these discontinuities. The formal accuracy of the finite differences at the points next to the internal boundaries is reduced to the first order. In addition, if the no slip boundary conditions are used in order to preserve in a simple way the major favorable features of the finite-differencing schemes (cf. Janjic, 1977; 1979; 1984a, 1984b), a nonphysical sink of momentum is introduced. Yet another problem is the representation of the physical processes in the surface layer and the planetary boundary layer (PBL). If one wants to represent these processes in a reasonably uniform way throughout the integration domain, including both low-lying and elevated terrain, an approximately equidistant spacing of the vertical levels is required in the lower few kilometers of the atmosphere. However, the vertical resolution needed in order to achieve this goal is still too high. This was indeed one of the major problems in the process of developing the physical package for the "Eta" model (Janjic, 1990; 1994; 1996; 2001). The problem has been alleviated by increasing vertical resolution over time, which eventually allowed meaningful application of the similarity theory over large parts of the integration domain (Lobocki, 1993; Janjic, 1996).

The hydrostatic Meso model with the step-mountains ("eta coordinate") was producing reasonable synoptic scale meteorological guidance. Apparently, the blocking by the step-mountains was able to depict reasonably well the synoptic scale flow around the obstacles. However, with the increasing model resolutions, several problems that could be associated with the step-mountain representation started to surface, particularly at smaller scales, and in mountainous areas. The difficulties appear to be associated with the flow over the obstacles. For example, the model using the step-mountain representation failed to reproduce a catabatic windstorm in the Rockies, while the forecast using the conventional sigma coordinate was quite successful in this respect (Janjic and DiMego, 2001). In addition, several studies (Adcroft et al, 1997; Gallus, 2000; Gallus and Klemp, 2000; Janjic and DiMego, 2001) indicate that more problems should be expected at higher resolutions.

Another problem possibly related to the mountain representation is that the NCEP Eta Model using the step-mountains was producing precipitation too far down on the slopes of major orographic obstacles (Staudenmeier and Mittelstadt, 1998, Janjic 1998). A similar problem was noticed independently in the operational high resolution runs in the Alpine region (Communicated by Pacagnella).

In response to the step-mountain problems the hybrid pressure-sigma vertical coordinate option (Sangster, 1960; Arakawa and Lamb, 1977) was introduced into the WRF NMM. However, for consistency with NCEP's global spectral model, the hybrid pressure sigma coordinate discussed by Eckermann (2009) is used in the NMMB. With the hybrid coordinate, the hydrostatic pressure is computed from the formula (2.0). A

version of the algorithm proposed by Eckermann (2009) is used for coordinate generation. The transition to the hydrostatic pressure vertical coordinate occurs around 300 hPa. Examples of thicknesses of 64 NMMB layers depending on surface pressure are shown in Figure 7 in [Pa]. Transition to the hydrostatic pressure coordinate occurs at the layer interface nearest to 300 hPa, and the top of the model atmosphere is at 10 hPa. Cumulative distribution of topography height in medium resolution global NMMB is also shown in 100 m bins in the lower right panel of the figure. The derivative of the curve in the plot shows the fraction of total grid points in each of the 56 100m bins. The cumulative curve shows the fraction of the topography points that are lower or equal to the heights of the corresponding bin on the abscissa. Note that the thicknesses of the layers above the transition point do not change with the change of the surface pressure, while the layers below shrink in order to accommodate the same number of layers within reduced pressure range.

With the hybrid coordinates, the coordinate surfaces are flat high above and away from the mountains. Over elevated terrain the hybrid coordinate has increased vertical resolution, and the equations are continuous, without the computational internal boundary conditions that have to be specified with the step-mountains. The sloping coordinate surfaces in the vicinity of the mountains, and the related inaccuracies, are the price to pay for these benefits. Since the hydrostatic pressure is currently used as the vertical coordinate above about 300 hPa, the possible inaccuracies due to the sloping coordinate surfaces are restricted only to the lower part of the mass of the atmosphere. Note that, generally, largest errors in the  $\sigma$ -coordinate occur in the stratosphere. Thus, with the hybrid coordinate, the most serious problems associated with the sloping  $\sigma$ -surfaces are eliminated. In addition, the increased resolution presumably acts in the direction of reducing the computational inaccuracies, and improves the representation of the vertical structure of the PBL over elevated terrain.

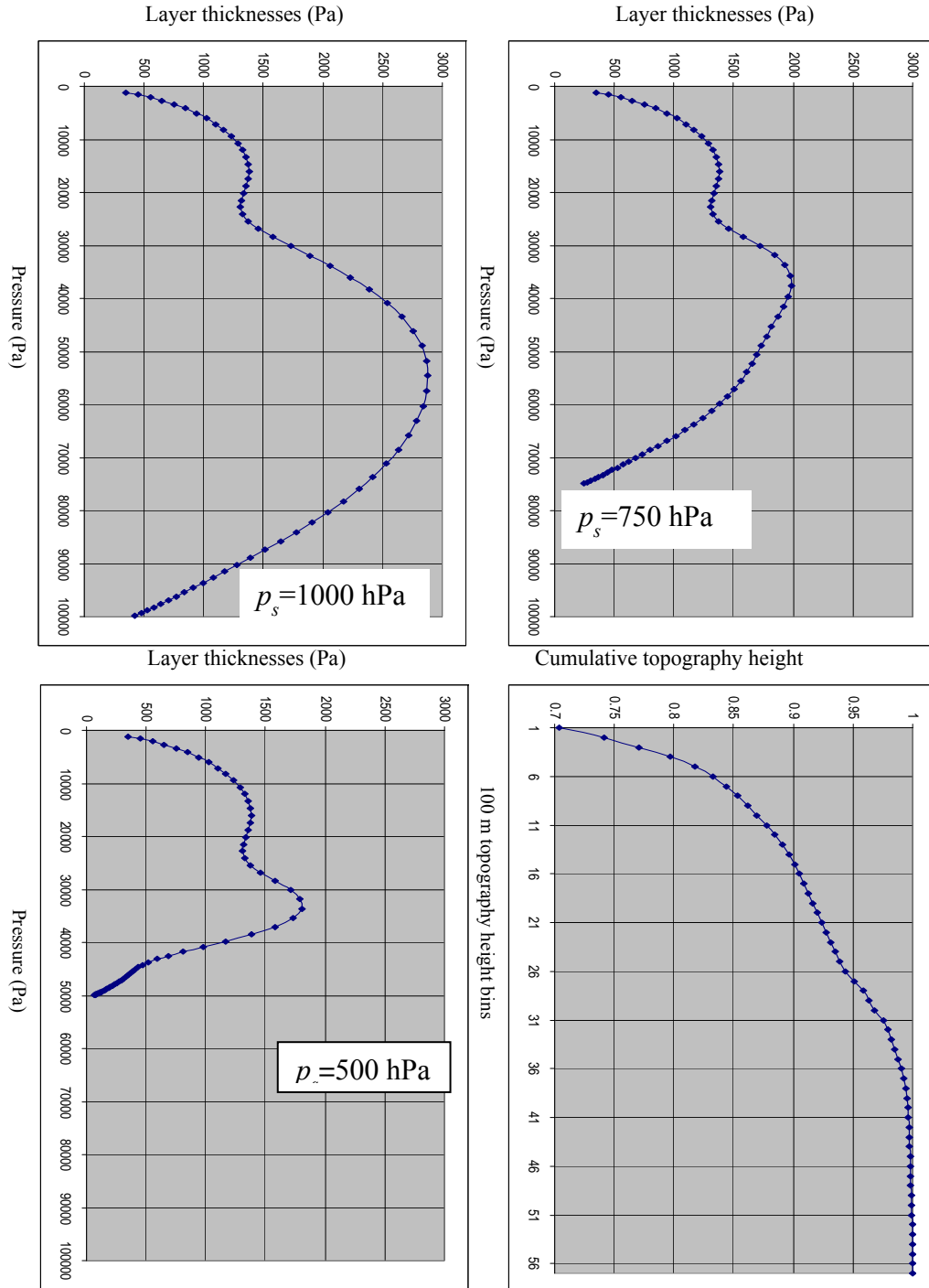


Figure 7. Examples of thicknesses of 64 NMMB layers in Pa depending on surface pressure, 1000 hPa (upper left panel), 750 hPa (upper right panel) and 500 hPa (lower left panel). Transition to hydrostatic pressure coordinate occurs at about 300 hPa, and the top of the model atmosphere is at 10 hPa. Cumulative distribution of topography height in medium resolution global NMMB is also shown in 100 m bins (lower right panel).

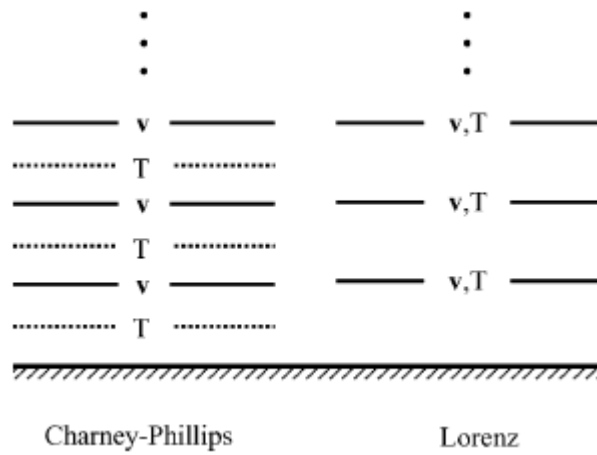


Figure 8. The difference between the Charney-Phillips and the Lorenz vertical staggering.

The usual Lorenz staggering of the variables is used in the vertical (Figure 8). The geopotential and the nonhydrostatic pressure are defined at the interfaces of the layers, while all three velocity components and temperature are carried in the middle of the model layers. The vertical velocity is defined at the B grid mass points.

## 6.0 TEMPORAL DISCRETIZATION

### 6.1 Overview of the time differencing approach

- Explicit schemes are used where possible for accuracy, computational efficiency and coding transparency:
  - Horizontal advection of  $u$ ,  $v$ ,  $T$ ;
  - Advection of various other variables such as specific humidity, cloud water, TKE, aerosols, tracer gases;
  - Adjustment terms.
- Implicit schemes are used for very fast processes that would require a restrictively short time step for numerical stability with explicit differencing:
  - Vertical advection;
  - Vertically propagating sound waves.

For the basic dynamic variables the NMMB uses four types of time integration: (i) modified Adams-Bashforth for horizontal advection of  $u$ ,  $v$ ,  $T$  and tracers, and for Coriolis terms, (ii) Crank Nicholson for vertical advection of  $u$ ,  $v$ ,  $T$  and tracers, (iii) forward-backward scheme for adjustment terms and (iv) an implicit scheme for vertically propagating sound waves.

### 6.2 Stabilization of Adams-Bashforth Time Differencing

The Adams-Bashforth scheme can be represented as

$$\frac{y^{n+1} - y^n}{\Delta t} = \frac{3}{2} f(y^n) - \frac{1}{2} f(y^{n-1}). \quad (6.2.1)$$

Note that this method has a very weak linear instability which can be tolerated in practice or stabilized by slight off-centering, as is done in the NMMB

$$\frac{y^{n+1} - y^n}{\Delta t} = 1.533 f(y^n) - 0.533 f(y^{n-1}). \quad (6.2.2)$$

Figure 9 shows the amplification factor of the physical mode (green) and the computational mode (red) for the scheme (6.2.1). The plot is for linear 1D centered second order advection with constant advection speed of 110 m/s and a time step equal to one third of the maximum allowed time step by the CFL criterion. Here wave number is on the  $x$  axis, with the wave number corresponding to the  $4\Delta x$  wave in the middle, the  $2\Delta x$  wave on the right end, and the wave with infinite wave length on the left end. The amplification rate of the physical mode is very near to unity, so that it is very weakly amplified. On the other hand the computational mode is strongly damped. The amplification rate of the physical mode is not exactly one, however, as shown in Figure 10 where the ordinate scale near one is magnified. The green curve in the figure again

corresponds to the physical mode of the scheme (6.2.1), while the orange curve uses (6.2.2). The slight instability of the meteorological mode of the traditional Adams-Bashforth scheme is seen in the green curve with a maximum at  $4\Delta x$ . The instability changes to a slight damping with (6.2.2) as indicated by the orange curve.

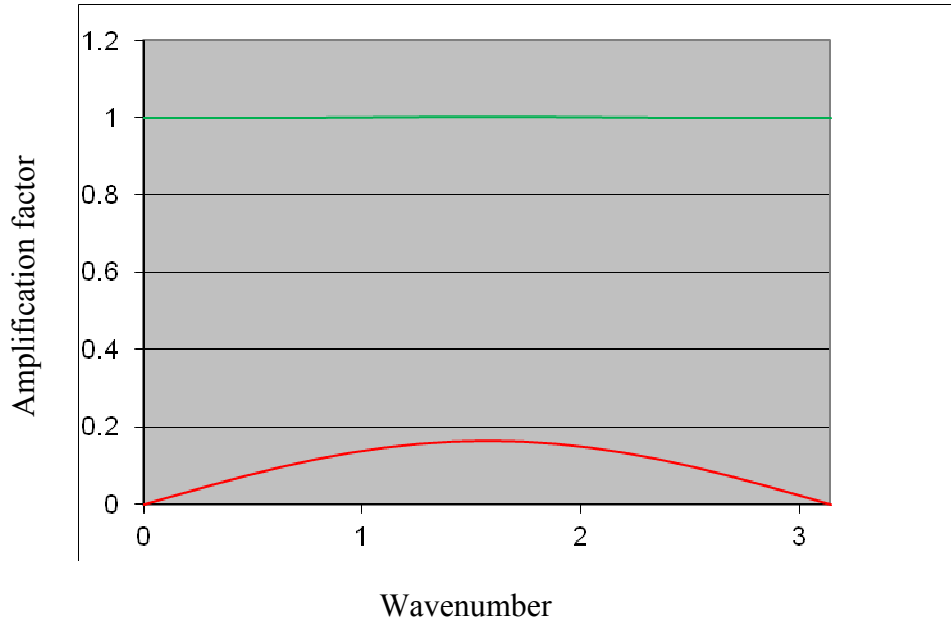


Figure 9. Amplification factors for the computational mode (red) and the physical mode (green) in the Adams-Bashforth time differencing scheme. Wave number in radians is shown along the abscissa with the  $4\Delta x$  wave in the center, the  $2\Delta x$  wave to the right and infinite wave number on the left.

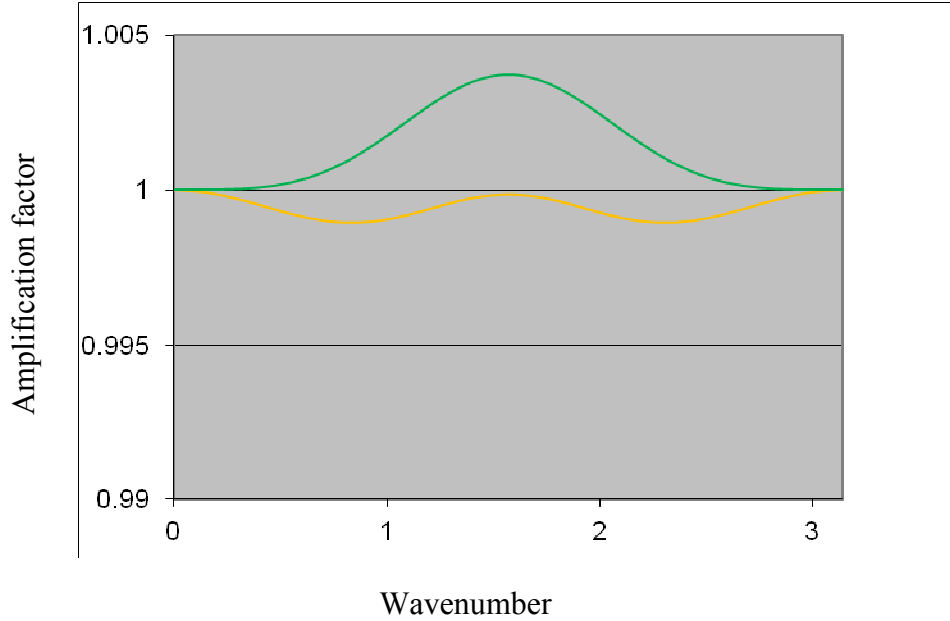


Figure 10. Same as figure 9 except the amplification factor scale near 1 is amplified. The green line shows the physical mode amplification factor for the Adams-Bashforth scheme (6.2.1), while the orange line corresponds to the modified scheme (6.2.2).

The instability of the Adams-Bashforth scheme is very weak, and experience shows that the scheme can be safely used with short time steps even without the stabilization by the off-centering. However, unstable schemes do not converge, and the stabilization is needed from the conceptual point of view. The damping of the computational mode (not shown) is unchanged. Note that the deviations of the amplification factors from unity shown in Figure 10 are about the maximum one would see for real data runs.

### 6.3 The Crank-Nicholson Differencing Scheme

The Crank-Nicholson scheme can be represented as

$$\frac{y^{n+1} - y^n}{\Delta t} = \frac{1}{2} \left[ f(y^{n+1}) + f(y^n) \right]. \quad (6.3.1)$$

This is an implicit scheme and so is always stable.

Implicit scheme is required for vertical advection because the fine spacing in vertical levels would control the time-step rather than the CFL condition for horizontally propagating fast waves. The Crank-Nicholson scheme is often off-centered by giving relative weight larger than 1/2 to the term  $f(y^{n+1})$  in order to make the scheme dissipative. However, as can be seen from the expression on the right hand side, the

values of  $y^n$  and  $y^{n+1}$  are given equal weights of  $1/2$ , and the scheme is centered in time.

#### 6.4 Time integration of the fast adjustment process

Time integration of terms involving the propagation of gravity waves is handled by a forward-backward process (Ames, 1968; Gadd, 1974; Janjic and Wiin-Nielsen, 1977; Janjic 1979; Mesinger, 1977). Using the shallow water equations to illustrate the process,

$$\frac{\partial u}{\partial t} = -g \frac{\partial h}{\partial x}, \quad \frac{\partial h}{\partial t} = -H \frac{\partial u}{\partial x}. \quad (6.4.1)$$

The mass tendency equation is advanced by a forward step

$$h^{n+1} = h^n - \Delta t H \frac{\partial u^n}{\partial x}, \quad (6.4.2)$$

and the velocity equation is then advanced with a backward step

$$u^{n+1} = u^n - \Delta t g \frac{\partial h^{n+1}}{\partial x}. \quad (6.4.3)$$

#### 6.5 Time integration of vertically propagating sound waves

The time integration of vertically propagating sound waves is hidden inside the implicit algorithm used to solve the full model equations. Details of this calculation are found in section 7.2.

## 7.0 TIME DISCRETE EQUATIONS

This section provides details of the time discrete equations that have been outlined in section 6.0. It is intended for readers who wish to work through the actual equations solved by the NMMB core. The basics are outlined above so readers not wishing this much detail can skip to the next section.

The numerical model described here uses the equations discussed in the section 2.0 cast into finite difference form. By using numerical methods that have been successful in hydrostatic models, it is expected that the model will behave well in the hydrostatic limit, i.e., when applied with resolutions that do not support significant vertical accelerations. For vanishing  $\varepsilon$ , the prognostic equations of the quasi-hydrostatic system of equations, i.e., (2.14), (2.24) and (2.10), together with the hydrostatic equation and the gas law, can be conveniently split into two energy conserving subsystems of prognostic equations (Janjic, 2003), i.e.,

$$\left(\frac{\partial \mathbf{v}}{\partial t}\right)_i = -\nabla_s \Phi - \alpha \nabla_s p + \mathbf{f} \mathbf{k} \times \mathbf{v}, \quad (7.1)$$

$$\left(\frac{\partial T}{\partial t}\right)_i = \frac{\alpha}{c_p} \left[ \mathbf{v} \cdot \nabla_s \pi - \int_0^s \nabla_{s'} \cdot \left( \mathbf{v} \frac{\partial \pi}{\partial s'} \right) ds' \right], \quad (7.2)$$

$$\left[ \frac{\partial}{\partial t} \left( \frac{\partial \pi}{\partial s} \right) \right]_s + \nabla_s \cdot \left( \mathbf{v} \frac{\partial \pi}{\partial s} \right) + \frac{\partial}{\partial s} \left( \dot{s} \frac{\partial \pi}{\partial s} \right) = 0, \quad (7.3)$$

$$\left(\frac{\partial \mathbf{v}}{\partial t}\right)_{ii} = -\mathbf{v} \cdot \nabla_s \mathbf{v} - \left( \dot{s} \frac{\partial \pi}{\partial s} \right) \frac{\partial \mathbf{v}}{\partial \pi}, \quad (7.4)$$

$$\left(\frac{\partial T}{\partial t}\right)_{ii} = -\mathbf{v} \cdot \nabla_s T - \left( \dot{s} \frac{\partial \pi}{\partial s} \right) \frac{\partial T}{\partial \pi}. \quad (7.5)$$

The time derivatives of the two subsystems are denoted by subscripts  $i$  and  $ii$ , respectively, and, as before, the subscript  $s$  indicates that the operator is applied along a constant vertical coordinate surface. As can be readily verified, the system (7.1)–(7.2), together with the continuity equation rewritten here in the form (7.3), conserves energy. The same applies to the system (7.4)–(7.5) combined with the continuity equation that links the two subsystems. Thus, these two subsystems are a natural choice for time splitting. However, note that large ratios between the advection time step, and the time step used for the remaining terms of the equations cannot be used in NWP applications. Since the wind speed can exceed  $100 \text{ ms}^{-1}$ , this ratio is restricted to 2 or 3 at most. Note, when using non-iterative schemes for advection terms in this situation, the discrete system without time splitting can be more computationally efficient and robust than a split scheme with iterative time differencing. This non-split approach is used in the NMMB.

## 7.1 Time differencing

The NMMB time differencing is presented in this section in order to illustrate how the extra terms appearing in the nonhydrostatic system are treated. The economical forward–backward scheme (Ames, 1969; Gadd, 1974; Janjic and Wiin-Nielsen, 1977; Janjic 1979) is used for the adjustment terms. Modified Adams-Bashforth scheme is used for the horizontal advection terms and the Coriolis force. Although the Adams-Bashforth scheme is slightly unstable, the instability is very weak so that the scheme can be safely used in practice. Nevertheless, for conceptual reasons, in the scheme used in NMMB the instability is removed by slight off-centering. After the off-centering, the modified scheme becomes weakly dissipative (Janjic et al., 2010). The Crank-Nicholson scheme is used for the vertical advection.

The superscripts  $n$  and  $n+1$  will be used to denote the time levels for all variables with the exception of the vertical velocity  $w$  which is defined at intermediate time levels indicated by superscripts  $n+1/2$  or  $n-1/2$ . The superscript  $n+1/2$  will be used also in the advection terms in order to indicate that centered in time schemes are used. Because the nonhydrostatic equations have been separated into two components, the subscript 1 will be used to indicate that a variable has been advanced in time only by the first component equation. For example, the solution of (2.24) starting from the time level  $n$  will be denoted by the subscript 1, since (2.23) remains to be solved before reaching the time level  $n+1$ .

The vertical velocity term in the hydrostatic  $s$  coordinate is computed integrating (2.10)

$$\left( \dot{s} \frac{\partial \pi}{\partial s} \right)_s^n = - \left( \frac{\partial \pi}{\partial t} \right)_s^n - \int_0^s \nabla_{s'} \cdot \left( \mathbf{v} \frac{\partial \pi}{\partial s'} \right)^n ds', \quad (7.1.1)$$

and the surface pressure tendency equation is

$$\mu^{n+1} = \mu^n - \Delta t \int_0^1 \nabla_{s'} \cdot \left( \mathbf{v} \frac{\partial \pi}{\partial s'} \right)^n ds'. \quad (7.1.2)$$

The first component of the nonhydrostatic pressure is computed using

$$p_1 = p^n + (1 + \varepsilon^n) \Delta t \left( \frac{\partial \pi}{\partial t} \right)^n. \quad (7.1.3)$$

Then

$$\omega_1 = \mathbf{v}^n \cdot \nabla_s p^n - (1 + \varepsilon^n) \int_0^s \nabla_{s'} \cdot \left( \mathbf{v} \frac{\partial \pi}{\partial s'} \right)^n ds', \quad (7.1.4)$$

and the first component of the thermodynamic equation is

$$T_1 = T^n + \frac{\Delta t}{c_p} \frac{RT^n}{p^n} \omega_1 - \Delta t \left[ \mathbf{v}^n \cdot \nabla_s T^{n+1/2} + \left( \dot{s} \frac{\partial \pi}{\partial s} \right)^n \frac{\partial T^{n+1/2}}{\partial \pi^n} \right]. \quad (7.1.5)$$

The superscript  $n + 1/2$  in the advection terms indicates symbolically that centered schemes are used.

The second component of the thermodynamic equation is

$$T^{n+1} - T_1 = \frac{1}{c_p} \frac{RT_1}{p_1} (p^{n+1} - p_1) . \quad (7.1.6)$$

The hypsometric equation yields the geopotential associated with the first component solutions for temperature and pressure,

$$\Phi_1 = \Phi_{sfc} + \int_s \frac{RT_1}{p_1} \left( \frac{\partial \pi}{\partial s'} \right)^{n+1} ds' , \quad (7.1.7)$$

and the second component equation yields

$$\Phi^{n+1} = \Phi_{sfc} + \int_s \frac{RT^{n+1}}{p^{n+1}} \left( \frac{\partial \pi}{\partial s'} \right)^{n+1} ds' . \quad (7.1.8)$$

The value of vertical velocity,  $w$ , associated with the first component solutions is obtained from

$$g w_1 = \frac{\Phi_1 - \Phi^n}{\Delta t} + \mathbf{v}^n \cdot \nabla_s \Phi_1 + \left( s \frac{\partial \pi}{\partial s} \right)^n \frac{\partial \Phi_1}{\partial \pi^n} . \quad (7.1.9)$$

Note that  $\Phi_1$  is an intermediate value of geopotential between  $\Phi^n$  and  $\Phi^{n+1}$ , i.e.,

$$\Phi^{n+1} - \Phi_1 \leq O(\Delta t) . \quad (7.1.10)$$

Therefore, using  $\Phi_1$  in the advection terms of (7.1.9) in order to compute  $w$  is a consistent numerical approximation. On the other hand, neglecting the contribution  $(\Phi^{n+1} - \Phi_1)/\Delta t$  would be wrong in view of (7.1.10). Thus,

$$w^{n+1/2} - w_1 = \frac{\Phi^{n+1} - \Phi_1}{g \Delta t} , \quad (7.1.11)$$

which must also satisfy the 3rd equation of motion,

$$w^{n+1/2} - g \Delta t \frac{\partial p^{n+1}}{\partial \pi^{n+1}} = w_1 - g \Delta t (1 + \varepsilon_1) . \quad (7.1.12)$$

The value of  $\varepsilon$  associated with the first component solutions is obtained from

$$g \varepsilon_1 = \frac{w_1 - w^{n-1/2}}{\Delta t} + \mathbf{v}^n \cdot \nabla_\sigma w_1 + \left( s \frac{\partial \pi}{\partial s} \right)^n \frac{\partial w_1}{\partial \pi^n} , \quad (7.1.13)$$

and the second component from

$$\varepsilon^{n+1} = \frac{\partial p^{n+1}}{\partial \pi^{n+1}} - 1. \quad (7.1.14)$$

Upon solution of the preceding equations for thermodynamic variables, the pressure gradient force at the time level  $n+1$  can be computed, and the horizontal equation of motion can be used to advance the wind components in time and thus complete the time step. The superscript  $n+1/2$  in the advection and Coriolis terms again indicates that centered schemes are used

$$\begin{aligned} \mathbf{v}^{n+1} = & \mathbf{v}^n - \Delta t [(1 + \varepsilon^{n+1}) \nabla_s \Phi^{n+1} + \alpha^{n+1} \nabla_s p^{n+1} - f \mathbf{k} \times \mathbf{v}^{n+1/2}] \\ & - \Delta t \left[ \mathbf{v}^n \cdot \nabla_{\sigma} \mathbf{v}^{n+1/2} + \left( \dot{s} \frac{\partial \pi}{\partial s} \right)^n \frac{\partial \mathbf{v}^{n+1/2}}{\partial \pi^n} \right]. \end{aligned} \quad (7.1.16)$$

Here, the specific volume  $\alpha^{n+1}$  is

$$\alpha^{n+1} = \frac{RT^{n+1}}{p^{n+1}}. \quad (7.1.16)$$

## 7.2 Solution of the coupled equations

Eqs. (7.1.6), (7.1.8), (7.1.11) and (7.1.12) are coupled equations. Their solution will be sought by eliminating all unknowns except  $p^{n+1}$  solving the resulting equation, and then back-substituting to obtain  $T^{n+1}$ ,  $\Phi^{n+1}$ ,  $w^{n+1/2}$  and  $\varepsilon^{n+1}$ . Namely, (7.1.7) and (7.1.8), together with (7.1.11) and (7.1.12), can be combined to give

$$R \int_s^1 \left( \frac{T^{n+1}}{p^{n+1}} - \frac{T_1}{p_1} \right) \left( \frac{\partial \pi}{\partial s'} \right)^{n+1} ds' = (g \Delta t)^2 \left[ \frac{1}{\left( \frac{\partial \pi}{\partial s'} \right)^{n+1}} \frac{\partial p^{n+1}}{\partial s} - (1 + \varepsilon_1) \right]. \quad (7.2.1)$$

Using (7.1.6) to eliminate  $T^{n+1}$ , (7.2.1) may be rewritten as

$$R(1 - \kappa) \int_s^1 T_1 \left( \frac{1}{p^{n+1}} - \frac{1}{p_1} \right) \left( \frac{\partial \pi}{\partial s'} \right)^{n+1} ds' = (g \Delta t)^2 \left[ \frac{1}{\left( \frac{\partial \pi}{\partial s'} \right)^{n+1}} \frac{\partial p^{n+1}}{\partial s} - (1 + \varepsilon_1) \right], \quad (7.2.2)$$

where  $\kappa \equiv R/c_p$ . Define a pressure  $p^*$  that satisfies the equation

$$\frac{1}{\left( \frac{\partial \pi}{\partial s'} \right)^{n+1}} \frac{\partial p^*}{\partial s} \equiv (1 + \varepsilon_1), \quad (7.2.3)$$

subject to the boundary condition  $p^* = \pi_T$  at  $s = 0$ . Upon inserting (7.2.3) into (7.2.2), one obtains

$$\frac{R(1-\kappa)}{g^2} \int_s^1 T_1 \left( \frac{1}{p^{n+1}} - \frac{1}{p_1} \right) \left( \frac{\partial \pi}{\partial s'} \right)^{n+1} ds' = \Delta t^2 \frac{1}{\left( \frac{\partial \pi}{\partial s'} \right)^{n+1}} \frac{\partial (p^{n+1} - p^*)}{\partial s}. \quad (7.2.4)$$

As pointed out in Janjic et al. (2001), after some manipulation, (7.2.4) can be solved iteratively. However, as will be shown here, it can be solved directly as well. Note that

$$p^{n+1} - p^* \leq O(\Delta t), \quad (7.2.5)$$

so that, from (7.2.4),

$$\frac{R(1-\kappa)}{g^2} \int_s^1 T_1 \left( \frac{1}{p^{n+1}} - \frac{1}{p_1} \right) \left( \frac{\partial \pi}{\partial s'} \right)^{n+1} ds' \leq O(\Delta t^3), \quad (7.2.6)$$

which illustrates how subtle the difference is between  $p_1$  and  $p^{n+1}$ . In order to visualize more clearly the procedure used to solve (7.2.4) for  $p^{n+1}$  directly, it is convenient to consider the vertically discretized form of (7.2.4). Let each of the  $lm$  model layers be denoted by index  $l$  increasing from top down, and let the corresponding layer interfaces be denoted by half-indices  $l-1/2$  and  $l+1/2$ . In addition, let temperature be defined at mid-layers, and pressure variables at layer interfaces. Then, using the simplest vertical two-point averaging and differencing operators denoted, respectively, by an overbar and symbol  $\Delta$ , a discrete version of (7.2.4) can be written as

$$\frac{R(1-\kappa)}{(g\Delta t)^2} \sum_{k=l}^{k=lm} T_{1l} \left( \frac{\overline{p_{1l}} - \overline{p^{n+1}_l}}{\overline{p^{n+1}_l} \overline{p_{1l}}} \right) \Delta \pi_l^{n+1} = \frac{\Delta p_l^{n+1} - \Delta p_l^*}{\Delta \pi_l^{n+1}}. \quad (7.2.7)$$

Define a pressure variable

$$p_{2l+1/2} = p_{1l+1/2} + \text{const}(p_{2l-1/2} + \varepsilon_1 \Delta \pi_l - p_{1l+1/2}), \quad (7.2.8)$$

by correcting  $p_1$  using the latest preliminary value of  $\varepsilon_1$ . Note that when  $\text{const} = 0$ ,  $p_{2l+1/2} = p_{1l+1/2}$ , and when  $\text{const} = 1$ ,  $p_{2l+1/2} = p_{1l+1/2}^*$ . Then, taking into account (7.2.6), (7.2.7) can be rewritten as

$$\frac{R(1-\kappa)}{(g\Delta t)^2} \sum_{k=l}^{k=lm} \frac{T_{1l}}{\overline{p_{2l}^2}} \left( \frac{\overline{p_{1l}} - \overline{p^{n+1}_l}}{\overline{p_{1l}} \overline{p^{n+1}_l}} \right) \Delta \pi_l^{n+1} = \frac{\Delta p_l^{n+1} - \Delta p_l^*}{\Delta \pi_l^{n+1}}. \quad (7.2.9)$$

In practice, the correction weight  $\text{const}$  in (7.2.8) is 0.35 (for historical reasons) but noticeable impact on the solution is not detected when varying this parameter between 0 and 1. Subtracting from (7.2.9) analogous expression defined on the level  $l+1$ , one obtains

$$\frac{R(1-\kappa)}{(g\Delta t)^2} \frac{T_{1l}}{\bar{p}_{2l}^2} \left( \frac{-\pi}{p_{1l}} - \overline{p^{n+1}} \frac{\pi}{l} \right) \Delta\pi_l^{n+1} = \frac{\Delta p_l^{n+1} - \Delta p_l^*}{\Delta\pi_l^{n+1}} - \frac{\Delta p_{l+1}^{n+1} - \Delta p_{l+1}^*}{\Delta\pi_{l+1}^{n+1}}. \quad (7.2.10)$$

Replacing averaging and differencing operators applied to  $p^{n+1}$  by explicit algebraic expressions, (7.2.10) can be rewritten as

$$\begin{aligned} \frac{R(1-\kappa)}{(g\Delta t)^2} \frac{T_{1l}}{\bar{p}_{2l}^2} \left[ \frac{-\pi}{p_{1l}} - \frac{1}{2} (p_{l-1/2}^{n+1} + p_{l+1/2}^{n+1}) \right] \Delta\pi_l^{n+1} = \\ \frac{p_{l+1/2}^{n+1} - p_{l-1/2}^{n+1} - \Delta p_l^*}{\Delta\pi_l^{n+1}} - \frac{p_{l+3/2}^{n+1} - p_{l+1/2}^{n+1} - \Delta p_{l+1}^*}{\Delta\pi_{l+1}^{n+1}}. \end{aligned} \quad (7.2.11)$$

Inspection of (7.2.11) reveals that the unknown  $p^{n+1}$  appears at three consecutive layer interfaces,  $l-1/2$ ,  $l+1/2$  and  $l+3/2$ . Thus (7.2.11) is a tri-diagonal system which can be solved with suitably chosen boundary conditions. A solution without the approximation (7.2.8) can be obtained by iterating (7.2.11), but that appears unnecessary in the light of (7.2.6).

In order to address the problem of specification of boundary conditions for (7.2.11), consider a horizontally homogenous atmosphere at rest and in hydrostatic equilibrium. Let the equations be linearized around such a basic state. Also, consider only the solutions that preserve horizontal homogeneity. As can be readily verified, the requirement for horizontal homogeneity eliminates all motions that belong to the first part of the time stepping procedure. In other words, the intermediate solutions denoted by subscript 1 will coincide with the initial values denoted by superscript  $n$ . The only solutions left will be those described by the linearized set of coupled equations leading to (7.2.4). In particular, from (7.1.6)

$$(T^{n+1} - T_0) - (T^n - T_0) = \frac{1}{c_p} \frac{RT_0}{\pi_0} \left[ (p^{n+1} - \pi_0) - (p^n - \pi_0) \right], \quad (7.2.12)$$

and after differentiation of (7.1.8) with respect to  $s$ , linearization and rearrangement,

$$g \frac{\partial(z^{n+1} - z_0)}{\partial\pi_0} = -\frac{R(T^{n+1} - T_0)}{\pi_0} + \frac{RT_0}{\pi_0} \frac{(p^{n+1} - \pi_0)}{\pi_0}. \quad (7.2.13)$$

Here,  $z$  is the height and the subscript 0 denotes the basic state variables. From (7.1.11) and (7.1.12)

$$w^{n+1/2} = \frac{(z^{n+1} - z_0) - (z^n - z_0)}{\Delta t} \quad (7.2.14)$$

$$\frac{w^{n+1/2} - w^{n-1/2}}{\Delta t} = g \frac{\partial(p^{n+1} - \pi_0)}{\partial\pi_0}. \quad (7.2.15)$$

Introducing primes to denote the deviations from the basic state, applying the simplest time differencing operator to (7.2.13) and using (7.2.14),

$$g \frac{\partial w^{n+1/2}}{\partial \pi_0} = - \frac{R(T'^{n+1} - T'^n)}{\pi_0 \Delta t} + \frac{RT_0}{\pi_0} \frac{(p'^{n+1} - p'^n)}{\pi_0 \Delta t}. \quad (7.2.16)$$

Using (7.2.12) to eliminate  $T'$  in (7.2.16), and differencing in time the resulting equation, one obtains

$$g \frac{\partial}{\partial \pi_0} \frac{w^{n+1/2} - w^{n-1/2}}{\Delta t} = \frac{c_v}{c_p} \frac{RT_0}{\pi_0^2} \frac{(p'^{n+1} - 2p'^n + p'^{n-1})}{\Delta t^2}. \quad (7.2.17)$$

On the other hand, differentiating (7.2.15) with respect to  $\pi_0$ ,

$$\frac{\partial}{\partial \pi_0} \frac{w^{n+1/2} - w^{n-1/2}}{\Delta t} = g \frac{\partial^2 p'^{n+1}}{\partial \pi_0^2}. \quad (7.2.18)$$

Thus, combining (7.2.17) and (7.2.18), and taking into account that the basic state is hydrostatic,

$$\frac{p'^{n+1} - 2p'^n + p'^{n-1}}{\Delta t^2} = \frac{c_p}{c_v} RT_0 \frac{\partial^2 p'^{n+1}}{\partial z_0^2}. \quad (7.2.19)$$

The equation for vertically propagating sound waves is readily recognized in (7.2.19), although finite differencing is used instead of differentiation with respect to time on the left-hand side.

Now that the physical nature of the processes involved in the second part of the integration procedure have been revealed, the question of the boundary conditions for (7.2.4) can be readdressed. It appears natural to keep the upper end of the oscillator described by (7.2.19) fixed, and the lower end free. Thus,  $p = \pi$  is set at  $s = 0$ , and  $\partial(p'^{n+1} - p'^n)/\partial s = 0$  is set at  $s = 1$ . Such an upper boundary condition is perfectly justified for vanishing pressure at the top of the atmosphere of the model.

### 7.3 Time stepping and time step

Figure 11 illustrates the time stepping process in NMMB. Here the fundamental time step  $\Delta t = t_2 - t_1$  is the time step for the dynamical process (shown by the short, thin arrows). The time step for passive substance advection is usually  $2\Delta t$  as illustrated by the longer, wide arrows. The physics is called even less frequently in order to save computational time. The longest interval between two consecutive calls is used for radiation which is the most expensive single component of a comprehensive physical package.

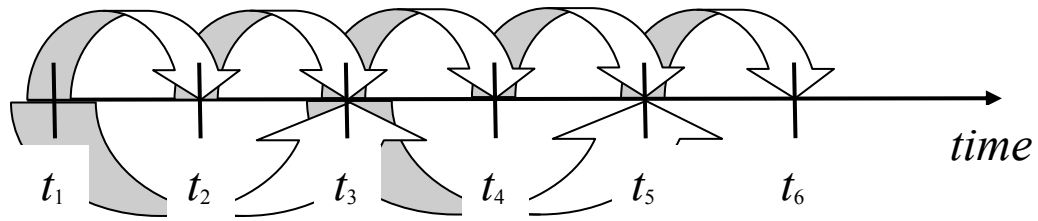


*Figure 11. Time stepping process in the NMMB.*

As a general rule of thumb, the adjustment time step  $\Delta t$  in seconds can be taken as 2.25 times the grid spacing in kilometers. For higher resolution model runs made without parameterized convection, a  $\Delta t$  in seconds of about 1.9 to 2.0 times the grid spacing may be more appropriate.

## 8.0 SPATIAL DISCRETE EQUATIONS

The general philosophy for the spatial discretization of the model equations includes the following:

- Conserve energy and enstrophy in case of nondivergent flow in order to control nonlinear energy cascade and, thus, reduce to the extent possible the generation of noise by the nonlinear terms.
- Use consistent formulations and order of accuracy for advection and divergence operators.
- Use energy conserving form of the omega-alpha term that provides consistent transformations between the kinetic and potential energy.
- Conserve a number of first order and quadratic quantities, such as momentum and other advected quantities.
- Reproduce in finite-difference operators certain properties of differential operators.
- Minimize the errors due to presence of topography.
- Avoid using numerical filters wherever possible.

### 8.1 Mass divergence and hydrostatic continuity equation

Consider the fluxes in the directions of the four coordinate axes connecting  $h$  points as shown in Figure 12.

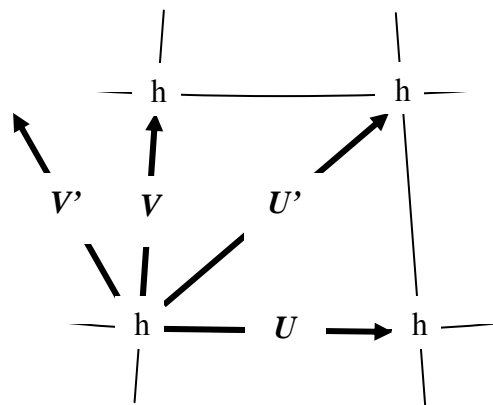


Figure 12. Schematic representation of mass fluxes in between  $h$  points on the  $B$  grid.

$$\begin{aligned}
U\Delta y &= \overline{\Delta\pi}^x \bar{u}^y \Delta y \\
V\Delta x &= \overline{\Delta\pi}^y \bar{v}^x \Delta x \\
U'd &= \overline{\Delta\pi}^{x'} (u\Delta y + v\Delta x) \\
V'd &= \overline{\Delta\pi}^{y'} (-u\Delta y + v\Delta x).
\end{aligned} \tag{8.1.1}$$

Here  $\Delta x$ ,  $\Delta y$  and  $d$  are as defined in figure 2. The mass divergence term is then defined as

$$D = - \left[ \frac{2}{3} \frac{\Delta_x(U\Delta y) + \Delta_y(V\Delta x)}{\Delta x \Delta y} + \frac{1}{3} \frac{\Delta_x'(U'd) + \Delta_y'(V'd)}{2\Delta x \Delta y} \right]. \tag{8.1.2}$$

Note that the ‘‘isotropic’’ four-flux form of the Arakawa Jacobian is used in the definition (8.1.2).

Vertically discretized hydrostatic mass continuity equation at a mid-layer level  $l$  can be written as

$$\left[ \delta_s \left( \frac{\partial \pi}{\partial t} \right) \right]_l + \nabla \cdot (\mathbf{v} \delta_s \pi)_l + [\delta_s (\dot{s} \delta_s \pi)]_l = 0, \tag{8.1.3}$$

or

$$\sum_{k=1}^l \nabla \cdot (\mathbf{v} \delta_s \pi)_k \Delta s_k = - \left( \frac{\partial \pi}{\partial t} \right)_{l+1/2} - (\dot{s} \delta_s \pi)_{l+1/2}, \tag{8.1.4}$$

In (8.1.4), the approximation

$$\nabla \cdot (\mathbf{v} \delta_s \pi)_k \Delta s_k = \nabla \cdot (\mathbf{v} \Delta_s \pi)_k = -D_k, \tag{8.1.5}$$

is used for horizontal discretization.

## 8.2 Hydrostatic pressure gradient force and the omega-alpha term

The hydrostatic pressure gradient force has the form

$$\begin{aligned}
\overline{\Delta\pi}^u \frac{\partial u}{\partial t} &= - \left( \frac{2}{3} \frac{\overline{\Delta\pi}^x \Delta_x \overline{\Phi}^s}{\Delta x} + \frac{1}{3} \frac{\overline{\Delta\pi}^{x'} \Delta_x' \overline{\Phi}^s - \overline{\Delta\pi}^{y'} \Delta_y' \overline{\Phi}^s}{2\Delta x} \right) \\
&\quad - \left[ \frac{2}{3} \frac{\overline{RT}_v}{\overline{\pi}^s} \Delta\pi \frac{\Delta_x \overline{\pi}^s}{\Delta x} + \frac{1}{3} \left( \frac{\overline{RT}_v}{\overline{\pi}^s} \Delta\pi \frac{\Delta_x' \overline{\pi}^s}{2\Delta x} - \frac{\overline{RT}_v}{\overline{\pi}^s} \Delta\pi \frac{\Delta_y' \overline{\pi}^s}{2\Delta x} \right) \right],
\end{aligned} \tag{8.2.1}$$

$$\begin{aligned} \overline{\Delta\pi}^v \frac{\partial v}{\partial t} = & - \left( \frac{2}{3} \frac{\overline{\Delta\pi}^y \Delta_y \overline{\Phi}^s}{\Delta y} + \frac{1}{3} \frac{\overline{\Delta\pi}^{x'} \Delta_x \overline{\Phi}^s + \overline{\Delta\pi}^{y'} \Delta_y \overline{\Phi}^s}{2\Delta y} \right) \\ & - \left[ \frac{2}{3} \frac{\overline{RT_v}^y \Delta_y \overline{\pi}^s}{\overline{\pi}^s \Delta y} + \frac{1}{3} \left( \frac{\overline{RT_v}^{x'} \Delta_x \overline{\pi}^s}{\overline{\pi}^s 2\Delta y} + \frac{\overline{RT_v}^{y'} \Delta_y \overline{\pi}^s}{\overline{\pi}^s 2\Delta y} \right) \right] \end{aligned} \quad (8.2.2)$$

Consider the 2/3 component of the first pressure gradient force term multiplied by corresponding velocity components

$$\overline{\Delta\pi}^u u \frac{\partial u}{\partial t} \Delta x \Delta y = -u \frac{\overline{\Delta\pi}^x \Delta_x \overline{\Phi}^s}{\Delta x} \Delta x \Delta y, \quad (8.2.3)$$

$$\overline{\Delta\pi}^v v \frac{\partial v}{\partial t} \Delta x \Delta y = -v \frac{\overline{\Delta\pi}^y \Delta_y \overline{\Phi}^s}{\Delta y} \Delta x \Delta y. \quad (8.2.4)$$

Summing up formulas (8.2.3) and (8.2.4)

$$\overline{\Delta\pi}^u u \frac{\partial u}{\partial t} \Delta x \Delta y + \overline{\Delta\pi}^v v \frac{\partial v}{\partial t} \Delta x \Delta y = -u \Delta y \frac{\overline{\Delta\pi}^x \Delta_x \overline{\Phi}^s}{\Delta x} - v \Delta x \frac{\overline{\Delta\pi}^y \Delta_y \overline{\Phi}^s}{\Delta y}, \quad (8.2.5)$$

and extending the summation over the entire integration domain, one obtains

$$\sum \left( \overline{\Delta\pi}^u u \frac{\partial u}{\partial t} + \overline{\Delta\pi}^v v \frac{\partial v}{\partial t} \right) \Delta x \Delta y = - \sum u \Delta y \frac{\overline{\Delta\pi}^x \Delta_x \overline{\Phi}^s}{\Delta x} + v \Delta x \frac{\overline{\Delta\pi}^y \Delta_y \overline{\Phi}^s}{\Delta y}. \quad (8.2.6)$$

If the summation is performed over a closed domain, or a domain with cyclic boundary conditions, (8.2.6) can be rewritten as

$$\sum \left( \overline{\Delta\pi}^u u \frac{\partial u}{\partial t} + \overline{\Delta\pi}^v v \frac{\partial v}{\partial t} \right) \Delta x \Delta y = - \sum \overline{\Delta\pi}^x \overline{u}^y \Delta y \Delta_x \overline{\Phi}^s + \overline{\Delta\pi}^y \overline{v}^x \Delta x \Delta_y \overline{\Phi}^s, \quad (8.2.7)$$

or,

$$\sum \left( \overline{\Delta\pi}^u u \frac{\partial u}{\partial t} + \overline{\Delta\pi}^v v \frac{\partial v}{\partial t} \right) \Delta x \Delta y = \sum \overline{\Phi}^s \left[ \Delta_x \left( \overline{\Delta\pi}^x \overline{u}^y \Delta y \right) + \Delta_y \left( \overline{\Delta\pi}^y \overline{v}^x \Delta x \right) \right], \quad (8.2.8)$$

and finally, as

$$\sum \left( \overline{\Delta\pi}^u u \frac{\partial u}{\partial t} + \overline{\Delta\pi}^v v \frac{\partial v}{\partial t} \right) \Delta x \Delta y = \sum \overline{\Phi}^s \left[ \Delta_x (U \Delta y) + \Delta_y (V \Delta x) \right]. \quad (8.2.9)$$

Following an analogous procedure for the “diagonal” 1/3 contribution to the first term of the pressure gradient force

$$\overline{\Delta\pi}^u \frac{\partial u}{\partial t} = -\frac{\overline{\Delta\pi}^{x'} \Delta_x \overline{\Phi}^s - \overline{\Delta\pi}^{y'} \Delta_y \overline{\Phi}^s}{2\Delta x}, \quad (8.2.10)$$

$$\overline{\Delta\pi}^v \frac{\partial v}{\partial t} = -\frac{\overline{\Delta\pi}^{x'} \Delta_x \overline{\Phi}^s + \overline{\Delta\pi}^{y'} \Delta_y \overline{\Phi}^s}{2\Delta y}, \quad (8.2.11)$$

one obtains

$$\overline{\Delta\pi}^u u \frac{\partial u}{\partial t} \Delta x \Delta y = -u \frac{\overline{\Delta\pi}^{x'} \Delta_x \overline{\Phi}^s - \overline{\Delta\pi}^{y'} \Delta_y \overline{\Phi}^s}{2\Delta x} \Delta x \Delta y. \quad (8.2.12)$$

$$\overline{\Delta\pi}^v v \frac{\partial v}{\partial t} \Delta x \Delta y = -v \frac{\overline{\Delta\pi}^{x'} \Delta_x \overline{\Phi}^s + \overline{\Delta\pi}^{y'} \Delta_y \overline{\Phi}^s}{2\Delta y} \Delta x \Delta y, \quad (8.2.13)$$

or after rearrangement,

$$\overline{\Delta\pi}^u u \frac{\partial u}{\partial t} \Delta x \Delta y = -u \frac{1}{2} \left( \overline{\Delta\pi}^{x'} \Delta_x \overline{\Phi}^s - \overline{\Delta\pi}^{y'} \Delta_y \overline{\Phi}^s \right) \Delta y, \quad (8.2.14)$$

$$\overline{\Delta\pi}^v v \frac{\partial v}{\partial t} \Delta x \Delta y = -v \frac{1}{2} \left( \overline{\Delta\pi}^{x'} \Delta_x \overline{\Phi}^s + \overline{\Delta\pi}^{y'} \Delta_y \overline{\Phi}^s \right) \Delta x. \quad (8.2.15)$$

Summing up formulas (8.2.14 and 8.2.15)

$$\begin{aligned} \overline{\Delta\pi}^u u \frac{\partial u}{\partial t} \Delta x \Delta y + \overline{\Delta\pi}^v v \frac{\partial v}{\partial t} \Delta x \Delta y = \\ -\frac{1}{2} \left[ u \left( \overline{\Delta\pi}^{x'} \Delta_x \overline{\Phi}^s - \overline{\Delta\pi}^{y'} \Delta_y \overline{\Phi}^s \right) \Delta y + v \left( \overline{\Delta\pi}^{x'} \Delta_x \overline{\Phi}^s + \overline{\Delta\pi}^{y'} \Delta_y \overline{\Phi}^s \right) \Delta x \right], \end{aligned} \quad (8.2.16)$$

and rearranging,

$$\begin{aligned} \left( \overline{\Delta\pi}^u u \frac{\partial u}{\partial t} + \overline{\Delta\pi}^v v \frac{\partial v}{\partial t} \right) \Delta x \Delta y = \\ -\frac{1}{2} \left[ \overline{\Delta\pi}^{x'} (u \Delta y + v \Delta x) \Delta_x \overline{\Phi}^s + \overline{\Delta\pi}^{y'} (-u \Delta y + v \Delta x) \Delta_y \overline{\Phi}^s \right]. \end{aligned} \quad (8.2.17)$$

Summing (8.2.2) over the entire closed integration domain, or a domain with cyclic boundary conditions

$$\begin{aligned} \sum \left( \overline{\Delta\pi}^u u \frac{\partial u}{\partial t} + \overline{\Delta\pi}^v v \frac{\partial v}{\partial t} \right) \Delta x \Delta y = \\ -\sum \frac{1}{2} \left[ \overline{\Delta\pi}^{x'} (u \Delta y + v \Delta x) \Delta_x \overline{\Phi}^s + \overline{\Delta\pi}^{y'} (-u \Delta y + v \Delta x) \Delta_y \overline{\Phi}^s \right], \end{aligned} \quad (8.2.18)$$

and rearranging taking into account the definitions of the “diagonal” fluxes (8.1.1),

$$\sum \left( \overline{\Delta\pi^u} u \frac{\partial u}{\partial t} + \overline{\Delta\pi^v} v \frac{\partial v}{\partial t} \right) \Delta x \Delta y = - \sum \frac{1}{2} \left( U' d \Delta_x \overline{\Phi^s} + V' d \Delta_y \overline{\Phi^s} \right), \quad (8.2.19)$$

one finally gets

$$\sum \left( \overline{\Delta\pi^u} u \frac{\partial u}{\partial t} + \overline{\Delta\pi^v} v \frac{\partial v}{\partial t} \right) \Delta x \Delta y = \sum \overline{\Phi^s} \frac{1}{2} \left[ \Delta_x (U' d) + \Delta_y (V' d) \right]. \quad (8.2.20)$$

Combining (8.2.9) and (8.2.20),

$$\sum \left( \overline{\Delta\pi^u} u \frac{\partial u}{\partial t} + \overline{\Delta\pi^v} v \frac{\partial v}{\partial t} \right) \Delta x \Delta y = \sum \overline{\Phi^s} \left\{ \frac{2}{3} \left[ \Delta_x (U \Delta y) + \Delta_y (V \Delta x) \right] + \frac{1}{3} \frac{1}{2} \left[ \Delta_x (U' d) + \Delta_y (V' d) \right] \right\} \quad (8.2.36)$$

and taking into account the definition of the divergence (8.1.2) one may write

$$\sum \left( \overline{\Delta\pi^u} u \frac{\partial u}{\partial t} + \overline{\Delta\pi^v} v \frac{\partial v}{\partial t} \right) \Delta x \Delta y = - \sum \overline{\Phi^s} D \Delta x \Delta y. \quad (8.2.37)$$

Since there are no special requirements on  $\overline{\Delta\pi^u}$  and  $\overline{\Delta\pi^v}$ ,

$$\overline{\Delta\pi^u} = \overline{\Delta\pi^v} = \overline{\Delta\pi^{xy}}, \quad (8.2.38)$$

is chosen as the most natural choice.

On the right hand side of (8.2.37) there are no horizontal differencing operators, so that only vertical summation at a grid point will be considered. Note that at a mid-layer level  $l$

$$\Delta_s \left( \Phi \sum_{1/2}^{l+1/2} D \right)_l = \overline{\Phi^s} D_l + (\Delta_s \Phi)_l \frac{1}{2} \left( \sum_{1/2}^{l-1/2} D + \sum_{1/2}^{l+1/2} D \right) \quad (8.2.39)$$

and, therefore,

$$\overline{\Phi^s} D_l = \Delta_s \left( \Phi \sum_{1/2}^{l+1/2} D \right)_l - (\Delta_s \Phi)_l \frac{1}{2} \left( \sum_{1/2}^{l-1/2} D + \sum_{1/2}^{l+1/2} D \right) \quad (8.2.40)$$

and

$$\overline{\Phi^s} D_l = \Delta_s \left( \Phi \sum_{1/2}^{l+1/2} D \right)_l - (\Delta_s \Phi)_l \frac{1}{2} \left( \sum_{1/2}^{l-1/2} D + \sum_{1/2}^{l+1/2} D \right). \quad (8.2.41)$$

Taking into account the mass continuity equation (8.1.4), the summation in the vertical of the first term on the right hand side of (8.2.41) yields

$$\sum_l \Delta_s \left( \Phi \sum_{1/2}^{l+1/2} D \right)_l = \Phi_{sfc} \frac{\partial \mu}{\partial t}, \quad (8.2.42)$$

and the second term can be rewritten as

$$(\Delta_s \Phi)_l \frac{1}{2} \left( \sum_{k=1/2}^{l-1/2} D_k + \sum_{k=1/2}^{l+1/2} D_k \right) = \left( \frac{RT_v}{\pi^s} \right)_l \left[ \frac{\partial \pi}{\partial t} + (\dot{s} \delta_s \pi) \right]_l^s \Delta \pi_l. \quad (8.2.43)$$

Thus, the second term defines the consistent finite difference approximation of the contributions of the local time change and the vertical advection of hydrostatic pressure in the omega-alpha term of the thermodynamic equation.

As can be verified by direct inspection, the consistent finite difference approximation of the contribution of the horizontal advection of hydrostatic pressure has the form

$$\frac{1}{\Delta \pi \Delta x \Delta y} \left[ \frac{2}{3} \frac{RT^x}{\pi^s} (U \Delta y) \Delta_x \bar{\pi}^s + \frac{RT^y}{\pi^s} (V \Delta x) \Delta_y \bar{\pi}^s + \frac{1}{3} \frac{1}{2} \left( \frac{RT^{x'}}{\pi^s} (U' d) \Delta_{x'} \bar{\pi}^s + \frac{RT^{y'}}{\pi^s} (V' d) \Delta_{y'} \bar{\pi}^s \right) \right] \quad (8.2.44)$$

Namely, in case of summation of (8.2.44) over all grid box volumes, the topmost averaging operators can be dropped leaving behind contributions of the second term of the pressure gradient force to the kinetic energy generation at the  $\mathbf{v}$  points.

### 8.3 Horizontal advection of momentum

Consider the four stream function points shown in Figure 13 in an orthogonal curvilinear coordinate system. Using the C grid energy and enstrophy conserving scheme, the advection of the nondivergent meridional wind component defined between the points 1 and 2 in the figure takes the form (c.f. Janjic, 1984a, 1984b)

$$\frac{\partial v_{12}}{\partial t} \Rightarrow -J_A(\bar{\psi}^{12}, v_{12}) = -J_A\left(\frac{\psi_1 + \psi_2}{2}, \frac{\psi_2 - \psi_1}{\Delta x_{12}}\right). \quad (8.3.1)$$

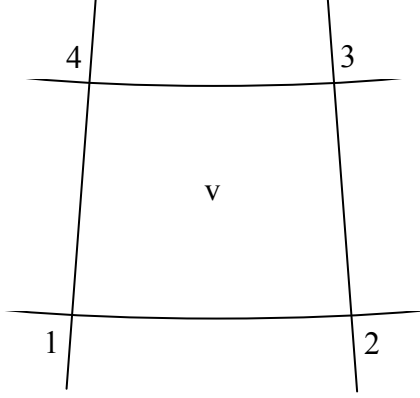


Figure 13. Stencil of stream function points used to derive analog of the C grid energy and enstrophy conserving scheme on the B grid.

Here the symbol  $\Rightarrow$  represents approximation by finite differences. In case of Cartesian, or a cylindrical coordinate system, we can write

$$-J_A\left(\frac{\psi_1 + \psi_2}{2}, \frac{\psi_2 - \psi_1}{\Delta x_{12}}\right) = -\frac{1}{2\Delta x_{12}} J_A(\psi_1 + \psi_2, \psi_2 - \psi_1). \quad (8.3.2)$$

In case of more general orthogonal curvilinear systems this formula holds only approximately, but with generally sufficient accuracy. Thus, using (8.3.2) and taking into account the properties of the Arakawa Jacobian (Janjic, 1984a, 1984b) we have

$$\frac{\partial v_{12}}{\partial t} \Rightarrow -\frac{1}{2\Delta x_{12}} J_A(\psi_1, \psi_2) + \frac{1}{2\Delta x_{12}} J_A(\psi_2, \psi_1) = -\frac{1}{\Delta x_{12}} J_A(\psi_1, \psi_2) = \frac{1}{\Delta x_{12}} J_A(\psi_2, \psi_1) \quad (8.3.3)$$

The equation (8.3.3) can be rewritten as

$$\Delta A_{12} \Delta x_{12} \frac{\partial v_{12}}{\partial t} \Rightarrow -\Delta x_{12} \Delta A_{12} J_A(\psi_2, -\psi_1), \quad (8.3.4)$$

or in a more compact form

$$\Delta A_{12} \Delta x_{12} \frac{\partial v_{12}}{\partial t} \Rightarrow -Z_A(\psi_2, -\psi_1) = -Z_A(\psi_1, \psi_2), \quad (8.3.5)$$

where  $Z_A$  is a new operator obtained by multiplying the Arakawa Jacobian by its grid box area and the grid distance used to define the velocity component at the grid point considered.

Analogously,

$$\Delta A_{23} \Delta y_{23} \frac{\partial u_{23}}{\partial t} \Rightarrow -Z_A(\psi_2, -\psi_3) = -Z_A(\psi_3, \psi_2), \quad (8.3.6)$$

$$\Delta A_{34} \Delta x_{34} \frac{\partial v_{34}}{\partial t} \Rightarrow -Z_A(\psi_4, \psi_3) = -Z_A(\psi_3, -\psi_4), \quad (8.3.7)$$

$$\Delta A_{41} \Delta y_{41} \frac{\partial u_{41}}{\partial t} \Rightarrow -Z_A(\psi_4, \psi_1) = -Z_A(\psi_1, -\psi_4). \quad (8.3.8)$$

Subtracting (8.3.6) from (8.3.5), and (8.3.8) from (8.3.7), yields

$$\Delta A_{12} \Delta x_{12} \frac{\partial v_{12}}{\partial t} - \Delta A_{23} \Delta y_{23} \frac{\partial u_{23}}{\partial t} \Rightarrow -Z_A(\psi_2, \psi_3 - \psi_1), \quad (8.3.9)$$

$$\Delta A_{34} \Delta x_{34} \frac{\partial v_{34}}{\partial t} - \Delta A_{41} \Delta y_{41} \frac{\partial u_{41}}{\partial t} \Rightarrow -Z_A(\psi_4, \psi_3 - \psi_1). \quad (8.3.10)$$

Summing up (8.3.9) and (8.3.10) we obtain

$$-\Delta A_{23} \Delta y_{23} \frac{\partial u_{23}}{\partial t} - \Delta A_{41} \Delta y_{41} \frac{\partial u_{41}}{\partial t} + \Delta A_{12} \Delta x_{12} \frac{\partial v_{12}}{\partial t} + \Delta A_{34} \Delta x_{34} \frac{\partial v_{34}}{\partial t} \Rightarrow -2Z_A\left(\frac{\psi_2 + \psi_4}{2}, \psi_3 - \psi_1\right) \quad (8.3.11)$$

On the other hand, summing up (8.3.5) and (8.3.8), and (8.3.6) and (8.3.7),

$$\Delta A_{12} \Delta x_{12} \frac{\partial v_{12}}{\partial t} + \Delta A_{41} \Delta y_{41} \frac{\partial u_{41}}{\partial t} \Rightarrow -Z_A(\psi_1, \psi_2 - \psi_4), \quad (8.3.12)$$

$$\Delta A_{23} \Delta y_{23} \frac{\partial u_{23}}{\partial t} + \Delta A_{34} \Delta x_{34} \frac{\partial v_{34}}{\partial t} \Rightarrow -Z_A(\psi_3, \psi_2 - \psi_4), \quad (8.3.13)$$

so that the sum of (8.3.12) and (8.3.13) takes the form

$$\Delta A_{23} \Delta y_{23} \frac{\partial u_{23}}{\partial t} + \Delta A_{41} \Delta y_{41} \frac{\partial u_{41}}{\partial t} + \Delta A_{12} \Delta x_{12} \frac{\partial v_{12}}{\partial t} + \Delta A_{34} \Delta x_{34} \frac{\partial v_{34}}{\partial t} \Rightarrow -2Z_A\left(\frac{\psi_1 + \psi_3}{2}, \psi_2 - \psi_4\right) \quad (8.3.14)$$

Subtracting (8.3.11) from (8.3.14), and summing up (8.3.11) and (8.3.14), we obtain, respectively,

$$\Delta A_{23} \Delta y_{23} \frac{\partial u_{23}}{\partial t} + \Delta A_{41} \Delta y_{41} \frac{\partial u_{41}}{\partial t} \Rightarrow Z_A\left(\frac{\psi_2 + \psi_4}{2}, \psi_3 - \psi_1\right) - Z_A\left(\frac{\psi_1 + \psi_3}{2}, \psi_2 - \psi_4\right), \quad (8.3.14)$$

$$\Delta A_{12} \Delta x_{12} \frac{\partial v_{12}}{\partial t} + \Delta A_{34} \Delta x_{34} \frac{\partial v_{34}}{\partial t} \Rightarrow -Z_A\left(\frac{\psi_2 + \psi_4}{2}, \psi_3 - \psi_1\right) - Z_A\left(\frac{\psi_1 + \psi_3}{2}, \psi_2 - \psi_4\right). \quad (8.3.15)$$

However, for a B grid scheme, we have to express the terms on the right hand sides of (8.3.14) and (8.3.15) in terms of the B grid nondivergent wind components. From the definition of the nondivergent wind

$$u = -\delta_y \bar{\psi}^x, \quad v = \delta_x \bar{\psi}^y,$$

we find that

$$\psi_3 - \psi_1 = -u\Delta y + v\Delta x \quad \text{and} \quad \psi_2 - \psi_4 = u\Delta y + v\Delta x. \quad (8.3.16)$$

Here, the notation for the B grid variables in the middle of the four stream function points are used without indices. Therefore, (8.3.14) and (8.3.15) can be rewritten as

$$\Delta A_{23}\Delta y_{23} \frac{\partial u_{23}}{\partial t} + \Delta A_{41}\Delta y_{41} \frac{\partial u_{41}}{\partial t} \Rightarrow Z_A(\bar{\psi}^y, -u\Delta y + v\Delta x) - Z_A(\bar{\psi}^x, u\Delta y + v\Delta x) \quad (8.3.17)$$

$$\Delta A_{12}\Delta x_{12} \frac{\partial v_{12}}{\partial t} + \Delta A_{34}\Delta x_{34} \frac{\partial v_{34}}{\partial t} \Rightarrow -Z_A(\bar{\psi}^y, -u\Delta y + v\Delta x) - Z_A(\bar{\psi}^x, u\Delta y + v\Delta x). \quad (8.3.18)$$

Using a formula analogous to (8.3.2), we may further write

$$\begin{aligned} \Delta A_{23}\Delta y_{23} \frac{\partial u_{23}}{\partial t} + \Delta A_{41}\Delta y_{41} \frac{\partial u_{41}}{\partial t} \Rightarrow \\ -\Delta y Z_A(\bar{\psi}^x, u) - \Delta y Z_A(\bar{\psi}^y, u) - \Delta x Z_A(\bar{\psi}^x, v) + \Delta x Z_A(\bar{\psi}^y, v) \end{aligned} \quad (8.3.19)$$

$$\begin{aligned} \Delta A_{12}\Delta x_{12} \frac{\partial v_{12}}{\partial t} + \Delta A_{34}\Delta x_{34} \frac{\partial v_{34}}{\partial t} \Rightarrow \\ -\Delta x Z_A(\bar{\psi}^x, v) - \Delta x Z_A(\bar{\psi}^y, v) - \Delta y Z_A(\bar{\psi}^x, u) + \Delta y Z_A(\bar{\psi}^y, u) \end{aligned} \quad (8.3.20)$$

Taking into account the definition of the operator  $Z_A$ , from (8.3.19) and (8.3.20) we choose

$$\frac{\partial u}{\partial t} \Rightarrow -J_A(\bar{\psi}^x, u) - J_A(\bar{\psi}^y, u) + \frac{\Delta x}{\Delta y} \left[ -J_A(\bar{\psi}^x, v) + J_A(\bar{\psi}^y, v) \right], \quad (8.3.21)$$

$$\frac{\partial v}{\partial t} \Rightarrow -J_A(\bar{\psi}^x, v) - J_A(\bar{\psi}^y, v) + \frac{\Delta y}{\Delta x} \left[ -J_A(\bar{\psi}^x, u) + J_A(\bar{\psi}^y, u) \right]. \quad (8.3.22)$$

as the scheme for the nondivergent wind components on the B grid. Note that if only the first two terms in (8.3.21) and (8.3.22) were used, that would be the Arakawa (1972) scheme. Thus, the last two terms in these two equations are the difference between the Janjic (1984a, 1984b) style scheme and the Arakawa (1972) B grid schemes.

In formulas (8.3.21) and (8.3.22), there are four nondivergent advection operators:

$$-J_A(\bar{\psi}^x, u), \quad -J_A(\bar{\psi}^y, u), \quad -J_A(\bar{\psi}^x, v), \quad -J_A(\bar{\psi}^y, v). \quad (8.3.23)$$

The operators (8.3.23) are generalized for the divergent flow following the procedure outlined e.g. in Janjic (1984a, 1984b). Consider the fluxes in the directions of the four coordinate axes that are located in between  $h$  points as shown in Figure 12, reproduced in Figure 14 for convenience.

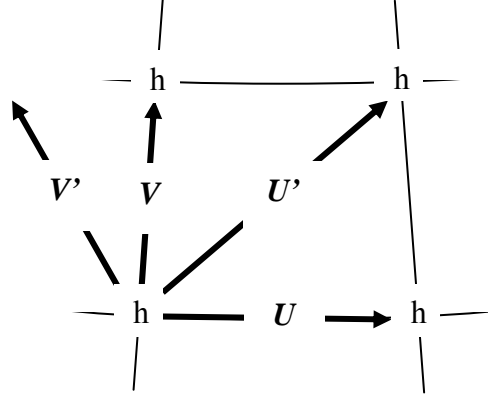


Figure 14. Schematic representation of fluxes in between  $h$  points on the  $B$  grid.

$$\begin{aligned}
 U\Delta y &= \overline{\Delta\pi^x} \overline{u^y} \Delta y \\
 V\Delta x &= \overline{\Delta\pi^y} \overline{v^x} \Delta x \\
 U'd &= \overline{\Delta\pi^{x'}} (u\Delta y + v\Delta x) \\
 V'd &= \overline{\Delta\pi^{y'}} (-u\Delta y + v\Delta x)
 \end{aligned} \tag{8.3.24}$$

However, in order to use the fluxes for momentum advection, they should be defined in between the  $\mathbf{v}$  points. This can be achieved by averaging the fluxes (8.3.24) along the coordinate axes  $x'$  and  $y'$  as indicated by averaging the stream function in nondivergent advection terms (8.3.23)

$$\overline{U\Delta y^{x'}}, \overline{V\Delta x^{x'}}, \overline{U'd^{x'}}, \overline{V'd^{x'}}, \overline{U\Delta y^{y'}}, \overline{V\Delta x^{y'}}, \overline{U'd^{y'}}, \overline{V'd^{y'}} \tag{8.3.25}$$

Using (8.3.25), the divergent analogs of the advection operators (8.3.23) multiplied by layer thicknesses take the form

$$\left( \overline{\Delta\pi^{x'}} \frac{\partial u}{\partial t} \right)_{x'} = - \left( \frac{2 \overline{U\Delta y^{x'}} \overline{\Delta x^x} \Delta_x u + \overline{V\Delta x^{x'}} \overline{\Delta y^y} \Delta_y u}{3 \Delta x \Delta y} + \frac{1 \overline{U'd^{x'}} \overline{\Delta x^x} \Delta_x u + \overline{V'd^{x'}} \overline{\Delta y^y} \Delta_y u}{3 \cdot 2 \Delta x \Delta y} \right), \tag{8.3.26a}$$

$$\left(\overline{\Delta\pi}^{y'} \frac{\partial u}{\partial t}\right)_{y'} = - \left[ \frac{2}{3} \frac{\overline{U\Delta y}^{y'} \overline{\Delta x}^x \Delta_x u + \overline{V\Delta x}^{y'} \overline{\Delta y}^y \Delta_y u}{\Delta x \Delta y} + \frac{1}{3} \frac{\overline{U'd}^{y'} \overline{\Delta x}^x \Delta_x u + \overline{V'd}^{y'} \overline{\Delta y}^y \Delta_y u}{2\Delta x \Delta y} \right],$$

(8.3.26b)

$$\left(\overline{\Delta\pi}^{x'} \frac{\partial v}{\partial t}\right)_{x'} = - \left[ \frac{2}{3} \frac{\overline{U\Delta y}^{x'} \overline{\Delta x}^x \Delta_x v + \overline{V\Delta x}^{x'} \overline{\Delta y}^y \Delta_y v}{\Delta x \Delta y} + \frac{1}{3} \frac{\overline{U'd}^{x'} \overline{\Delta x}^x \Delta_x v + \overline{V'd}^{x'} \overline{\Delta y}^y \Delta_y v}{2\Delta x \Delta y} \right], \quad (8.3.26c)$$

$$\left(\overline{\Delta\pi}^{y'} \frac{\partial v}{\partial t}\right)_{y'} = - \left[ \frac{2}{3} \frac{\overline{U\Delta y}^{y'} \overline{\Delta x}^x \Delta_x v + \overline{V\Delta x}^{y'} \overline{\Delta y}^y \Delta_y v}{\Delta x \Delta y} + \frac{1}{3} \frac{\overline{U'd}^{y'} \overline{\Delta x}^x \Delta_x v + \overline{V'd}^{y'} \overline{\Delta y}^y \Delta_y v}{2\Delta x \Delta y} \right]. \quad (8.3.26d)$$

Note that the first two of Eqs. (8.3.26) conserve the volume integral of  $u^2/2$ , while the last two conserve the volume integral of  $v^2/2$ .

Combining formulas (8.3.26) and dividing them by the mean layer depth in pressure, analogs of formulas (8.3.21) and (8.3.22) for divergent flow are obtained

$$\frac{\partial u}{\partial t} \Rightarrow \frac{1}{\overline{\Delta\pi}^{x'y'}} \left\{ \left(\overline{\Delta\pi}^{x'} \frac{\partial u}{\partial t}\right)_{x'} + \left(\overline{\Delta\pi}^{y'} \frac{\partial u}{\partial t}\right)_{y'} + \frac{\Delta x}{\Delta y} \left[ \left(\overline{\Delta\pi}^{x'} \frac{\partial v}{\partial t}\right)_{x'} - \left(\overline{\Delta\pi}^{y'} \frac{\partial v}{\partial t}\right)_{y'} \right] \right\}, \quad (8.3.27)$$

$$\frac{\partial v}{\partial t} \Rightarrow \frac{1}{\overline{\Delta\pi}^{x'y'}} \left\{ \left(\overline{\Delta\pi}^{x'} \frac{\partial v}{\partial t}\right)_{x'} + \left(\overline{\Delta\pi}^{y'} \frac{\partial v}{\partial t}\right)_{y'} + \frac{\Delta y}{\Delta x} \left[ \left(\overline{\Delta\pi}^{x'} \frac{\partial u}{\partial t}\right)_{x'} - \left(\overline{\Delta\pi}^{y'} \frac{\partial u}{\partial t}\right)_{y'} \right] \right\}. \quad (8.3.28)$$

#### 8.4 Horizontal advection of temperature and other mass point variables

The horizontal advection of temperature is computed using the scheme

$$\frac{\partial T}{\partial t} \Rightarrow - \frac{1}{\Delta\pi} \left( \frac{2}{3} \frac{\overline{U\Delta y} \overline{\Delta x} T^x + \overline{V\Delta x} \overline{\Delta y} T^y}{\Delta x \Delta y} + \frac{1}{3} \frac{\overline{U'd} \overline{\Delta x} T^{x'} + \overline{V'd} \overline{\Delta y} T^{y'}}{2\Delta x \Delta y} \right) \quad (8.4.1)$$

The scheme (8.4.1) conserves the first and the second moments of the advected quantity and reduces to the Arakawa Jacobian in case of nondivergent flow. The horizontal advection of other mass point variables, with the exception of positive definite tracers, is computed analogously.

For positive definite tracers, the square root of the tracer is advected using (8.4.1) (e.g., Janjic et al., 2009; Schneider, 1984). In this way positive definiteness is preserved, and due to the quadratic conservativeness of the scheme, the total mass of the tracer is conserved. However, with this technique a conservative *a posteriori* monotoneization is applied in order to prevent over-steepening.

As another option carried over from earlier versions of the model, a very basic upstream Lagrangian algorithm forward in time can be used. In the one dimensional case, the first guess is computed using

$$\frac{y_j^{\tau+1*} - y_j^\tau}{\Delta t} = -u \frac{y_j^\tau - y_{j-1}^\tau}{\Delta x}, u > 0. \quad (8.4.2)$$

This is followed by a negative diffusion step to reduce smoothing

$$\frac{y_j^{\tau+1} - y_j^{\tau+1*}}{\Delta t} = -f\left(\frac{u\Delta t}{\Delta x}\right) \frac{y_{j-1}^{\tau+1*} - 2y_j^{\tau+1*} + y_{j+1}^{\tau+1*}}{\Delta x^2}, f\left(\frac{u\Delta t}{\Delta x}\right) > 0. \quad (8.4.3)$$

Finally, conservation is enforced *a posteriori* after each anti-diffusion step to maintain a global sum of the advected quantity and prevent generation of new extrema. Due to open boundary conditions and decoupling from the continuity equation, the total mass of tracers cannot be conserved with acceptable accuracy using this approach.

## 8.5 Vertical Advection

At the mass points the vertical advection is computed from the formula

$$\frac{\partial H}{\partial t} \Rightarrow -\frac{1}{\Delta \pi} \overline{(\dot{s} \delta_s \pi)} \Delta_s H^s, \quad (8.5.1)$$

while at the velocity points the formula

$$\frac{\partial V}{\partial t} \Rightarrow -\frac{1}{\Delta \pi^{xy}} \overline{(\dot{s} \delta_s \pi)^{xy}} \Delta_s V^s \quad (8.5.2)$$

is used. As can be verified using (8.1.3), (8.5.1) and (8.5.2) conserve the first and second moments of the advected quantity.

## 8.6 Nonhydrostatic pressure gradient force, momentum conservation, omega-alpha term

Considering that in the case of nonhydrostatic equations,

$$\frac{d\mathbf{v}}{dt} = -(1 + \varepsilon) \nabla \Phi - \alpha \nabla_s p + \mathbf{f} \mathbf{k} \times \mathbf{v}, \quad (8.6.1)$$

and

$$\frac{\partial p}{\partial \pi} = 1 + \varepsilon, \quad (8.6.2)$$

the first term of the pressure gradient force is approximated by

$$\overline{\Delta_s \pi}^a A_{fd} \left[ (1 + \varepsilon) \frac{\partial \Phi}{\partial a} \right] = \overline{\Delta_s \pi}^a A_{fd} \left( \frac{\partial p}{\partial \pi} \frac{\partial \Phi}{\partial a} \right) \Rightarrow \overline{\Delta_s p}^a \delta_a \overline{\Phi}^s \quad (8.6.3)$$

In (8.6.3)  $a$  denotes a coordinate axis,  $s$  is the vertical coordinate, and the operator  $A_{fd}$  denotes a finite difference approximation. The approximation of the second term is obtained requiring that the momentum is conserved. Namely, the sum of the two pressure gradient force terms can be written as

$$\begin{aligned} \overline{\Delta_s p}^a \Delta_a \overline{\Phi}^s + A_{fd} \left( \Delta a \Delta_s \pi \frac{RT_v}{p} \frac{\partial p}{\partial a} \right) = \\ \Delta_s (\overline{p}^a \Delta_a \Phi) - \overline{p}^a \Delta_s (\Delta_a \Phi) + A_{fd} \left( \Delta a \Delta_s \pi \frac{RT_v}{p} \frac{\partial p}{\partial a} \right), \end{aligned} \quad (8.6.4)$$

and rearranging the formula (8.6.4) step by step,

$$\begin{aligned} \overline{\Delta_s p}^a \Delta_a \overline{\Phi}^s + A_{fd} \left( \Delta a \Delta_s \pi \frac{RT_v}{p} \frac{\partial p}{\partial a} \right) = \\ - \overline{p}^a \Delta_s (\Delta_a \Phi) + A_{fd} \left( \Delta a \Delta_s \pi \frac{RT_v}{p} \frac{\partial p}{\partial a} \right) + \Delta_s (\overline{p}^a \Delta_a \Phi), \end{aligned} \quad (8.6.5)$$

$$\begin{aligned} \overline{\Delta_s p}^a \Delta_a \overline{\Phi}^s + A_{fd} \left( \Delta a \Delta_s \pi \frac{RT_v}{p} \frac{\partial p}{\partial a} \right) = \\ - \Delta_a (\overline{p}^s \Delta_s \Phi) + \overline{\Delta_s \Phi}^a \Delta_a \overline{p}^s + A_{fd} \left( \Delta a \Delta_s \pi \frac{RT_v}{p} \frac{\partial p}{\partial a} \right) + \Delta_s (\overline{p}^a \Delta_a \Phi), \end{aligned} \quad (8.6.6)$$

$$\begin{aligned} \overline{\Delta_s p}^a \Delta_a \overline{\Phi}^s + A_{fd} \left( \Delta a \Delta_s \pi \frac{RT_v}{p} \frac{\partial p}{\partial a} \right) = \\ \overline{\Delta_s \Phi}^a \Delta_a \overline{p}^s + A_{fd} \left( \Delta a \Delta_s \pi \frac{RT_v}{p} \frac{\partial p}{\partial a} \right) + \Delta_s (\overline{p}^a \Delta_a \Phi) - \Delta_a (\overline{p}^s \Delta_s \Phi), \end{aligned} \quad (8.6.7)$$

one finally obtains

$$\begin{aligned} \overline{\Delta_s p}^a \Delta_a \overline{\Phi}^s + A_{fd} \left( \Delta a \Delta_s \pi \frac{RT_v}{p} \frac{\partial p}{\partial a} \right) = \\ - \left( \overline{\frac{RT_v}{\overline{p}^s} \Delta_s \pi} \right)^a \Delta_a \overline{p}^s + A_{fd} \left( \Delta a \Delta_s \pi \frac{RT_v}{p} \frac{\partial p}{\partial a} \right) + \Delta_s (\overline{p}^a \Delta_a \Phi) - \Delta_a (\overline{p}^s \Delta_s \Phi) \end{aligned} \quad (8.6.8)$$

From (8.6.8), it follows that the momentum conserving form of the second term of the pressure gradient force is

$$A_{fd} \left( \Delta a \Delta_s \pi \frac{RT_v}{p} \frac{\partial p}{\partial a} \right) \Rightarrow \left( \overline{\frac{RT_v}{\overline{p}^s} \Delta_s \pi} \right)^a \Delta_a \overline{p}^s. \quad (8.6.9)$$

Thus, the pressure gradient force is computed using

$$\begin{aligned} \overline{\Delta\pi}^{xy} \frac{\partial u}{\partial t} = & - \left[ \frac{2}{3} \frac{\overline{\Delta p}^x \Delta_x \overline{\Phi}^s}{\Delta x} + \frac{1}{3} \frac{\overline{\Delta p}^{x'} \Delta_x \overline{\Phi}^s - \overline{\Delta p}^{y'} \Delta_y \overline{\Phi}^s}{2\Delta x} \right] \\ & - \left[ \frac{2}{3} \frac{\overline{RT_v}^x \Delta\pi}{\overline{p}^s} \frac{\Delta_x \overline{p}^s}{\Delta x} + \frac{1}{3} \left( \frac{\overline{RT_v}^{x'} \Delta\pi}{\overline{p}^s} \frac{\Delta_x \overline{p}^s}{2\Delta x} - \frac{\overline{RT_v}^{y'} \Delta\pi}{\overline{p}^s} \frac{\Delta_y \overline{p}^s}{2\Delta x} \right) \right], \end{aligned} \quad (8.6.10)$$

and

$$\begin{aligned} \overline{\Delta\pi}^{xy} \frac{\partial v}{\partial t} = & - \left[ \frac{2}{3} \frac{\overline{\Delta p}^y \Delta_y \overline{\Phi}^s}{\Delta y} + \frac{1}{3} \frac{\overline{\Delta p}^{x'} \Delta_x \overline{\Phi}^s + \overline{\Delta p}^{y'} \Delta_y \overline{\Phi}^s}{2\Delta y} \right] \\ & - \left[ \frac{2}{3} \frac{\overline{RT_v}^y \Delta\pi}{\overline{p}^s} \frac{\Delta_y \overline{p}^s}{\Delta y} + \frac{1}{3} \left( \frac{\overline{RT_v}^{x'} \Delta\pi}{\overline{p}^s} \frac{\Delta_x \overline{p}^s}{2\Delta y} + \frac{\overline{RT_v}^{y'} \Delta\pi}{\overline{p}^s} \frac{\Delta_y \overline{p}^s}{2\Delta y} \right) \right]. \end{aligned} \quad (8.6.11)$$

From (8.6.10) and (8.6.11), one obtains the horizontal pressure advection term in the omega-alpha term in the form

$$\frac{1}{\Delta\pi\Delta x\Delta y} \left[ \frac{2}{3} \frac{\overline{RT_v}^x}{\overline{p}^s} (U\Delta y)\Delta_x \overline{p}^s + \frac{\overline{RT_v}^y}{\overline{p}^s} (V\Delta x)\Delta_y \overline{p}^s + \frac{1}{3} \frac{1}{2} \left( \frac{\overline{RT_v}^{x'}}{\overline{p}^s} (U'd)\Delta_x \overline{p}^s + \frac{\overline{RT_v}^{y'}}{\overline{p}^s} (V'd)\Delta_y \overline{p}^s \right) \right] \quad (8.6.12)$$

The remaining two terms in (2.19) are computed multiplying the right hand side of (8.2.43) by  $(1+\varepsilon)$ , i.e. using

$$(1+\varepsilon) \left( \frac{RT_v}{\pi} \right)_l \left[ \frac{\partial \pi}{\partial t} + (\dot{s}\mathcal{D}_s\pi) \right]_l^s \Delta\pi_l. \quad (8.6.13)$$

## 8.7 Polar filtering

The Fourier filtering is applied south and north of the latitudes where

$$r(\varphi) = \frac{\cos \varphi \Delta\lambda}{\Delta\varphi} < c, \quad (8.7.1)$$

and  $c$  is a constant with the default value of 1. For the variable

$$X_k = \frac{k\Delta\lambda}{2} \quad (8.7.2)$$

corresponding to the zonal wavenumber  $k$ , an equivalent variable is sought corresponding to the same wave length, but with  $\Delta y$  grid size,

$$X_e = \min\left(\frac{\frac{k\Delta\lambda}{2}}{\frac{\cos\varphi\Delta\lambda}{\Delta\varphi}}c, \frac{\pi}{2}\right) = \min\left(\frac{k\Delta\varphi}{2\cos\varphi}c, \frac{\pi}{2}\right), \quad (8.7.3)$$

and with an upper limit set at  $\frac{\pi}{2}$  corresponding to the maximum admissible zonal wave number.

The frequency of a wave propagating in the zonal direction is assumed to be proportional to

$$\sin(X_k) + \frac{1}{2}w\sin(2X_k). \quad (8.7.4)$$

Here, the first term represents the contribution of gravity waves, and the second term appears due to advection. The parameter  $w$  is the ratio between frequencies of gravity waves and advection, and its default value is 1/3. Approximately, the maximum values of the expression (8.7.4) are on the order of unity as its argument approaches  $X_k = \frac{\pi}{2}$  corresponding to the maximum zonal wave number. The frequency of a wave with the same wavelength propagating in the  $y$  direction is proportional to

$$\sin(X_e) + \frac{1}{2}w\sin(2X_e). \quad (8.7.5)$$

The condition for filtering at that wave number is

$$c \left[ \sin(X_e) + \frac{1}{2}w\sin(2X_e) \right] \geq \frac{\cos\varphi\Delta\lambda}{\Delta\varphi}. \quad (8.7.6)$$

The filter response function has the form

$$(\cos X_k)^n, \quad (8.7.7)$$

where the power  $n$  is such that

$$(\cos X_k)^n X_e(1+w) \leq \sin(X_e) + \frac{1}{2}w\sin(2X_e). \quad (8.7.8)$$

The additional assumption introduced here is that the frequencies of the filtered waves are computed with sufficient resolution (and therefore accuracy) at the filtered latitude, so that the phase errors due to finite differencing can be ignored.

The role of the filter is to reduce these frequencies to those corresponding with (8.7.5). Note that the filter is applied only to tendencies, and thus acts as a decelerator similar, e.g., to the effect of application of the semi-implicit scheme.

## 9.0 GENERAL COMMENTS ON CONSERVATION PROPERTIES IN THE NMMB

The conservation of major integral properties such as energy and enstrophy has been the basic philosophy of the discretization that can be traced back as a modeling principle to the paper by Janjic (1977). Since then, however, the numerical schemes used in the model have been greatly refined and the resolutions increased by more than an order of magnitude. Perhaps the most significant upgrade was the introduction of the new schemes for calculating the contribution of the nonlinear advection terms and the horizontal divergence operators on the E grid (Janjic, 1984a, 1984b). Some properties of the momentum advection scheme were discussed in Gavrilov and Janjic (1989). In the current NMMB formulation, all divergence operators are computed using the fluxes between each point and its eight nearest neighbors. This, ‘‘isotropic’’, divergence operator is used in the Arakawa Jacobians, but also, e.g., in the hydrostatic continuity equation in order to compute the divergence of mass.

In the case of rotational flow and cyclic boundary conditions, among other things, the scheme for horizontal advection of momentum on the B grid conserves the following properties:

- Enstrophy as defined on the staggered grid C (i.e., using the most accurate second-order approximation of the Laplacian)

$$\sum_{i,j} (\delta_{xx}\psi + \delta_{yy}\psi)^2 \Delta A. \quad (9.1)$$

- Rotational kinetic energy as defined on the staggered grid C, i.e.,

$$\sum_{i,j} \frac{1}{2} [(\delta_y\psi)^2 + (\delta_x\psi)^2] \Delta A. \quad (9.2)$$

- Rotational momentum as defined on the staggered grid C.
- A quadratic quantity proportional to rotational kinetic energy as defined on the semi-staggered grid B

$$\begin{aligned} \sum_{i,j} \frac{1}{2} [(-\delta_y\bar{\psi}^x \Delta y + \delta_x\bar{\psi}^y \Delta x)^2 + (\delta_y\bar{\psi}^x \Delta y + \delta_x\bar{\psi}^y \Delta x)^2] \Delta A = \\ \sum_{i,j} [(-\delta_y\bar{\psi}^x \Delta y)^2 + (\delta_x\bar{\psi}^y \Delta x)^2] \Delta A \end{aligned} \quad (9.3)$$

- A first order quantity proportional to rotational momentum as defined on the semi-staggered grid B

$$\sum_{i,j} (-\delta_y\bar{\psi}^x \Delta y + \delta_x\bar{\psi}^y \Delta x) \Delta A, \quad \sum_{i,j} (\delta_y\bar{\psi}^x \Delta y + \delta_x\bar{\psi}^y \Delta x) \Delta A$$

$$\text{and} \tag{9.4}$$

$$\sum_{i,j} \left( -\delta_y \bar{\psi}^x \Delta y \right) \Delta A, \sum_{i,j} \left( \delta_x \bar{\psi}^y \Delta x \right) \Delta A.$$

The Z grid equivalent of the B grid (c.f. Janjic, 1984a, 1984b) used to define the quantities (9.1)–(9.4) is shown in Figure 3 together with orientations of the coordinate axes  $x, y$  appearing in (9.1)–(9.4). As before,  $\chi$  and  $\psi$  are the velocity potential and stream function, respectively, and  $h$  stands for mass point variables. The symbol  $\Delta A$  denotes the areas of grid boxes, and the summation sign with the subscripts  $i, j$  represents summation in the horizontal.

In case of general flow, the scheme conserves:

- Quadratic quantities proportional to kinetic energy as defined on the semi-staggered grid B and their sum

$$\sum_{i,j} \frac{1}{2} \left[ \left( \delta_x \bar{\phi}^x - \delta_y \bar{\psi}^x \right) \Delta y + \left( \delta_x \bar{\phi}^x + \delta_x \bar{\psi}^y \right) \Delta x \right]^2 \Delta V$$

$$\text{and} \tag{9.5}$$

$$\sum_{i,j} \frac{1}{2} \left[ - \left( \delta_x \bar{\phi}^x - \delta_y \bar{\psi}^x \right) \Delta y + \left( \delta_x \bar{\phi}^x + \delta_x \bar{\psi}^y \right) \Delta x \right]^2 \Delta V.$$

- First order quantity proportional to momentum as defined on the semi-staggered grid B and their sum.

$$\sum_{i,j} \frac{1}{2} \left[ \left( \delta_x \bar{\phi}^x - \delta_y \bar{\psi}^x \right) \Delta y + \left( \delta_x \bar{\phi}^x + \delta_x \bar{\psi}^y \right) \Delta x \right] \Delta V$$

$$\text{and} \tag{9.6}$$

$$\sum_{i,j} \frac{1}{2} \left[ - \left( \delta_x \bar{\phi}^x - \delta_y \bar{\psi}^x \right) \Delta y + \left( \delta_x \bar{\phi}^x + \delta_x \bar{\psi}^y \right) \Delta x \right] \Delta V.$$

In (9.5) and (9.6), the summation sign indicates the summation over all grid points, and the symbol  $\Delta V$  denotes the grid box volume in hydrostatic vertical coordinates.

The scheme for horizontal advection of temperature also conserves the first and the second moments of temperature. Finally, in the hydrostatic limit, i.e., when  $dw/dt$  tends to zero, the exact cancellation is achieved between the contributions of the pressure gradient force to the kinetic energy generation, and the  $\omega\alpha$  term of the continuity equation, which guarantees consistent transformations between the kinetic and the potential energy and the conservation of total energy. The relevant finite-difference schemes were presented in Janjic (1977), and their generalizations for the “isotropic”, 8-flux divergence operators were discussed in Janjic (1984a, 1984b) and further documented, e.g., in Mesinger et al (1988).

The exact energy conservation is not currently required in the case of the fully nonhydrostatic equations. In this case the terms involving  $\varepsilon = (dw/dt)/g$  are of the order higher than quadratic, and  $\varepsilon = (dw/dt)/g$  is small compared to unity in weakly nonhydrostatic flows that can be expected in NWP applications. On the other hand, on the scales and in the flow regimes where the contribution of  $\varepsilon = (dw/dt)/g$  becomes significant, the dissipation starts to play a prominent role creating strong energy sinks.

In addition, a conservative, positive definite and monotone Eulerian scheme for the tracers is applied. The positive definiteness is guaranteed by advecting the square root of the tracer (c.f. e.g., Schneider, 1984). The conservation is achieved due to conservation of quadratic quantities by the advection scheme. However, a forced conservative a posteriori monotone scheme is used to prevent creation of new extrema (Janjic, 2008, Janjic et al., 2009).

## 10.0 BOUNDARY CONDITIONS

### 10.1 Lateral and polar boundary conditions

Figure 15 illustrates the lateral boundary conditions used in the regional NMMB. The values of velocity and the mass variables are specified only on the outermost rows and columns, with the outer boundary running through mass points. In the first three rows inside the domain, upstream differences are used for advection. Thus, the lateral boundary conditions for advection are well posed. In addition a boundary blending zone is introduced, where the solution obtained by solving the model's equations is blended with prescribed boundary conditions. The best results are obtained with blending zone that is five rows wide, and with the weight of the prescribed boundary conditions decreasing linearly as the distance from the boundary increases (communicated by Pyle).

The “across the pole” polar boundary conditions were implemented by introducing two ghost rows with wind and mass variables respectively as shown in Figure 16. The polar rows of points carry mass variables. The mass points along the ghost lines carry the values of mass variables that lie on the same meridians, but on the other sides of the poles. Similarly, the wind points at the ghost lines carry the wind components on the other sides of the poles, but with changed signs since the coordinate axes change their directions as the poles are crossed along a meridian. The remapping of the variables onto the ghost lines is schematically shown in Figure 17. Note that reordering of the values of the variables for the remapping on the ghost line is not necessary since what matters at the poles is the sum of the polar fluxes, and not the order in which the summation of the fluxes is performed. This greatly simplifies the code and speeds up computation on parallel computers by reducing communication.

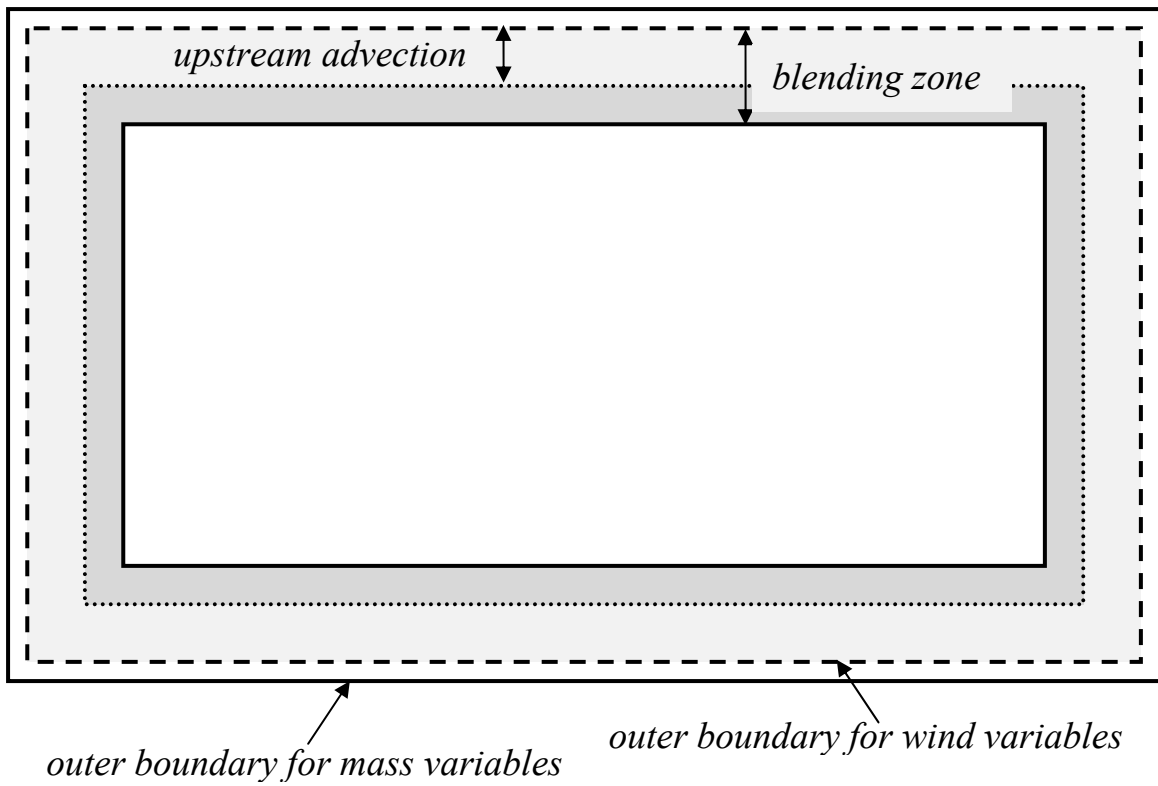
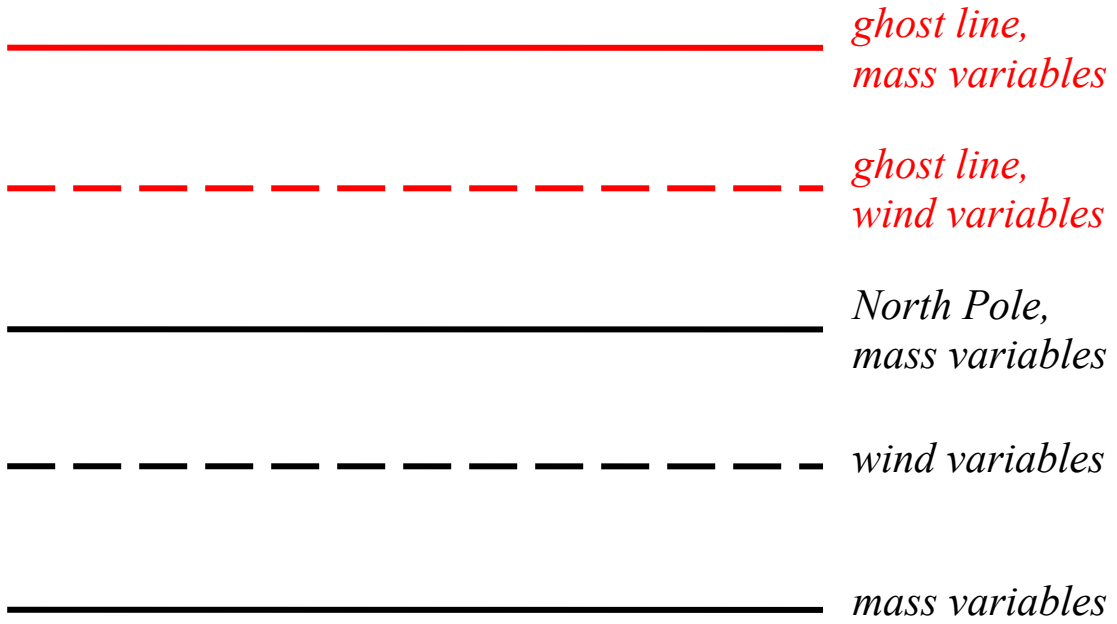


Figure 15. Lateral boundary conditions used in NMMB when used as a regional model



*Figure 16. Schematic representation of the distribution of variables near the North Pole.*

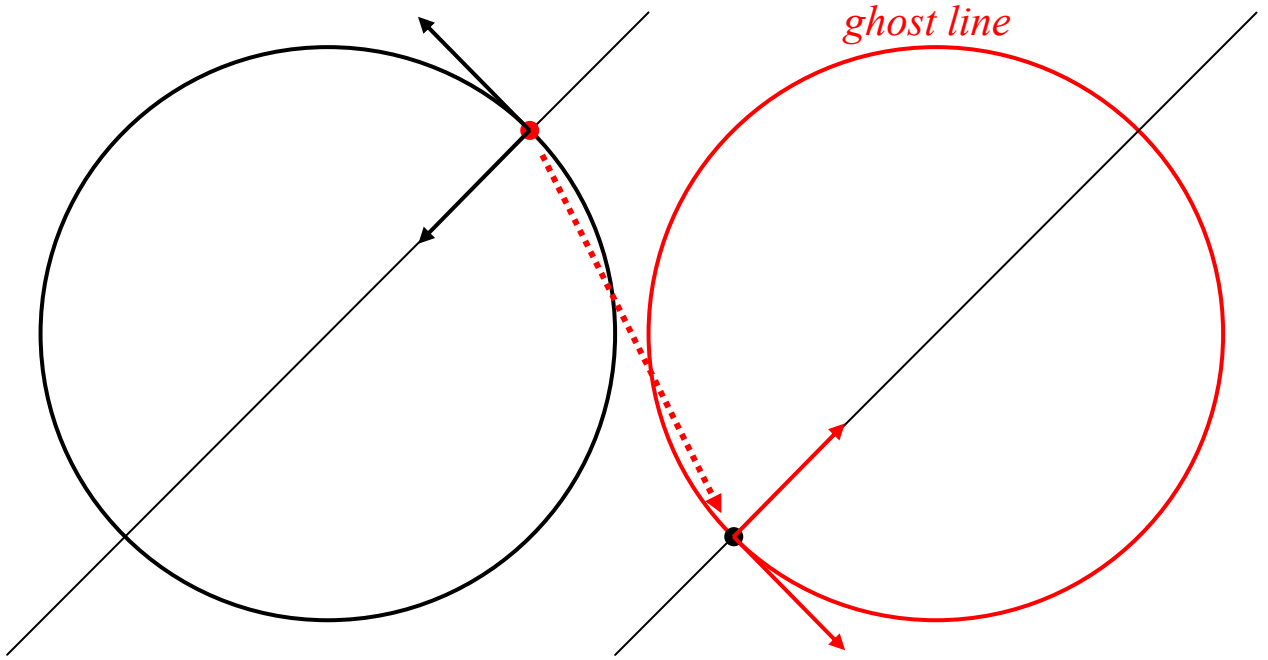


Figure 17. Remapping variable values from real to ghost latitudinal circles near the poles.

## 10.2 Vertical boundary conditions

The vertical boundary conditions are:

$$\dot{s} = 0 \text{ and } p = \pi \text{ at } s = 0, \quad (8.2.1)$$

$$\dot{s} = 0 \text{ and } \frac{\partial(p - p^*)}{\partial s} = 0 \text{ at } s = 1, \quad (8.2.2)$$

where  $p^*$  is defined by (7.2.3). Note that the second part of (8.2.1) and (8.2.2) are required for the nonhydrostatic calculations as discussed in more detail in Section 7.2.

## 11.0 TURBULENT MIXING AND MODEL FILTERS

The model has two types of parameterized dissipative processes (that is filters that are not part of the numerical scheme); explicit lateral diffusion (often called horizontal diffusion) and a process called horizontal divergence damping. These components are simply added to the tendencies whose calculations were described earlier.

### 11.1 Explicit lateral diffusion

For horizontal diffusion, the NMMB uses a 2nd order, nonlinear Smagorinsky-type approach (Janjic, 1990). The diffusion has the form

$$\frac{\partial V}{\partial t} = \frac{1}{\Delta\pi} \nabla \cdot (\Delta\pi K_M \nabla V), \quad \frac{\partial H}{\partial t} = \frac{1}{\Delta\pi} \nabla \cdot (\Delta\pi K_H \nabla H). \quad (11.1.1)$$

Here  $V$  and  $H$  stand for any  $\mathbf{v}$  point or  $h$  point variable, respectively, and the subscripts  $M$  and  $H$  denote the exchange coefficients for momentum and mass point variables. In the NMMB the exchange coefficient  $K$  is flow dependant

$$K = c_S^2 l^2 |\Delta|, \quad (11.1.2)$$

where  $c_S$  is the Smagorinsky constant that usually takes on values in the range [0.2,0.4],  $l$  is a mixing length comparable to grid distance and  $\Delta$  is proportional to modified horizontal deformation which in the NMMB includes contributions of turbulent kinetic energy (Janjic 1990) and vertical shear

$$|\Delta| = \left\{ 2 \left[ \left( \frac{\overline{\Delta_x u \Delta y^y} - \overline{\Delta_y v \Delta x^x}}{\Delta x \Delta y} \right)^2 + \left( \frac{\overline{\Delta_y u \Delta x^y} + \overline{\Delta_x v \Delta y^y}}{\Delta x \Delta y} \right)^2 + c' \frac{q^2}{\Delta x \Delta y} \right] + 2c'' \left[ \overline{(\delta_x w)^2}^x + \overline{(\delta_y w)^2}^y \right] \right\}^{\frac{1}{2}} \quad (11.1.3)$$

Here,  $q^2$  is twice the TKE and  $c'$  and  $c''$  are constants. The  $q^2$  term is included to account for the effects of horizontal mixing due to dry convective entrainment and detrainment. The default values of the constants  $c'$  and  $c''$  are 50 and 1, respectively. The vertical velocity  $w$  terms are present only if the model is run in the nonhydrostatic mode. A constraint is imposed on  $|\Delta|$  such that

$$|\Delta|_{\min} \leq |\Delta| \leq |\Delta|_{\max}, \quad (11.1.4)$$

where the lower and upper bounds are empirically determined by the need for residual computational damping and the stability criterion, respectively. The default values of the bounds are 0 and infinity (in regional applications), respectively. Since  $\Delta$  is computed at mass points, the diffusion coefficients for velocity and mass point variables in the directions of the coordinate axes  $x$  and  $y$  are averaged differently

$$(\Delta\pi K)_{Mx} = \overline{\Delta\pi K^y}, (\Delta\pi K)_{My} = \overline{\Delta\pi K^x}, (\Delta\pi K)_{Hx} = \overline{\Delta\pi K^x}, (\Delta\pi K)_{Hy} = \overline{\Delta\pi K^y}. \quad (11.1.5)$$

The subscripts  $Mx$ ,  $My$  and  $Hx$ ,  $Hy$  denote mass weighted momentum and mass point turbulent exchange coefficients, respectively, in the directions of coordinate axes  $x$ ,  $y$ . If the slope of the model surfaces exceeds 0.45% (4.5 m/km) the turbulent flux between mass points is set to zero in order to avoid unphysical results at the tops of pointed mountains and at the bottoms of valleys.

From (11.1.1), (11.1.2) and (11.1.5), the final formulas for lateral diffusion at mass and velocity points are, respectively,

$$\frac{1}{\Delta\pi} \nabla \cdot (\Delta\pi K_H \nabla H) \Rightarrow \frac{1}{\Delta\pi} \frac{\Delta_x \left[ \left( \overline{\Delta\pi K^x} \delta_x H \right) \Delta y \right] + \Delta_y \left[ \left( \overline{\Delta\pi K^y} \delta_y H \right) \Delta x \right]}{\Delta x \Delta y}, \quad (11.1.6)$$

$$\frac{1}{\Delta\pi} \nabla \cdot (\Delta\pi K_M \nabla V) \Rightarrow \frac{1}{\Delta\pi} \frac{\Delta_x \left[ \left( \overline{\Delta\pi K^y} \delta_x V \right) \Delta y \right] + \Delta_y \left[ \left( \overline{\Delta\pi K^x} \delta_y V \right) \Delta x \right]}{\Delta x \Delta y}. \quad (11.1.7)$$

However, in the global domain it is difficult to apply formulas (11.1.6)-(11.1.7) due to huge difference in resolution in the  $x$  and  $y$  directions. In regional domains the grid distances in the  $x$  and  $y$  directions generally remain close to each other, but the operation count is very high. For these reasons, the formulas actually used in the model are simplified preserving the nonlinear dependence.

## 11.2 Horizontal Divergence Damping

Dispersion of gravity-inertia waves alone can explain linear geostrophic adjustment on an infinite plain. However, “In a finite domain, unless viscosity is introduced, gravity waves will forever ‘slosh’ without dissipating” (Vallis, 1992). Numerical experiments by Farge and Sadourny (1989) strongly support the idea of dissipative geostrophic adjustment.

Consider the mass divergence at a single vertical level (see Figure 12 again reproduced here in Figure 18 for convenience)

$$D_l = \frac{2}{3} \frac{\Delta_x (U \Delta y) + \Delta_y (V \Delta x)}{\Delta x \Delta y} + \frac{1}{3} \frac{\Delta_x' (U' d) + \Delta_y' (V' d)}{2 \Delta x \Delta y}, \quad (11.2.1)$$

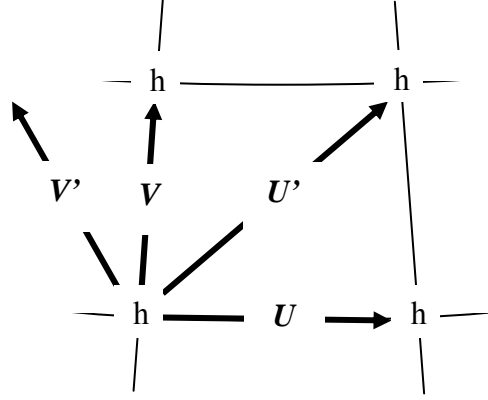


Figure 18. Schematic representation of fluxes in between  $h$  points on the  $B$  grid.

whereas before the mass fluxes are defined as

$$\begin{aligned}
 U\Delta y &= \overline{\Delta\pi^x} \bar{u}^y \Delta y \\
 V\Delta x &= \overline{\Delta\pi^y} \bar{v}^x \Delta x \\
 U'd &= \overline{\Delta\pi^{x'}} (u\Delta y + v\Delta x) \\
 V'd &= \overline{\Delta\pi^{y'}} (-u\Delta y + v\Delta x),
 \end{aligned} \tag{11.2.2}$$

and  $\pi$  is the hydrostatic pressure. In the NMMB the horizontal divergence damping is implemented as

$$\begin{aligned}
 \frac{\partial u}{\partial t} &= K_1 \frac{1}{\overline{\Delta\pi^{xy}}} \overline{\delta_x D_l^y} \\
 \frac{\partial v}{\partial t} &= K_1 \frac{1}{\overline{\Delta\pi^{xy}}} \overline{\delta_y D_l^x}
 \end{aligned} \tag{11.2.3}$$

The horizontal divergence damping damps both internal and external gravity wave modes. Enhanced divergence damping damps spurious fast modes which may be important for data assimilation or for controlling computational stability.

Now consider the external mode mass divergence

$$D_{ext} = \sum_{top}^{bottom} D_l \tag{11.2.4}$$

The external mode divergence damping used in the NMMB has the form

$$\frac{\partial u}{\partial t} = K_2 \frac{1}{\overline{\mu^{xy}}} \overline{\delta_x D_{ext}^y}$$

$$\frac{\partial v}{\partial t} = K_2 \frac{1}{\bar{\mu}^{xy}} \overline{\delta_y D_{ext}}^x, \quad (11.2.5)$$

where, as before,

$$\mu = \pi_{bottom} - \pi_{top}. \quad (11.2.6)$$

Integrating formulas (11.2.5) with respect to mass from the top to the bottom of a grid column, one obtains

$$\begin{aligned} \sum_{top}^{bottom} \frac{\partial u}{\partial t} \overline{\Delta \pi}^{xy} &= K_2 \overline{\delta_x D_{ext}}^y \frac{1}{\bar{\mu}^{xy}} \sum_{top}^{bottom} \overline{\Delta \pi}^{xy} \\ \sum_{top}^{bottom} \frac{\partial v}{\partial t} \overline{\Delta \pi}^{xy} &= K_2 \overline{\delta_y D_{ext}}^x \frac{1}{\bar{\mu}^{xy}} \sum_{top}^{bottom} \overline{\Delta \pi}^{xy}, \end{aligned} \quad (11.2.7)$$

and finally,

$$\begin{aligned} \sum_{top}^{bottom} \frac{\partial u}{\partial t} \overline{\Delta \pi}^{xy} &= K_2 \overline{\delta_x D_{ext}}^y \\ \sum_{top}^{bottom} \frac{\partial v}{\partial t} \overline{\Delta \pi}^{xy} &= K_2 \overline{\delta_y D_{ext}}^x. \end{aligned} \quad (11.2.8)$$

Thus, only the external mode is affected.

The combination of the horizontal and external mode divergence damping also can be used in the NMMB and has the form

$$\begin{aligned} \frac{\partial u}{\partial t} &= K_1 \frac{1}{\overline{\Delta \pi}^{xy}} \overline{\delta_x D_l}^y + K_2 \frac{1}{\bar{\mu}^{xy}} \overline{\delta_x D_{ext}}^y \\ \frac{\partial v}{\partial t} &= K_1 \frac{1}{\overline{\Delta \pi}^{xy}} \overline{\delta_y D_l}^x + K_2 \frac{1}{\bar{\mu}^{xy}} \overline{\delta_y D_{ext}}^x \end{aligned} \quad (11.2.9)$$

The divergence damping is applied after equation 4.2.1. The default value controlling the horizontal divergence damping is 6.4 for both external and internal modes which corresponds to weak divergence damping.

### 11.3 Filters

As a general rule, application of explicit or implied non-physical, numerical, filters is avoided in the NMMB since such filters alter the governing equations and, thus, can have adverse effect on the solution. The exception is the technique for filtering of low frequency short-wave noise resulting from inaccurate computation of the divergence

term on the semi-staggered grids discussed in section 4.2. This technique will be introduced following the ideas and derivations from Janjic (1974, 1979). The interested reader is directed to these papers for more details.

The horizontal mass divergence term in the hydrostatic continuity equation (8.1.3) can be rewritten as

$$\nabla_B \cdot \left( \overline{\Delta\pi^*} \mathbf{v} \right) = \nabla_B \cdot \left( \overline{\Delta\pi^{xy}} \mathbf{v} \right) + \nabla_B \cdot \left[ \left( \overline{\Delta\pi^*} - \overline{\Delta\pi^{xy}} \right) \mathbf{v} \right] \quad (11.3.1)$$

Here, the divergence operator on the left hand side is computed using the approximation (8.1.2), and

$$\nabla_B \cdot \mathbf{A} = \frac{2}{3} \frac{\Delta_x \left( \overline{A_x^y} \Delta y \right) + \Delta_y \left( \overline{A_y^x} \Delta x \right)}{\Delta x \Delta y} + \frac{1}{3} \frac{\Delta_x \left( A_x \Delta y + A_y \Delta x \right) + \Delta_y \left( -A_x \Delta y + A_y \Delta x \right)}{2 \Delta x \Delta y}, \quad (11.3.2)$$

where  $\mathbf{A}$  is an arbitrary vector with scalar components  $(A_x, A_y)$ , and the subscript  $B$  indicates that the finite difference approximation of the divergence operator is applied on the B grid. As can be verified in a straightforward manner, in the linear case (11.3.2) further simplifies to

$$\nabla_B \cdot \mathbf{A} = \frac{\Delta_x \left( \overline{A_x^y} \Delta y \right) + \Delta_y \left( \overline{A_y^x} \Delta x \right)}{\Delta x \Delta y}. \quad (11.3.3)$$

Applying the operator (11.3.3) to  $\overline{\Delta\pi^{xy}} \mathbf{v}$  we obtain

$$\nabla_B \cdot \left( \overline{\Delta\pi^{xy}} \mathbf{v} \right) = \frac{\Delta_x \left( \overline{\overline{\Delta\pi^{xy} u}^y} \Delta y \right) + \Delta_y \left( \overline{\overline{\Delta\pi^{xy} v}^x} \Delta x \right)}{\Delta x \Delta y}. \quad (11.3.4)$$

However, if  $\Delta_t$  denotes time changes between time levels  $n-1$  and  $n$ , at the time level  $n$

$$\nabla_B \cdot \left( \overline{\Delta\pi^{xy}} \mathbf{v}^n \right) = \frac{\Delta_x \left[ \overline{\overline{\Delta\pi^{xy} \left( u^{n-1} + \Delta_t u \right)^y}} \right] \Delta y + \Delta_y \left[ \overline{\overline{\Delta\pi^{xy} \left( v^{n-1} + \Delta_t v \right)^x}} \right] \Delta x}{\Delta x \Delta y}, \quad (11.3.5)$$

or,

$$\nabla_B \cdot \left( \overline{\Delta\pi}^{xy} \mathbf{v}^n \right) = \frac{\Delta_x \left( \overline{\Delta\pi}^{xy} \Delta_t u \Delta y \right) + \Delta_y \left( \overline{\Delta\pi}^{xy} \Delta_t v \Delta x \right)}{\Delta x \Delta y} + \frac{\Delta_x \left( \overline{\Delta\pi}^{xy} u^{n-1} \Delta y \right) + \Delta_y \left( \overline{\Delta\pi}^{xy} v^{n-1} \Delta x \right)}{\Delta x \Delta y} \quad (11.3.6)$$

and

$$\nabla_B \cdot \left( \overline{\Delta\pi}^{xy} \mathbf{v}^n \right) = \nabla_B \cdot \left( \overline{\Delta\pi}^{xy} \mathbf{v}^{n-1} \right) + \frac{\Delta_x \left( \overline{\Delta\pi}^{xy} \Delta_t u \Delta y \right) + \Delta_y \left( \overline{\Delta\pi}^{xy} \Delta_t v \Delta x \right)}{\Delta x \Delta y}. \quad (11.3.7)$$

For brevity, define the contributions of the pressure gradient force to time changes of  $u$  and  $v$  in (8.6.10) and (8.6.11) by

$$P_{x1} = -\Delta t \frac{2}{3} \left( \overline{\frac{\Delta p^x \Delta_x \overline{\Phi}^s}{\Delta x} + \frac{RT_v}{\bar{p}^s} \Delta \pi \frac{\Delta_x \bar{p}^s}{\Delta x}} \right)^y, \quad (11.3.8)$$

$$P_{x2} = -\Delta t \frac{1}{3} \frac{\left( \overline{\frac{\Delta p^{x'} \Delta_{x'} \overline{\Phi}^s + \frac{RT_v}{\bar{p}^s} \Delta \pi \Delta_{x'} \bar{p}^s} \right) - \left( \overline{\frac{\Delta p^{y'} \Delta_{y'} \overline{\Phi}^s + \frac{RT_v}{\bar{p}^s} \Delta \pi \Delta_{y'} \bar{p}^s} \right)}{2 \Delta x}, \quad (11.3.9)$$

$$P_{y1} = -\Delta t \frac{2}{3} \left( \overline{\frac{\Delta p^y \Delta_y \overline{\Phi}^s + \frac{RT_v}{\bar{p}^s} \Delta \pi \frac{\Delta_y \bar{p}^s}{\Delta y}} \right)^x, \quad (11.3.10)$$

$$P_{y2} = -\Delta t \frac{2}{3} \frac{\left( \overline{\frac{\Delta p^{x'} \Delta_{x'} \overline{\Phi}^s + \frac{RT_v}{\bar{p}^s} \Delta \pi \Delta_{x'} \bar{p}^s} \right) + \left( \overline{\frac{\Delta p^{y'} \Delta_{y'} \overline{\Phi}^s + \frac{RT_v}{\bar{p}^s} \Delta \pi \Delta_{y'} \bar{p}^s} \right)}{2 \Delta y}. \quad (11.3.11)$$

Then,

$$\overline{\Delta\pi}^{xy} \Delta_t u = P_{x1}^n + P_{x2}^n + \Delta C_x + \Delta A_x, \quad (11.3.12)$$

$$\overline{\Delta\pi}^{xy} \Delta_t v = P_{y1}^n + P_{y2}^n + \Delta C_y + \Delta A_y, \quad (11.1.13)$$

and

$$\frac{\Delta_x \left( \overline{\Delta \pi^{xy} \Delta u}^y \Delta y \right) + \Delta_y \left( \overline{\Delta \pi^{xy} \Delta v}^x \Delta x \right)}{\Delta x \Delta y} = \frac{\Delta_x \left( \overline{P_{x1}^n + P_{x2}^n}^y \Delta y \right) + \Delta_y \left( \overline{P_{y1}^n + P_{y2}^n}^x \Delta x \right)}{\Delta x \Delta y}, \quad (11.3.14)$$

$$+ \frac{\Delta_x \left( \overline{\Delta C_x + \Delta A_x}^y \Delta y \right) + \Delta_y \left( \overline{\Delta C_y + \Delta A_y}^x \Delta x \right)}{\Delta x \Delta y}$$

where  $\Delta C_x$ ,  $\Delta A_x$ ,  $\Delta C_y$ ,  $\Delta A_y$  are the components of the contributions of the Coriolis and advection terms. Consider first the contribution of the terms

$$\frac{\Delta_x \left( \overline{P_{x1}^n}^y \Delta y \right) + \Delta_y \left( \overline{P_{y1}^n}^x \Delta x \right)}{\Delta x \Delta y}. \quad (11.3.15)$$

Using (11.3.8) and (11.3.10) we obtain

$$- \Delta t \frac{2}{3} \frac{1}{\Delta x \Delta y} \left\{ \Delta_x \left[ \overline{\left( \frac{\Delta p^x \Delta_x \bar{\Phi}^s}{\Delta x} + \frac{RT_v}{\bar{p}^s} \Delta \pi \frac{\Delta_x \bar{p}^s}{\Delta x} \right)^{n^y y}} \right] \Delta y + \Delta_y \left[ \overline{\left( \frac{\Delta p^y \Delta_y \bar{\Phi}^s}{\Delta y} + \frac{RT_v}{\bar{p}^s} \Delta \pi \frac{\Delta_y \bar{p}^s}{\Delta y} \right)^{n^x x}} \right] \Delta x \right\} \quad (11.3.16)$$

The expression (11.3.16) can be rearranged to take the form

$$- \Delta t \frac{2}{3} \frac{1}{2} \frac{1}{\Delta x \Delta y} \left\{ \Delta_x \left[ \overline{\left( \frac{\Delta p^x \Delta_x \bar{\Phi}^s}{\Delta x} + \frac{RT_v}{\bar{p}^s} \Delta \pi \frac{\Delta_x \bar{p}^s}{\Delta x} \right)^{n^y y}} \right] \Delta y + \overline{\left( \frac{\Delta p^y \Delta_y \bar{\Phi}^s}{\Delta y} + \frac{RT_v}{\bar{p}^s} \Delta \pi \frac{\Delta_y \bar{p}^s}{\Delta y} \right)^{n^x x}} \Delta x \right] \right. \\ \left. + \Delta_y \left[ \overline{\left( \frac{\Delta p^x \Delta_x \bar{\Phi}^s}{\Delta x} + \frac{RT_v}{\bar{p}^s} \Delta \pi \frac{\Delta_x \bar{p}^s}{\Delta x} \right)^{n^y y}} \right] \Delta y + \overline{\left( \frac{\Delta p^y \Delta_y \bar{\Phi}^s}{\Delta y} + \frac{RT_v}{\bar{p}^s} \Delta \pi \frac{\Delta_y \bar{p}^s}{\Delta y} \right)^{n^x x}} \Delta x \right] \right\} \quad (11.3.17)$$

To elucidate the impact of the operator (11.3.17), assume that  $\Delta x = \Delta y$  and that the terms

$\Delta p = \overline{\overline{\Delta p}}$  and  $\frac{RT_v}{\bar{p}} \Delta \pi = \overline{\overline{\frac{RT_v}{\bar{p}} \Delta \pi}}$  do not vary in space. Then (11.3.17) takes the form

$$- \Delta t \frac{2}{3} \frac{1}{2} \frac{1}{\Delta x \Delta y} \left\{ \begin{array}{l} \Delta_{x'} \left[ \overline{\overline{\left( \overline{\overline{\Delta p \Delta_x \Phi^s + \frac{RT_v}{\bar{p}} \Delta \pi \Delta_x \bar{p}^s} \right)^{n^y}}} + \overline{\overline{\left( \overline{\overline{\Delta p \Delta_y \Phi^s + \frac{RT_v}{\bar{p}} \Delta \pi \Delta_y \bar{p}^s} \right)^{n^x}}} \right]} \\ + \Delta_{y'} \left[ - \overline{\overline{\left( \overline{\overline{\Delta p \Delta_x \Phi^s + \frac{RT_v}{\bar{p}} \Delta \pi \Delta_x \bar{p}^s} \right)^{n^y}}} + \overline{\overline{\left( \overline{\overline{\Delta p \Delta_y \Phi^s + \frac{RT_v}{\bar{p}} \Delta \pi \Delta_y \bar{p}^s} \right)^{n^x}}} \right]} \end{array} \right\} \quad (11.3.18)$$

and

$$- \Delta t \frac{2}{3} \frac{1}{2} \frac{1}{\Delta x \Delta y} \left[ \Delta_{x'} \left( \overline{\overline{\Delta p \Delta_x \Phi^s + \frac{RT_v}{\bar{p}} \Delta \pi \Delta_x \bar{p}^s}} \right)^n + \Delta_{y'} \left( \overline{\overline{\Delta p \Delta_y \Phi^s + \frac{RT_v}{\bar{p}} \Delta \pi \Delta_y \bar{p}^s}} \right)^n \right] \quad (11.3.19)$$

The operator (11.3.19) provides communication only with the neighboring points in the diagonal directions  $x'$  and  $y'$ , but not with the nearest neighboring points in the directions  $x$  and  $y$ . Weak interaction between the nearest neighboring points is still possible due to the nonlinear terms that are missing in (11.3.19), but this interaction generally is not sufficient to effectively prevent the grid separation and the resulting small-scale low-frequency noise.

Now, consider the remaining term in the divergence of the pressure gradient force contribution

$$\frac{\Delta_x \left( \overline{\overline{P_{x2}^n}} \Delta y \right) + \Delta_y \left( \overline{\overline{P_{y2}^n}} \Delta x \right)}{\Delta x \Delta y} \quad (11.3.20)$$

Using (11.3.9) and (11.3.11), (11.3.20) takes the form

$$\left. -\Delta t \frac{1}{3} \frac{1}{2} \frac{1}{\Delta x \Delta y} \left\{ \begin{aligned} & \Delta_x \left[ \frac{\left( \overline{\Delta p}^{x'} \Delta_x \overline{\Phi}^s + \frac{\overline{RT}_v}{\overline{p}^s} \Delta \pi \Delta_x \overline{p}^s \right)^n - \left( \overline{\Delta p}^{y'} \Delta_y \overline{\Phi}^s + \frac{\overline{RT}_v}{\overline{p}^s} \Delta \pi \Delta_y \overline{p}^s \right)^n }{\Delta x} \Delta y \right. \\ & \left. + \Delta_y \left[ \frac{\left( \overline{\Delta p}^{x'} \Delta_x \overline{\Phi}^s + \frac{\overline{RT}_v}{\overline{p}^s} \Delta \pi \Delta_x \overline{p}^s \right)^n + \left( \overline{\Delta p}^{y'} \Delta_y \overline{\Phi}^s + \frac{\overline{RT}_v}{\overline{p}^s} \Delta \pi \Delta_y \overline{p}^s \right)^n}{\Delta y} \Delta x \right] \right\} \right. \\ & \hspace{15em} (11.3.21)
 \end{aligned}$$

In particular, if  $\Delta x = \Delta y$ , we obtain

$$\left. -\Delta t \frac{1}{3} \frac{1}{2} \frac{1}{\Delta x \Delta y} \left\{ \begin{aligned} & \Delta_x \left[ \frac{\left( \overline{\Delta p}^{x'} \Delta_x \overline{\Phi}^s + \frac{\overline{RT}_v}{\overline{p}^s} \Delta \pi \Delta_x \overline{p}^s \right)^n - \left( \overline{\Delta p}^{y'} \Delta_y \overline{\Phi}^s + \frac{\overline{RT}_v}{\overline{p}^s} \Delta \pi \Delta_y \overline{p}^s \right)^n}{\Delta x} \right. \\ & \left. + \Delta_y \left[ \frac{\left( \overline{\Delta p}^{x'} \Delta_x \overline{\Phi}^s + \frac{\overline{RT}_v}{\overline{p}^s} \Delta \pi \Delta_x \overline{p}^s \right)^n + \left( \overline{\Delta p}^{y'} \Delta_y \overline{\Phi}^s + \frac{\overline{RT}_v}{\overline{p}^s} \Delta \pi \Delta_y \overline{p}^s \right)^n}{\Delta y} \right] \right\} \right. \\ & \hspace{15em} (11.3.22)
 \end{aligned}$$

and

$$-\Delta t \frac{1}{3} \frac{1}{2} \frac{1}{\Delta x \Delta y} \left\{ \Delta_x \left( \overline{\Delta p}^{x'} \Delta_x \overline{\Phi}^s + \frac{\overline{RT}_v}{\overline{p}^s} \Delta \pi \Delta_x \overline{p}^s \right)^n + \Delta_y \left( \overline{\Delta p}^{y'} \Delta_y \overline{\Phi}^s + \frac{\overline{RT}_v}{\overline{p}^s} \Delta \pi \Delta_y \overline{p}^s \right)^n \right\}. \tag{11.3.23}$$

Again, the operator (11.3.23) does not provide communication with the nearest neighboring points in the directions  $x$  and  $y$ , so it is ineffective in preventing the small scale noise.

On the other hand, define

$$P_{x0} = -\Delta t \left( \frac{\overline{\Delta p}^x \Delta_x \overline{\Phi}^s}{\Delta x} + \frac{\overline{RT_v}^x \Delta \pi}{\overline{p}^s} \frac{\Delta_x \overline{p}^s}{\Delta x} \right) \quad (11.3.24)$$

$$P_{y0} = -\Delta t \left( \frac{\overline{\Delta p}^y \Delta_y \overline{\Phi}^s}{\Delta y} + \frac{\overline{RT_v}^y \Delta \pi}{\overline{p}^s} \frac{\Delta_y \overline{p}^s}{\Delta y} \right), \quad (11.3.25)$$

and the operator that at time level  $n$  has the form

$$\frac{\Delta_x (P_{x0}^n \Delta y) + \Delta_y (P_{y0}^n \Delta x)}{\Delta x \Delta y} = \frac{-\Delta t}{\Delta x \Delta y} \left\{ \Delta_x \left[ \left( \frac{\overline{\Delta p}^x \Delta_x \overline{\Phi}^s}{\Delta x} + \frac{\overline{RT_v}^x \Delta \pi}{\overline{p}^s} \frac{\Delta_x \overline{p}^s}{\Delta x} \right)^n \Delta y \right] + \Delta_y \left[ \left( \frac{\overline{\Delta p}^y \Delta_y \overline{\Phi}^s}{\Delta y} + \frac{\overline{RT_v}^y \Delta \pi}{\overline{p}^s} \frac{\Delta_y \overline{p}^s}{\Delta y} \right)^n \Delta x \right] \right\}. \quad (11.3.26)$$

Note that the right hand side of (11.3.26) reduces to

$$\frac{-\Delta t}{\Delta x \Delta y} \left[ \Delta_x \left( \overline{\Delta p}^x \Delta_x \overline{\Phi}^s + \frac{\overline{RT_v}^x}{\overline{p}^s} \Delta \pi \Delta_x \overline{p}^s \right)^n + \Delta_y \left( \overline{\Delta p}^y \Delta_y \overline{\Phi}^s + \frac{\overline{RT_v}^y}{\overline{p}^s} \Delta \pi \Delta_y \overline{p}^s \right)^n \right] \quad (11.3.27)$$

if  $\Delta x = \Delta y$ .

In case of (11.3.26) full communication between the nearest neighboring points is ensured, and apparently, a term of the form (11.3.26) is what is missing on the right hand side of (11.3.14). Therefore, we modify (11.3.14) to include the term (11.3.26) as follows

$$\frac{\Delta_x \left( \overline{\Delta \pi}^{xy} \Delta_y \Delta u \Delta y \right) + \Delta_y \left( \overline{\Delta \pi}^{xy} \Delta_x \Delta v \Delta x \right)}{\Delta x \Delta y} = (1-C) \frac{\Delta_x \left( \overline{P_{x1}^n + P_{x2}^n}^y \Delta y \right) + \Delta_y \left( \overline{P_{y1}^n + P_{y2}^n}^x \Delta x \right)}{\Delta x \Delta y} + C \frac{\Delta_x (P_{x0}^n \Delta y) + \Delta_y (P_{y0}^n \Delta x)}{\Delta x \Delta y} + \frac{\Delta_x \left( \overline{\Delta C_x + \Delta A_x}^y \Delta y \right) + \Delta_y \left( \overline{\Delta C_y + \Delta A_y}^x \Delta x \right)}{\Delta x \Delta y} \quad (11.3.28)$$

or after rearrangement,

$$\begin{aligned}
\frac{\Delta_x \left( \overline{\Delta\pi^{xy}}^y \Delta_t u \Delta y \right) + \Delta_y \left( \overline{\Delta\pi^{xy}}^x \Delta_t v \Delta x \right)}{\Delta x \Delta y} &= \frac{\Delta_x \left( \overline{P_{x1}^n + P_{x2}^n}^y \Delta y \right) + \Delta_y \left( \overline{P_{y1}^n + P_{y2}^n}^x \Delta x \right)}{\Delta x \Delta y} \\
&+ \frac{\Delta_x \left( \overline{\Delta C_x + \Delta A_x}^y \Delta y \right) + \Delta_y \left( \overline{\Delta C_y + \Delta A_y}^x \Delta x \right)}{\Delta x \Delta y} \quad (11.3.29) \\
&+ C \frac{\Delta_x \left( P_{x0}^n \Delta y \right) + \Delta_y \left( P_{y0}^n \Delta x \right) - \Delta_x \left( \overline{P_{x1}^n + P_{x2}^n}^y \Delta y \right) - \Delta_y \left( \overline{P_{y1}^n + P_{y2}^n}^x \Delta x \right)}{\Delta x \Delta y}
\end{aligned}$$

Substituting (11.3.29) back into (11.3.6) we obtain

$$\begin{aligned}
\nabla_B \cdot \left( \overline{\Delta\pi^{xy}} \mathbf{v}^n \right) &= \frac{\Delta_x \left( \overline{\Delta\pi^{xy}}^y u^n \Delta y \right) + \Delta_y \left( \overline{\Delta\pi^{xy}}^x v^n \Delta x \right)}{\Delta x \Delta y} \\
&+ C \frac{\Delta_x \left( P_{x0}^n \Delta y \right) + \Delta_y \left( P_{y0}^n \Delta x \right) - \Delta_x \left( \overline{P_{x1}^n + P_{x2}^n}^y \Delta y \right) - \Delta_y \left( \overline{P_{y1}^n + P_{y2}^n}^x \Delta x \right)}{\Delta x \Delta y} \quad (11.3.30)
\end{aligned}$$

so that, combining (11.3.1) with (11.3.30), the corrected divergence in the hydrostatic continuity equation finally takes the form

$$\begin{aligned}
\nabla_B \cdot \left( \overline{\Delta\pi^*} \mathbf{v} \right)_*^n &= \nabla_B \cdot \left( \overline{\Delta\pi^*} \mathbf{v} \right)^n \\
&+ C \frac{\Delta_x \left( P_{x0}^n \Delta y \right) + \Delta_y \left( P_{y0}^n \Delta x \right) - \Delta_x \left( \overline{P_{x1}^n + P_{x2}^n}^y \Delta y \right) - \Delta_y \left( \overline{P_{y1}^n + P_{y2}^n}^x \Delta x \right)}{\Delta x \Delta y} \quad (11.3.31)
\end{aligned}$$

In the NMMB code the approximate formulas (11.3.23) and (11.3.27) are used in (11.3.31) in order to reduce the operation count.

## 12.0 REFERENCES

- Adcroft, A, C. Hill, and J. Marshall 1997: Representation of topography by shaved cells in a height coordinate ocean model. *Monthly Weather Review*, **125**: 2293–2315.
- Ames, W.F., 1969: *Numerical methods for partial differential equations*. London: Nelson, 291 pp.
- Arakawa, A., 1972: Design of the UCLA general circulation model. Tech. Report No. 7, Department of Meteorology, University of California, Los Angeles, 116 pp.
- Arakawa, A., V.R., Lamb, 1977: Computational design of the basic dynamical processes of the UCLA general circulation model. *Methods of Computational Physics*, **17**, 173–265.
- Davies, T., M. Cullen, A. Malcolm, M. Mawson, A. Staniforth, A. White, N. Wood, 2005: A new dynamical core for the Met Office’s global and regional modelling of the atmosphere. *Quarterly Journal of the Royal Meteorological Society*, **131**, 1759–1782.
- Bryan, K., 1969: A numerical method for the study of the circulation of the World Ocean. *Journal of Computational Physics*, 347–376.
- Doms, G. and U. Schaettler, 1997: The nonhydrostatic limited-area model LM (Lokal Modell) of DWD. Part I: Scientific Documentation. Deutscher Wetterdienst, 155 pp.
- Eckermann, S., 2009: Hybrid  $\sigma$ - $p$  coordinate choices for a global model. *Monthly Weather Review*, **137** (1), 224-245
- Farge, M., and R. Sadourny, 1989: Wave-vortex dynamics in rotating shallow water. *Journal of Fluid Mechanics*, **206**, 433-462.
- Gadd, A.J., 1974: An economical explicit integration scheme. Tech. Note 44, Meteorological Office, Bracknell, RG12 2SZ, U.K., 7 pp.
- Gallus, W.A. Jr., 2000: The impact of step orography on flow in the Eta model: Two contrasting examples. *Weather and Forecasting*, **15**, 630–639.
- Gallus, W.A. Jr., and J. B. Klemp, 2000: Behavior of flow over step orography. *Monthly Weather Review*, **128**, 1153–1164.
- Gavrilov, M.B. and Z.I. Janjic, 1989: Computed rotational energy spectra of two energy and enstrophy conserving schemes on semi-staggered grids. *Meteorology and Atmospheric Physics*, **41**, 1-4.
- Janjic, Z.I., 1977: Pressure gradient force and advection scheme used for forecasting with steep and small scale topography. *Contributions to Atmospheric Physics*, **50**, 186-199.
- \_\_\_\_\_, 1979: Forward-backward scheme modified to prevent two-grid-interval noise and its application in sigma coordinate models. *Contributions to Atmospheric Physics*, **52**, 69-84.

- \_\_\_\_\_, 1984a: Non-linear advection schemes and energy cascade on semi-staggered grids. *Monthly Weather Review*, **112**, 1234-1245.
- \_\_\_\_\_, 1984b: Non-linear advection Eulerian schemes. Workshop on Limited Area Numerical Weather Prediction Models for Computers of Limited Power, Part I. WMO, Programme on Short- and Medium-range Weather Prediction Research, PSMP Rept. Series No. 8, 117-156, Case Postale 2300, CH-1211 Geneve 2.
- \_\_\_\_\_, 1990: The step-mountain co-ordinate: physical package. *Monthly Weather Review*, **118**, 1429-1443.
- \_\_\_\_\_, 1994: The step-mountain eta coordinate model: further developments of the convection, viscous sub layer and turbulence closure schemes. *Monthly Weather Review*, **122**, 927-945.
- \_\_\_\_\_, 1996: The surface layer parameterization in the NCEP Eta Model. *Research Activities in Atmospheric and Oceanic Modeling*, WMO, Geneva, CAS/JSC WGNE, 4.16-4.17.
- \_\_\_\_\_, 1997: Advection scheme for passive substances in the NCEP Eta model. *Research Activities in Atmospheric and Oceanic Modeling*, WMO, Geneva, CAS/JSC WGNE, 3.14.
- \_\_\_\_\_, 1998: Capabilities of limited area numerical models in predicting heavy precipitation events and possibilities for further improvement. In: *Meeting of the World Federation of Scientists, Working Group on Defense Against Floods and Unexpected Meteorological Events, Geneva, 19-20 Nov. 1998 (invited introductory lecture)*.
- \_\_\_\_\_, 2001: Nonsingular Implementation of the Mellor-Yamada Level 2.5 Scheme in the NCEP Meso model. *National Centers for Environmental Prediction Office Note #437*.
- \_\_\_\_\_, 2003: A Nonhydrostatic Model Based on a New Approach. *Meteorology and Atmospheric Physics*, **82**, 271-285. <http://dx.doi.org/10.1007/s00703-001-0587-6>
- \_\_\_\_\_, 2004: The NCEP WRF Core. *Extended abstract, 20th Conference on Weather Analysis and Forecasting/16th Conference on Numerical Weather Prediction*, AMS, Seattle, Washington, 10-15 January 2004, 21 pp.
- \_\_\_\_\_, 2005: A unified model approach from meso to global scales. *Geophysical Research Abstracts*, **7**, 05582, SRef-ID: 1607-7962/gra/EGU05-A-05582, European Geosciences Union, General Assembly, April 24 – 29, 2005, Vienna, Austria.
- \_\_\_\_\_, 2009: Further development of a model for a broad range of spatial and temporal scales. *Preprints, 23d Conference on Weather Analysis and Forecasting/19th Conference on Numerical Weather Prediction*, American Meteorological Society, May 31-June 5 2009, Omaha, Nebraska.
- \_\_\_\_\_ and T. Black 2007: An ESMF unified model for a broad range of spatial and temporal scales. *Geophysical Research Abstracts*, **9**, 05025, 2007, SRef-ID:

- 1607-7962/gra/EGU2007-A-05025, European Geosciences Union, General Assembly, April 15-20, 2007, Vienna, Austria.
- \_\_\_\_\_, T. L. Black and G. DiMego, 1998: Recent NCEP contributions toward development of a mesoscale model. *Research Activities in Atmospheric and Oceanic Modeling*. WMO, Geneva, CAS/JSC WGNE.
- \_\_\_\_\_, and G. DiMego, 2001: Effects of mountain representation and nonhydrostatic dynamics in a case of orographic precipitation. *Preprints, Symposium on Precipitation Extremes: Prediction, Impacts and Responses. 81<sup>st</sup> Annual Meeting of the American Meteorological Society*, January 14-18, 2001, Albuquerque, NM, American Meteorological Society, Boston, MA, 24-28.
- \_\_\_\_\_, Gall, R., and M.E. Pyle, 2010: Scientific Documentation for the NMM Solver. NCAR Technical Note NCAR/TN-477+STR, 54 pp.  
<http://nldr.library.ucar.edu/collections/technotes/asset-000-000-000-845.pdf>
- \_\_\_\_\_, J.P. Gerrity, Jr. and S. Nickovic, 2001: An alternative approach to nonhydrostatic modeling. *Monthly Weather Review*, **129**, 1164-1178.
- \_\_\_\_\_, H. Huang and S. Lu, 2009: A unified atmospheric model suitable for studying transport of mineral aerosols from meso to global scales. *IOP/Electronic Journals, Conf.Series: Earth and Environmental Science (collection of papers from WMO/GEO Expert Meeting on an International Sand and Dust Storm Warning System Meeting, 7-9 November, Barcelona, Spain)*, Vol. **9**, 6pp.  
<http://www.iop.org/EJ/toc/1755-1315/7/1>
- \_\_\_\_\_, and F. Mesinger, 1984: Finite-difference methods for the shallow water equations on various horizontal grids. *Numerical Methods for Weather Prediction, Vol. 1*, Seminar, ECMWF, 1983, Reading, U.K., 29-101, Shinfield Park, Reading, Berkshire RG2 9AX, U.K.
- \_\_\_\_\_, and F. Mesinger, 1989: Response to small-scale forcing on two staggered grids used in finite-difference models of the atmosphere. *Quarterly Journal of the Royal Meteorological Society*, Vol. **115**, 1167-1176.
- \_\_\_\_\_, and A. Wiin-Nielsen, 1977: On geostrophic adjustment and numerical procedures in a rotating fluid. *Journal Atmospheric Science*, **34**, 297-310.
- Laprise, R., 1992: The Euler equation of motion with hydrostatic pressure as independent coordinate. *Monthly Weather Review*, **120** (1), 197-207.
- Lobocki L., 1993: A procedure for the derivation of surface layer bulk relationships from simplified second-order closure models. *J. Appl Meteor*, **32**: 126–138.
- Mesinger, F., 1977: Forward-backward scheme, and its use in a limited area model. *Beitr. Phys. Atmos.*, **50**, 200-210.
- Mesinger, F., Z.I. Janjic, S. Nickovic, D. Gavrilo and D.G. Deaven, 1988: The step-mountain coordinate: model description and performance for cases of Alpine lee cyclogenesis and for a case of an Appalachian redevelopment. *Monthly Weather Review*, **116**, 1493-1518.
- Randall, D.A., 1994: Geostrophic adjustment and the finite difference shallow-water equations. *Monthly Weather Review*, **122**, 1371–1380.

- Room, R., A. Mannik and A. Luhamaa, 2006: Nonhydrostatic adiabatic kernel for HIRLAM Part IV, Semi-implicit semi-Lagrangian scheme. HIRLAM Technical Reports, 65, 42 pp.
- Saito, K., J. Ishida, K. Aranami, T. Hara, T. Segawa, M. Narita and Y. Honda, 2007: Nonhydrostatic atmospheric models and operational development at JMA. *Journal of Meteorological Society of Japan*, **85B**, 271-304.
- Sangster, W. E. 1960: A method of representing the horizontal pressure force without reduction of station pressures to sea level. *Journal of Meteorology*, **17(2)**, (April 1960) pp. 166-176
- Schneider, H. R., 1984: A Numerical Transport Scheme which Avoids Negative Mixing Ratios. *Monthly Weather Review*, **112**, 1206–1217.
- Simmons, A.J. and D.M. Burridge, 1981: An energy and angular-momentum conserving vertical finite-difference scheme and hybrid vertical coordinates. *Monthly Weather Review*, **109**, 758–766.
- Skamarock, W.C. and J.B. Klemp, 2008: A time-split nonhydrostatic atmospheric model for weather research and forecasting applications. *Journal of Computational Physics*, **227**, 3465–3485.
- Staudenmeier, M.J., and J. Mittelstadt, 1998: Results of the western region evaluation of the Eta-10 model. *Preprints, 12th Conf. on Numerical Weather Prediction*, Phoenix, AZ, 11–16 January, 1998; AMS, Boston, MA, 131–134.
- Steppeler, J., U. Schaettler, H.W. Bitzer, A. Gassman, U. Damrath, and G. Gregoric, 2003: Meso gamma scale forecasts by nonhydrostatic model LM. *Meteorology and Atmospheric Physics*, **82**, 75-96.
- Vallis, G., 1992: Mechanism and parameterizations of geostrophic adjustment and a variational approach to balanced flow. *Journal of Atmospheric Science*, **49(13)**, 1144–1160
- Winninghoff, F. J., 1968: On the adjustment toward a geostrophic balance in a simple primitive equation model with application to the problems of initialization and objective analysis. Ph.D. Thesis, Dept. Meteor. Univ. California, Los Angeles, CA
- Yeh, K.-S., J. Côté, S. Gravel, A. Méthot, A. Patoine, M. Roch, and A. Staniforth, 2002: The CMC–MRB Global Environmental Multiscale (GEM) Model. Part III: Nonhydrostatic Formulation. *Monthly Weather Review*, **130**, 339–356.